PN-AAW-996

49920

3860465

# OPTICAL DESIGNS FOR NON-TRACKING CONCENTRATORS

TECHNICAL REPORT 3

by

Bing Man Kwan
Richard B. Bannerot

Mechanical Engineering Department
University of Houston - University Park
Houston, Texas 77004

September, 1984

Any opinions, findings, conclusions or recommendations expressed in this publication are those of the author(s) and do not necessarily reflect the views of the U.S. Agency for International Development (USAID).

# OPTICAL DESIGNS FOR NON-TRACKING CONCENTRATORS

TECHNICAL REPORT 2

Prepared by: Bing Man Kwan

Approved by: Richard B. Bannerot, Principal Investigator

Prepared as part of the project, "Medium Temperature, High Efficiency Tracking and Non-tracking Solar Energy Collectors for Rural and Industrial Applications" for the Agency for International Development under the Atgreement for Projects under USAID Grant Agreement Dated August 26, 1978, between the President of India and USAID for Technologies for the Rural Poor. AID Project Grant No. 386-0465

September, 1984

Acknowledgements

This work was supported by United States Agency for International Development (USAID).

Bing Man Kwan
Richard B. Bannerot

September, 1984

## EXECUTIVE SUMMARY

The sun's energy represents the largest and most dependable source of energy in our solar system. However, by the time solar energy reaches the earth it has been diffused to a rather low intensity (about 1353 $W/m^2$). This energy is sufficient to drive the earth's live cycle and to heat water and air for the comfort of humankind. Unfortunately, its intensity is too low to be very useful for high temperatures (above 100°C) without concentration. The Laws of Thermodynamics limit the thermal efficiencies of devices which attempt to utilize this low grade energy. Hence it would be very useful to develop methods to concentrate this energy resource and thereby render it more useful. The most effective method to concentrate solar energy is with a device utilizing optical quality components that tracks the movement of the sun. Such concentrating solar collectors have been developed and have been utilized with varying degrees of success. The major technical problems encountered with their use have been the degradation of the optical surfaces exposed to the environment and the lack of a reliable tracking system. An additional problem is that the tracking solar collector systems have generally not been able to compete economically with the available "conventional" energy. All of these shortcomings are addressed by considering an alternative concept: a non-tracking, concentrating solar energy collector. The disadvantage of the non-tracking concept is that the attainable concentration ratio is much smaller than that achievable with a tracking system. The advantages are that the non-tracking co llector obviously does not require a tracking system, the quality of the optical surfaces is not so critical as in the

tracking collector and finally since it is intrinsically a simplier and lower technology device, it should be cheaper and more suitable for technically less developed environments.

This technical report describes the efforts towards developing low-cost (i.e., flat reflectors), non-tracking, concentrating solar collectors. The main thrust of the work reported here is on the design of the optical aspects of the collector.

## ABSTRACT

Non-tracking concentrators usually take the form of symmetric grooves aligned East-West so that the sun moves approximately along the groove during the day. Such concentrators do not continuously follow the movement of the sun. However, due to the North-South swing of the sun between the summer and winter solstices, seasonal tilt adjustments are necessary in order to keep the groove approximately aligned with the sun. One such type of non-tracking concentrator is the compound parabolic concentrator or CPC. Such collectors can achieve very high concentration ratios, but they can be expensive to manufacture and in some less-developed countries the technology to build such collectors may not exist. Another type of non-tracking concentrator has a trapezoidal geometry in cross-section. Flat side mirrors on both sides of the groove direct insolation to the base absorber. The performance of the trapezoidal concentrator does not compare favorably with the theoretical performance of the CPC. However when practical considerations are evaluated (e.g., cost and sophistication of fabrication), the choice between the two designs is not so obvious.

Optimal optical designs based on a "one reflection or less criterion" (i.e. requiring the solar radiation incident within the acceptance angle of the collector to strike the base with one or less reflection) have been previously developed for the trapezoidal one-facet and two-facet concentrators. The one reflection or less criterion has proven to be a very conservative design. A significant amount of insolation outside the design acceptance angle of the collector still strikes the absorber after two or more reflections. In effect a higher

concentration ratio could have been achieved in practice for the same acceptance angle.

A two reflections or less criterion has been developed and is described in this thesis. Collector designs resulting from this criterion have been evaluated with the aid of a ray-trace computer simulation which includes the effects of non-ideal reflectors. Annual tilt routines for this class of non-tracking concentrators are developed.

TABLE OF CONTENTS


| | Page |
|---|---|
| Acknowledgements | iv |
| Executive Summary | v |
| Abstract | vii |
| Table of Contents | ix |
| List of Figures | xi |
| List of Tables | xiv |
| Nomenclature | xv |
| Chapter 1 Introduction | 1 |
| Chapter 2 General Characteristics of Solar Collectors | 8 |
| 2.1 Solar Angles | 8 |
| 2.2 Tabor Angle | 16 |
| 2.3 Thermodynamic Concentration Ratio Limit | 17 |
| 2.4 Compound Parabolic Concentrator (CPC) | 20 |
| 2.5 Trapezoidal Groove Concentrator | 24 |
| Chapter 3 Non-Tracking Concentrator Concepts | 26 |
| 3.1 Design Criteria (one reflection or less) | 26 |
| 3.2 Computer Simulation | 28 |
| 3.3 Results for the One Reflection or Less Criterion | 32 |
| 3.4 The Two Reflections or Less Criterion | 34 |
| 3.5 Performance Characteristics | 40 |
| Chapter 4 Performance | 43 |
| 4.1 90% Actual Acceptance Angle Criterion | 43 |
| 4.2 Design Comparison with Perfect Walls | 43 |
| 4.3 Design Comparison with Imperfect Walls | 51 |
| Chapter 5 Annual Performance of Trapezoidal Collectors | 59 |

5.1 Annual Time Distribution of Tabor Angle 59

Page

5.2 The Daily North-South Swing Curve 61

5.3 Atmospheric Absorption of Solar Radiation 63

5.4 Criterion for Tilt Routine 65

Chapter 6 Conclusions 71

References 73

Appendix A Mathematical Model 76

Appendix B Additional Results 90

## LIST OF FIGURES


| Figure | Title | Page |
|---|---|---|
| 1-1 | Basic design of a flat plate solar collector | 4 |
| 1-2 | All glass evacuated, tubular receiver | 6 |
| 2-1 | Northern (Southern) hemisphere earth-sun relationship | 9 |
| 2-2 | Graph to determine the solar declination | 10 |
| 2-3 | Sun paths for equinox, summer and winter solstices for a site at $30^{\circ}$ N latitude | 12 |
| 2-4 | Solar zenith angle ($\gamma_s$), solar azimuth angle ($\theta_s$) and Tabor angle ($\phi$) | 14 |
| 2-5 | The effect of sun angle on the amount of insolation striking a collector | 15 |
| 2-6 | Schematics of radiation concentrator | 18 |
| 2-7 | Compound Parabolic Concentrator | 21 |
| 2-8 | Illustration of the sharp cut off angle of CPC (perfect wall) | 22 |
| 2-9 | Reflector/Aperture ratio as function of concentration ratio for full and truncated CPC's | 23 |
| 3-1 | Geometric constraint imposed by the one reflection or less criterion for trapezoidal groove collectors | 27 |
| 3-2 | Performance of one-facet groove based on one reflection or less criterion (perfect wall) | 29 |
| 3-3 | Performance of two-facet groove based on one reflection or less criterion (perfect wall) | 30 |
| 3-4 | Effect of incident angle on the performance of a given one reflection or less design (perfect wall) | 33 |
| 3-5 | Geometric constraints imposed by the two reflection or less criterion for a two-facet groove | 35 |
| 3-6 | Performance of the one-facet groove based on a two reflection or less criterion (perfect wall) | 38 |

| Figure | Title | Page |
|---|---|---|
| 3-7 | Performance of the two-facet groove based on a two reflection or less criterion (perfect wall) | 39 |
| 3-8 | Effect of incident angle on the performance of a given two reflection or less design (perfect wall) | 41 |
| 4-1 | Illustration of the design, actual and 90% acceptance angle | 44 |
| 4-2 | Comparison of the performance of one- and two-facet designs based on a two reflection or less criterion (perfect wall) | 46 |
| 4-3 | Performance comparison among designs based on design acceptance angle, 90% actual acceptance angle and CPC with acceptance angle of 4° | 48 |
| 4-4 | Performance comparison among designs based on design acceptance angle, 90% actual acceptance angle and CPC with acceptance angle of 7° | 49 |
| 4-5 | Performance comparison among designs based on design acceptance angle, 90% actual acceptance angle and CPC with acceptance angle of 9° | 50 |
| 4-6 | Effect of real walls on the performance $\delta_{A}^{*} = 9°$ | 52 |
| 4-7 | Effect of real walls on the performance $\delta_{A}^{*} = 7°$ | 53 |
| 5-1 | The time probability function in hours per degree vs. Tabor angle for several values of cut off time $t_c$ | 60 |
| 5-2 | Air mass vs. time for the year | 62 |
| 5-3 | Variation of the Tabor angle throughout the year | 64 |
| 5-4 | Tilt routine for a collector with acceptance angle of 9° | 66 |
| 5-5 | Tilt routine for a collector with acceptance angle of 7° | 67 |
| A-1 | Location of the orthogonal co-ordinate system in the base plane | 77 |
| A-2 | Incident and reflected beam in transformed coordinate system | 82 |
| A-3 | Possible fates of a beam reflected from lower left wall (specular or diffuse reflection) | 84 |

| Figure | Title | Page |
|---|---|---|
| B-1 | Performance of one-facet groove based on two reflection or less criterion (perfect wall) | 90 |
| B-2 | Performance of one-facet groove based on two reflection or less criterion (perfect wall) | 91 |
| B-3 | Performance of one-facet groove based on two reflection or less criterion (perfect wall) | 92 |
| B-4 | Performance of two-facet groove based on two reflection or less criterion (perfect wall) | 93 |
| B-5 | Performance of one-facet groove based on two reflection or less criterion (real wall) | 94 |

## LIST OF TABLES


| Table | Title | Page |
|---|---|---|
| 2-1 | Declination Angle | 11 |
| 4-1(a) | Effects of Realistic Reflectors on Performance $\delta_A* = 7^\circ$ | 54 |
| 4-1(b) | Effects of Realistic Reflectors on Performance $\delta_A* = 9^\circ$ | 56 |

## NOMENCLATURE

| | |
|---|---|
| $A$ | Groove opening (See Fig. 3-5) |
| $A_c$ | Aperture area of the collector |
| $A_e$ | Area of the receiver |
| $B$ | Width of groove base |
| CR | Concentration ratio |
| $D_1$ | Height of lower sidewall (See Fig. 3-5) |
| $D_2$ | Height of upper sidewall (See Fig. 3-5) |
| $F$ | Shape factor |
| $f$ | Fraction of wall specular reflections |
| $I_b$ | Beam intensity |
| $n$ | Day of the year (From Jan. 1) |
| $q_s$ | Total available energy per unit area of aperture |
| $q_u$ | Useful energy collected per unit area of aperture |
| $R$ | Total reflector area |
| $R_1$, $R_2$ | Random number |
| $T_a$ | Average ambient temperature |
| $T_e$ | Average receiver temperature |
| $t_c$ | Cut off time |
| $U$ | Overall thermal loss coefficient for the collector |
| $x$, $y$, $z$ | Base coordinate system |

Greek Letters

| | |
|---|---|
| $\alpha_1$ | Angle between lower wall with vertical axis (See Fig. 3-5) |
| $\alpha_2$ | Angle between upper wall with vertical axis (See Fig. 3-5) |
| $\alpha_{sw}$ | Solar absorptivity of sidewall |
| $\gamma$ | Incident solar angle |
| $\gamma_s$ | Solar zenith angle |

| | |
|---|---|
| $\delta$ | Design acceptance angle |
| $\delta_A$ | Actual acceptance angle |
| $\delta_{A^*}$ | 90% actual acceptance angle |
| $\delta_s$ | Solar declination angle |
| $\varepsilon$ | Angle of tilt from the local latitude |
| $\eta$ | Instantaneous collector efficiency |
| $\theta_s$ | Solar azimuth angle |
| $\lambda$ | Local latitude at a location |
| $\sigma$ | Stefan-Boltzman constant |
| $\phi$ | Tabor angle |
| $\omega$ | Hour angle, solar noon being zero and each hour equaling $15^\circ$ with mornings positive and afternoons negative |

# Chapter One

## Introduction

As the price of fossil fuel continues to rise, alternative sources of energy such as geothermal, wind and solar energy become more attractive. Solar energy has some distinct advantages over the fossil fuels. For example it is renewable and non-polluting. The major obstacle in the development of solar energy is economics, although many have argued that economics is a false issue due to the lack of reasonable future alternatives to fossil fuels and the fact that the present pricing and taxing structure favor the status quo. In any event solar applications do require a large initial investment although the operations and maintenance costs are relatively low once it is installed.

The utilization of solar energy is capital intensive. The expense is due largely to the diffuse and intermittent nature of solar energy which results in large collector arrays and energy storage requirements. The primary thrust of current solar activity by researchers and engineers is to reduce the cost of the equipment required by making it operate more efficiently and by reducing material and construction costs. Also, in the USA at least changes in tax laws at both the federal and state level have been considered to encourage both household and industrial installation of solar energy equipment. Such special tax considerations, already enjoyed by the more conventional alternatives, could make solar energy more competitive.

In order to utilize solar radiation, systems have to be built to collect and convert it either to thermal, chemical, or electrical

energy. The collectors themselves are the most important component of a solar energy system and possibly the most expensive component. How well the whole system works depends largely on how well the collectors perform. Therefore it is desirable to know what factors affect the efficiency of a collector.

The useful energy collected by a collector can be expressed as

$$q_u A_c = (\tau \alpha)_{eff} q_s A_c - \bar{U} A_e(T_e - T_a) - \epsilon_e \sigma A_c(T_e^4 - T_a^4) \qquad (1.1)$$

where

$q_u$: the rate at which useful energy is collected per unit area of aperture

$q_s$: the rate at which solar energy is available per unit area of aperture, normal to the aperture

$A_c$: aperture area of the collector

$(\tau \alpha)_{eff}$: fraction of insolation striking the collector aperture that is absorbed by the receiver

$\bar{U}$: overall thermal loss coefficient

$A_e$: area of the receiver

$T_e$: average receiver temperature

$T_a$: average ambient temperature

$\epsilon_e$ : effective emittance of the receiver

The term on the left side of eqn. (1.1) represents the useful energy that can be removed from the collector, that is, the useable energy. The first term on the right of the equation is the total energy absorbed by the receiver. The second term on the right is the convective and conductive thermal loss term. The last term of the equation represents the radiative losses. Equation (1.1) actually represents the energy

balance for the collector.

Collector efficiency $\eta$ is defined as the instantaneous ratio of the rate at which useful energy can be extracted from the collector to the rate at which solar energy is available to the collector.

$$\eta = \frac{q_u A_c}{q_s A_c} = (\tau \alpha)_{eff} - U \frac{A_e}{q_s A_c} (T_e - T_a) - \epsilon_e \sigma \frac{A_e}{q_s A_c} (T_e^4 - T_a^4) \qquad (1.2)$$

From eqn. (1.2), it is clear that the efficiency of a collector is directly related to the thermal loss terms. Therefore design changes which reduce thermal losses which do not reduce the absorbed energy will undoubtedly increase the efficiency of the collector.

The most common type of solar collector for thermal collection at moderate temperatures is the flat plate collector, depicted in Fig. 1-1. It consists of an absorber to absorb the radiant energy, a transparent cover to protect the absorber surface from weathering, tubes attached to the absorber in which a fluid flows to carry away the energy collected by the absorber and finally insulation material at the bottom to reduce thermal loss. However, flat plate collectors operate efficiently only to about 80° C. At higher temperatures, the radiative and convective thermal losses become significant. Thus applications of solar energy with flat plate collectors at higher temperatures such as for industrial process heat and absorption air conditioning are severely limited. In a report [1] [1] from the Solar Energy Research Institute, it is estimated that industrial process heat accounts for about 18% to 25% of the total energy consumed in the United States. If preheating with solar energy

[1]Number in [ ] refers to references listed at the end

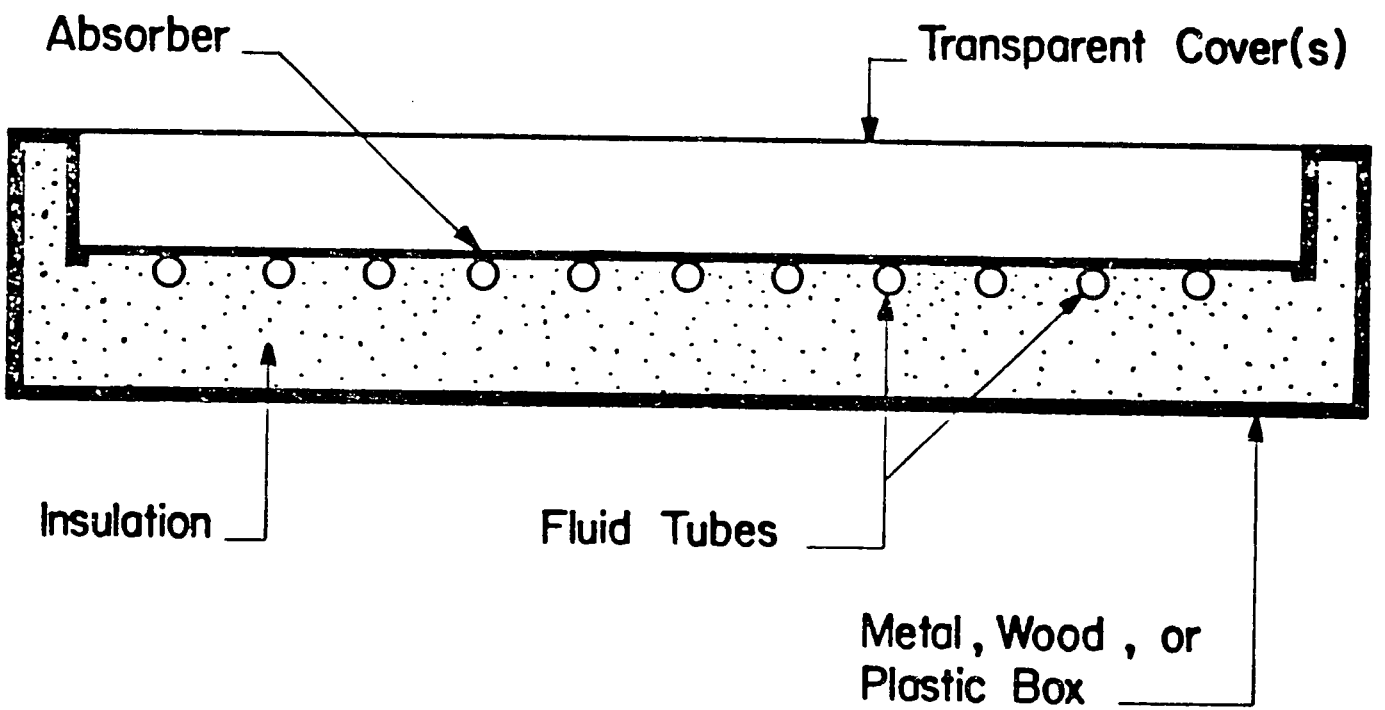


Figure 1-1 Basic Design of a Flat Plate Solar Collector

is feasible to about 280° C, then over half of the industrial process heat could potentially be supplied by solar energy.

As mentioned, high temperture performance of a solar collector can be enhanced by reducing thermal losses. These losses can be reduced in various ways. One method is to use radiatively selective surfaces on the absorber to maximize the amount of energy captured and minimize the re-radiation of the absorbed energy. Coatings with solar absorptance of 0.9 - 0.95 and infrared emittance between 0.06 and 0.3 are commercially available. Another way to reduce losses is by evacuation of the space around the absorber which can eliminate convective and greatly reduce conductive thermal losses from the absorber. At the present time several evacuated tubular designs are available commercially. General Electric Company has produced such a collector which is enclosed with soda lime glass (fluorescent lamp tubing) and is evacuated and sealed at the factory. Similar design have been available from Owens-Illinois. Figure 1-2 is a sketch of a evacuated tubular receiver coupled to a compound parabolic reflector. Technology currently used in glass and lighting industries are expected to reduce the cost of such receivers.

Concentration also helps to improve high temperature performance by reducing the area of the absorbing surface for a given aperture, thus, even though the amount of energy available to a given aperture remains the same, the collector can operate efficiently at a higher temperature since thermal losses have been reduced. Also the reflective surfaces on both sides of the receiver serve as a wind shield to help reduce convective losses.

Fully tracking focusing solar collectors, which follow the motion

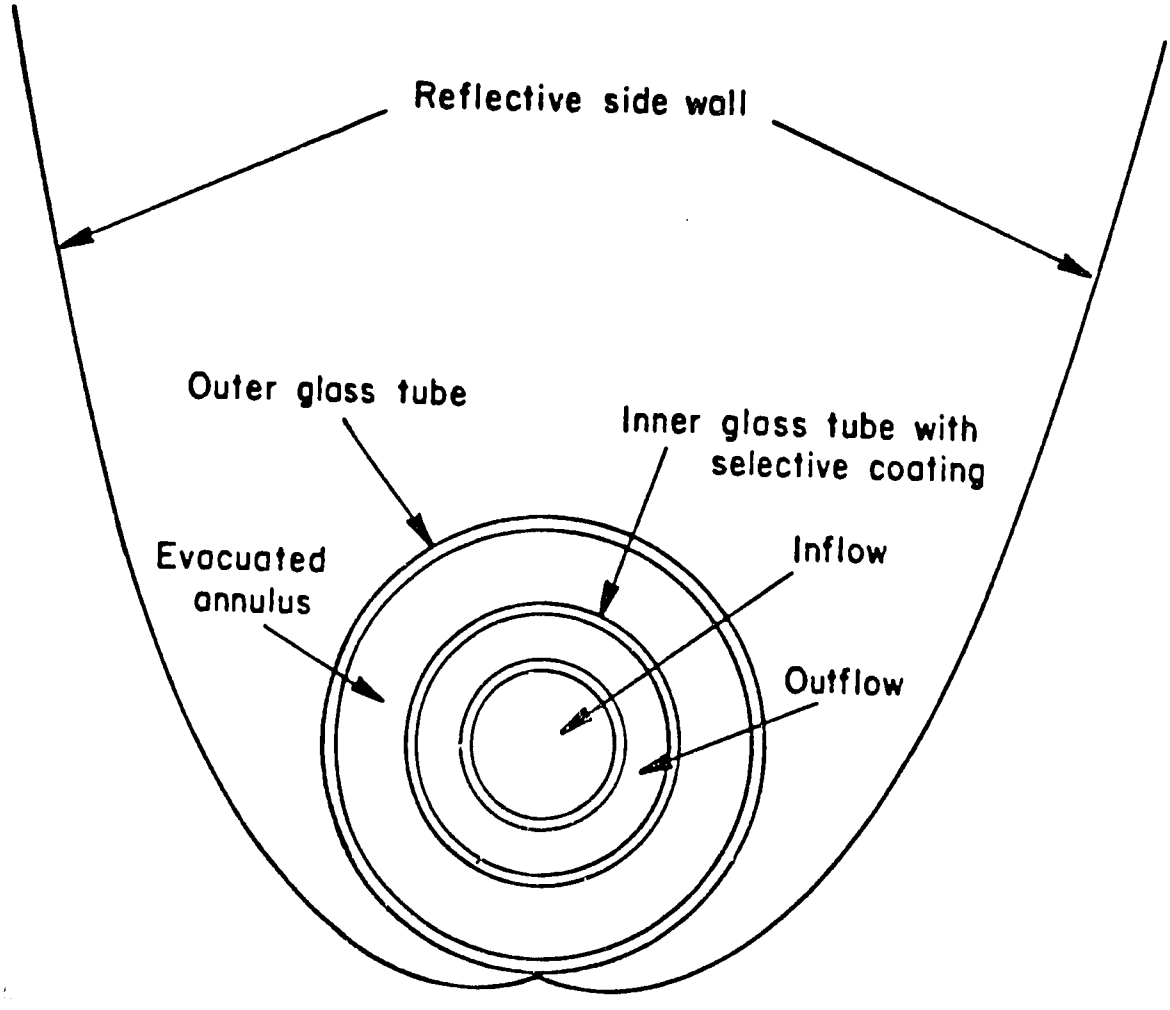


Figure 1-2 All Glass Evacuated, Tubular Receiver

of the sun continuously, can achieve very high concentration ratios which lead to efficient operation at extremely high temperatures. For example, the Georgia Tech Solar Thermal Test Facility [2] has 550 individual mirrors which are driven mechanically to follow the sun and to focus its rays onto the receiver suspended from a tower. The test facility can generate steam at 1110° F and 2200 psi. However, such a system is understandably expensive to fabricate and to operate. The gain in performance for such systems may be outweighed by the increased cost. Material selection as well as environmental degradation in the optical performance of the reflective surfaces is a major problem of such systems. An alternative to high quality focusing systems may be a non-tracking concentrator for operating temperatures up to about 150° C. The main objective of this study is to examine and compare the optical characteristics of various non-tracking concentrators.

## Chapter Two

## General Characteristics of Solar Collectors

### 2.1 Solar Angles

Knowledge of the earth's motion relative to the sun is necessary for the proper design of any solar energy system. It is especially important for concentrating collectors since this type of collector primarily uses only the beam component of insolation. Focusing devices must be designed to follow the path of the sun. Non-tracking concentrators have only a limited acceptance angle so they must be carefully designed and oriented to utilize as much of the insolation as possible.

As the earth rotates about the sun, it spins about an axis which tilts at an angle of $23.45^\circ$ from the orbital plane as illustrated in Fig. 2-1. As a result, the angle between the earth's equatorial plane and earth-sun line varies between $\pm 23.45^\circ$ throughout the year. This angle is called the declination $\delta_s$. Declinations north of the equator are positive (summer in the northern hemisphere); those south are negative. The declinations are tabulated in Table 2-1 and represented graphically in Fig. 2-2. It can also be approximated by

$$\delta_s \cong 23.45^\circ \sin\left(360^\circ \frac{(284 + n)}{365}\right) \tag{2.1}$$

where n is the day of the year. The value of $\delta_s$ calculated from eqn. (2-1) will be correct within $\pm 0.37^\circ$ (with maximum positive deviation on May 1) and $-1.7^\circ$ (with maximum negative deviation on October 9).

It is the earth's inclination with the orbital plane which accounts for the earth's seasonal variation, differences in the day length and

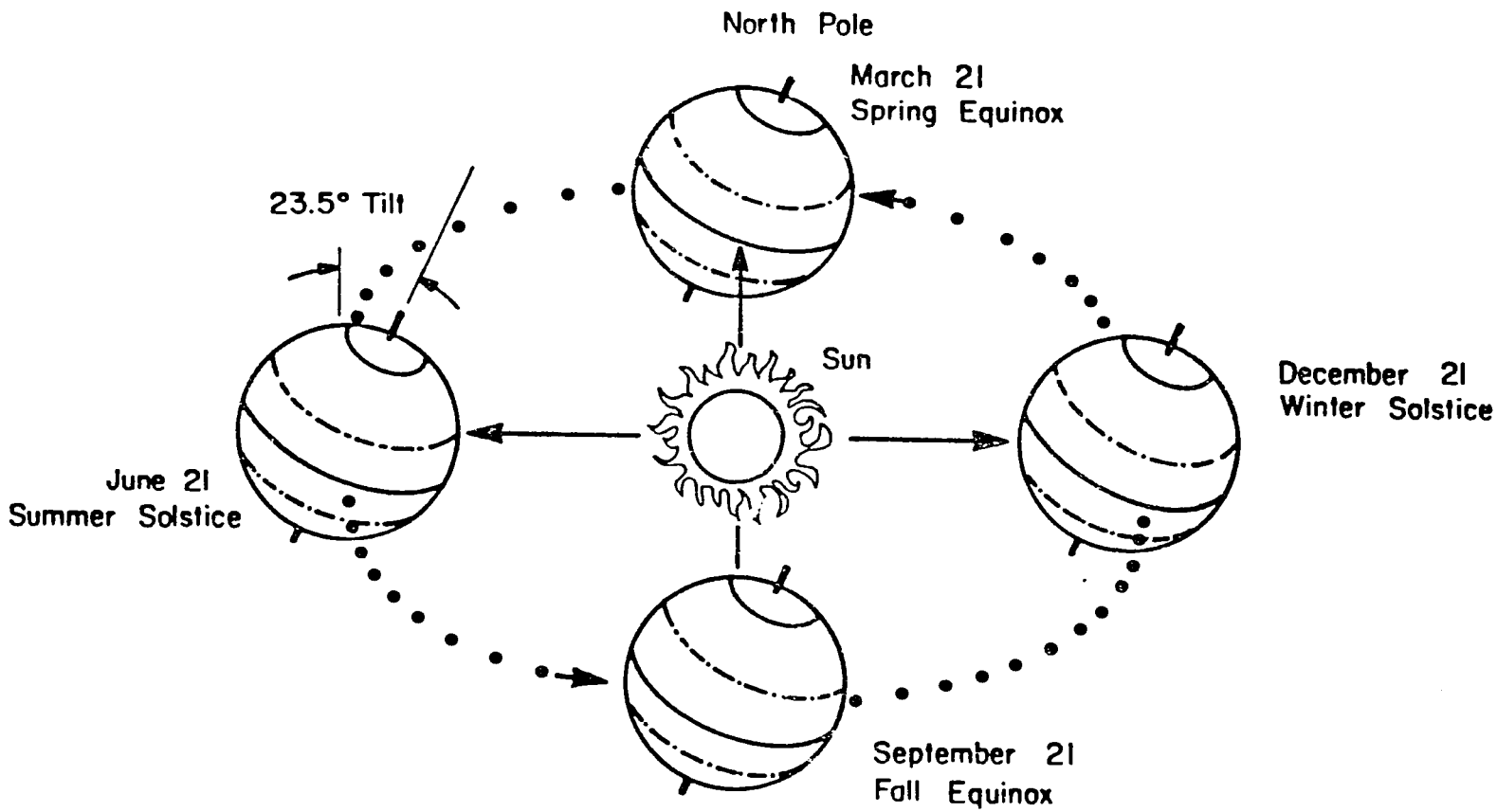


Figure 2-1 Northern (Southern) Hemisphere Earth-Sun Relationship

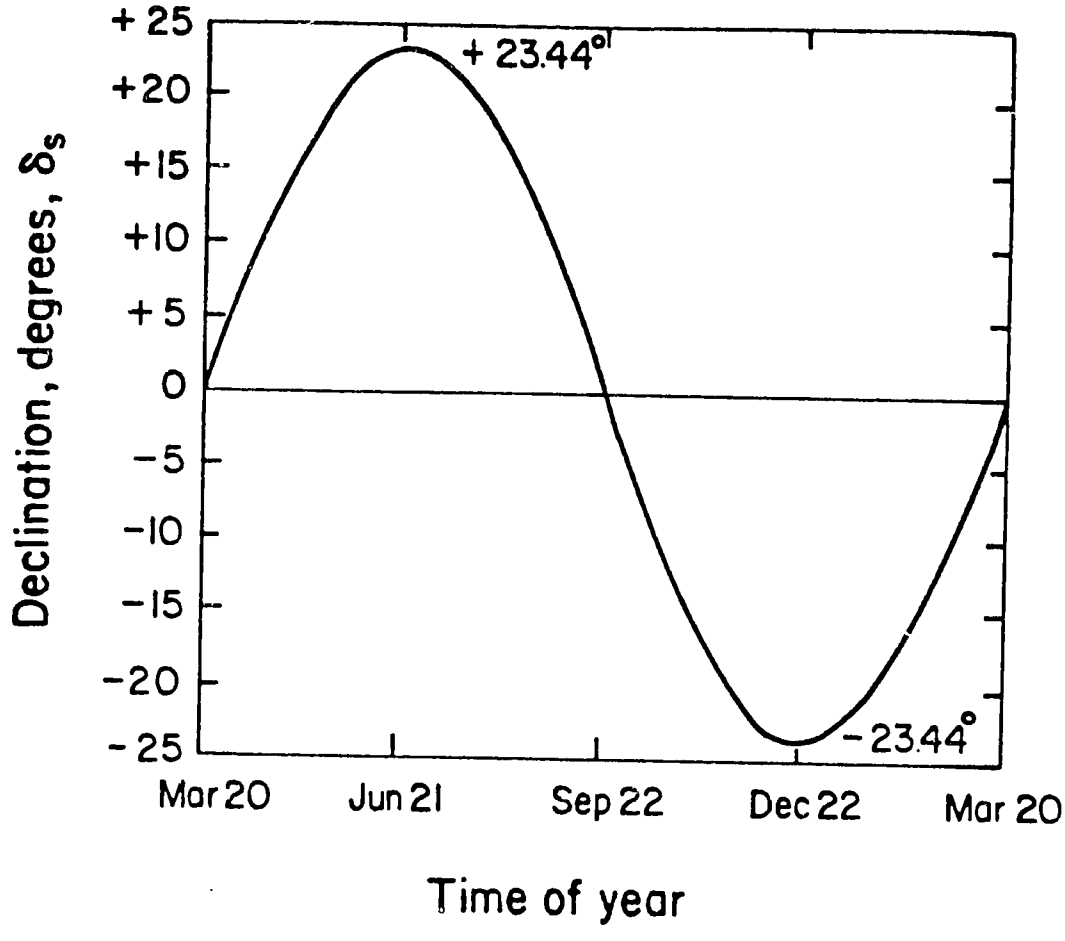


Figure 2-2 Graph to Determine the Solar Declination

Table 2-1 Declination

| Date | | Day n | Declination deg † δ s | Date | | Day n | Declination deg‡ δ s |
|---|---|---|---|---|---|---|---|
| Jan. | 1 | 1 | -23.0 | July | 9 | 190 | +22.9 |
| | 10 | 10 | -22.0 | | 19 | 200 | 20.9 |
| | 20 | 20 | -20.2 | | 29 | 210 | 18.8 |
| Feb. | 9 | 40 | -14.8 | Aug. | 8 | 220 | 16.2 |
| | 19 | 50 | -11.4 | | 18 | 230 | 13.2 |
| | | | | | 28 | 240 | 9.8 |
| Mar. | 1 | 60 | -7.7 | Sept. | 7 | 250 | 6.2 |
| | 11 | 70 | -3.9 | | 17 | 260 | 2.4 |
| | 21 | 80 | +0.1 | | 27 | 270 | -1.5 |
| | 31 | 90 | 4.0 | | | | |
| | | | | Oct. | 7 | 280 | -5.4 |
| Apr. | 10 | 100 | 7.8 | | 17 | 290 | -9.1 |
| | 20 | 110 | 11.4 | | 27 | 300 | -12.7 |
| | 30 | 120 | 14.7 | | | | |
| | | | | Nov. | 6 | 310 | -15.9 |
| May | 10 | 130 | 17.5 | | 16 | 320 | -18.7 |
| | 20 | 140 | 19.9 | | 26 | 330 | -20.9 |
| | 30 | 150 | 21.7 | | | | |
| | | | | Dec. | 6 | 340 | -22.5 |
| June | 9 | 160 | 22.9 | | 16 | 350 | -23.3 |
| | 19 | 170 | 23.4 | | 26 | 360 | -23.4 |
| | 29 | 180 | 23.3 | | 31 | 365 | -23.1 |

relative movement of the sun in the North-South direction during a year. For example, at the summer solstice, the northern hemisphere is tilted toward the sun which results in a higher insolation level and more day light hours. To an observer standing in the northern hemisphere facing south, the sun rises north of due east and sets north of due west as shown in Fig. 2-3. At equinox, the earth's equatorial plane is parallel to the earth-sun line resulting in equal day and night hours. The sun also will rise due east and set due west. At the winter solstice, the northern hemisphere is tilted away from the sun, thus increasing the

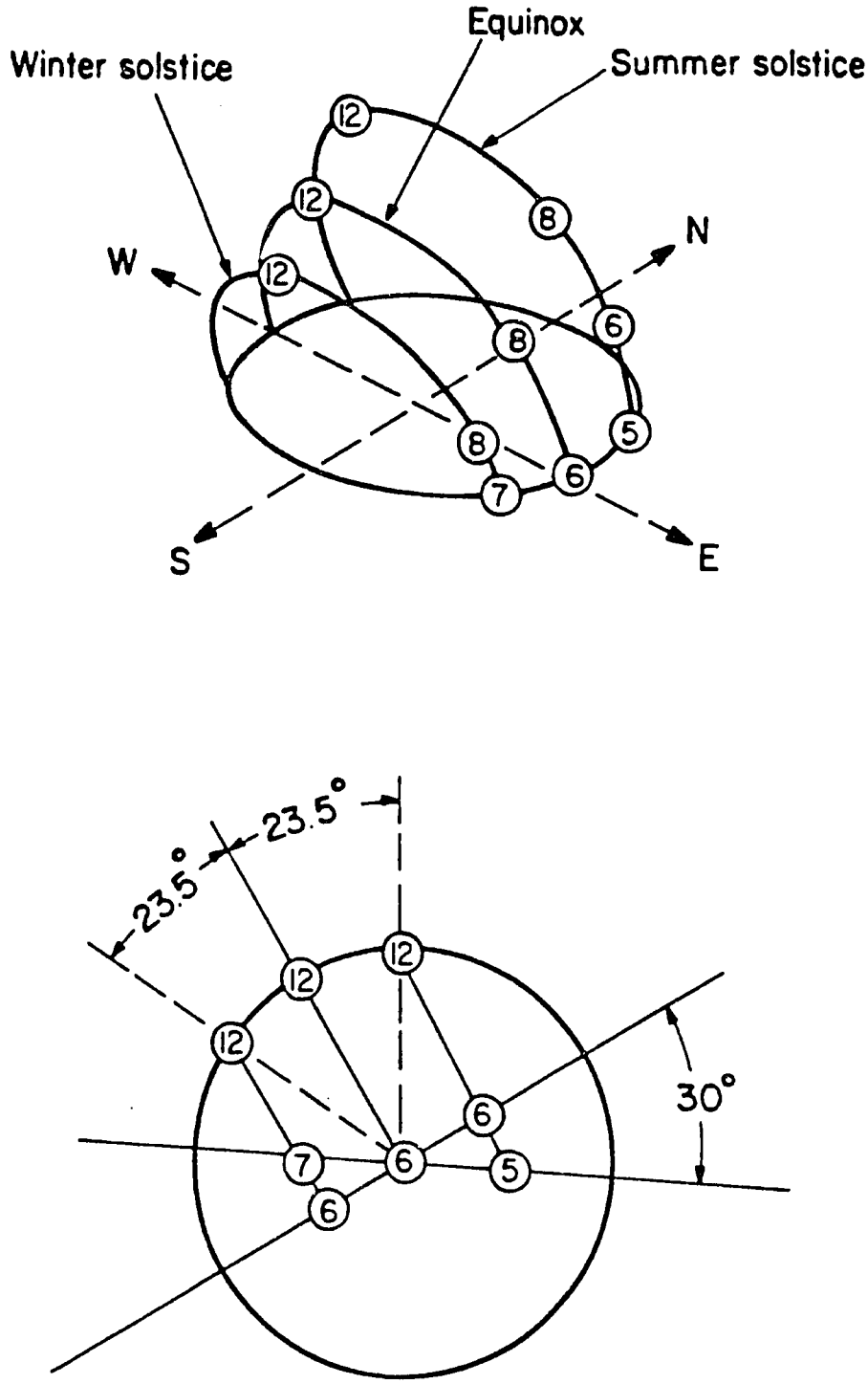


Figure 2-3 Sun Paths for Equinox, Summer and Winter Solstices for a Site at 30°N Latitude

path length which the solar radiation must travel to reach the ground in the northern hemisphere. Therefore, weaker insolation is anticipated. The sun rises south of due east and sets south of due west, resulting in shorter day light hours. So the sun not only moves east-west during a day but also moves north-south throughout a year.

At any time, the position of the sun in the sky relative to a point on earth can be represented by two angles.

(1) The solar zenith angle, $\gamma_s$, is the angle between the vertical at the point on the earth and the direction of the solar beam

(2) The solar azimuth angle, $\theta_s$, is the projected angle of the sun measured in the horizontal plane eastward from due south. It is positive measured to the east and negative to the west as illustrated in Fig. 2-4

These two angles can be determined from the following formulas:

$$\gamma_s = \cos^{-1} (\cos \lambda \ \sin \delta_s + \cos \lambda \ \cos \delta_s \ \cos \omega) \tag{2.2}$$

$$\theta_s = \sin^{-1} \left(\frac{\cos \delta_s \ \sin \omega}{\sin \gamma_s}\right) \tag{2.3}$$

where $\lambda$ is the local latitude and $\omega$ is the hour angle; solar noon being zero and each hour equalling 15° with morning positive and afternoons negative.

A principle factor in determining the intensity of the solar radiation that strikes the collector aperture is the angle between the normal to the aperture and the incoming ray. The intensity of solar radiation intercepted by a surface as shown in Fig. 2-5, varies as the cosine of

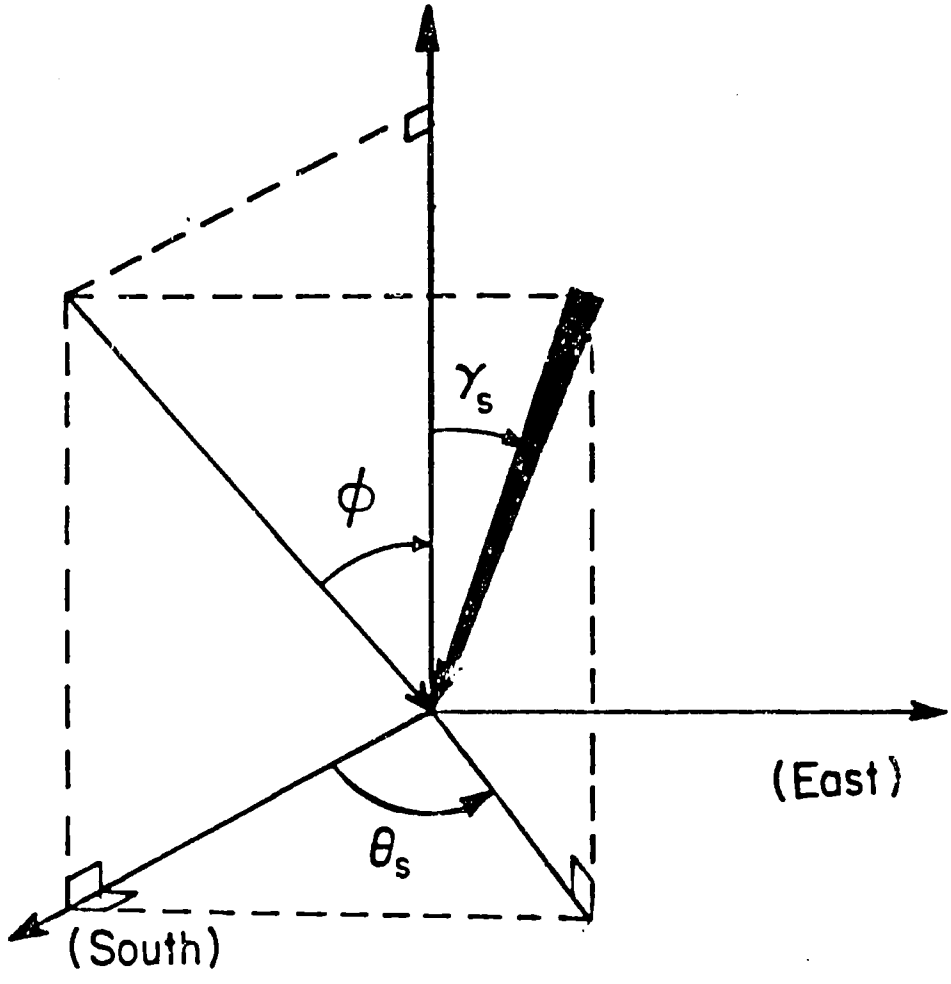


Figure 2-4 Solar Zenith Angle ($\gamma_s$), Solar Azimuth Angle ($\theta_s$) and Tabor Angle ($\phi$)

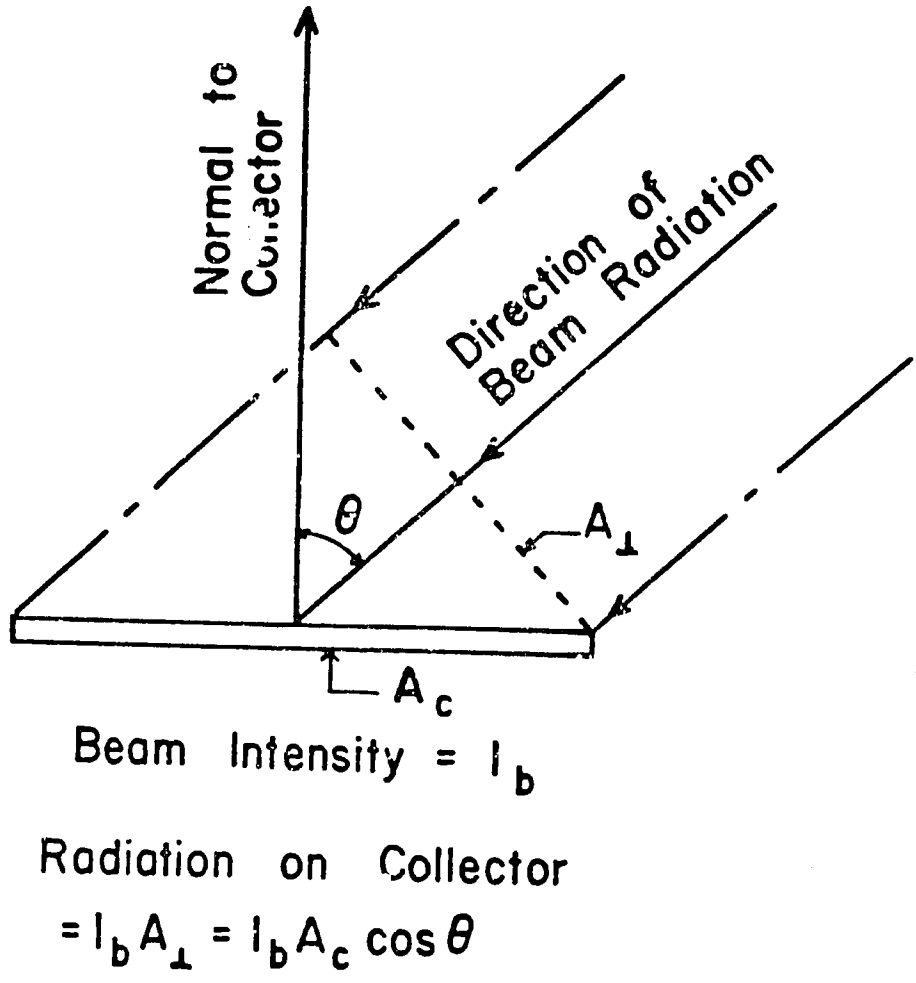


Figure 2-5 The Effect of Sun Angle on the Amount of Insolation Striking a Collector

the incident angle $\theta$ . This effect is called the cosine effect.

Non-tracking concentrators usually take the form of symmetric grooves aligned East-West so that the sun moves approximately along the groove during the day. Such concentrators do not continuously follow the movement of the sun. However, due to the North-South swing of the sun between summer and winter solstices as previously mentioned in this chapter, seasonal tilt adjustments are necessary in order to keep the groove approximately aligned with the sun. The frequency of tilt adjustment depends on the acceptance angle of the collector. Acceptance angle of a collector is defined as the largest incident angle for which all the direct insolation would reach the receiver of the collector if the collector optics were ideal. Insolation outside the acceptance angle of the collector may or may not reach the receiver depending on where it strikes the reflector.

## 2.2 Tabor Angle

As first described by Tabor [3] and later utilized by Hollands [4] the radiative performance of an East-West aligned groove depends on the angle between the collector normal and the projection of the insolation direction into a North-South plane. This angle $\phi$ can be expressed as

$$\phi = \tan^{-1}\left(\frac{\tan \delta_s}{\cos(\frac{\pi t}{12})}\right) \tag{2.4}$$

where t is the time in hours from solar noon. If a grooved collector is oriented East-West and its normal is tilted from the zenith (vertical) by an angle equal to the geographical latitude, the projected angle

of incidence of the solar rays onto the North-South plane measured from normal is $\phi$ . If the collector is tilted from this position by an angle $\varepsilon$ , the projected angle of incidence (relative to the collector) of the solar ray $\beta$ is

$$\beta = \phi - \varepsilon \tag{2.5}$$

If the beam's projected angle $\phi$ (or $\beta$ ) exceeds the acceptance angle of the collector, part or none of the beam reaches the receiver, depending upon the design of the collector.

## 2.3 Thermodynamic Concentration Ratio Limit

At this point it will be interesting to introduce the relationship between the acceptance angle and the concentration ratio of a concentrator. The following discussion has been adopted from Ref. 5.

Consider two black surfaces of area $A_1$ and $A_2$ of arbitrary geometry, and for the purpose of simplicity, assume both surfaces are surrounded by vacuum. Suppose surfaces 1 and 2 have temperatures $T_1$ and $T_2$ respectively, whereas the surroundings are at absolute zero. The energy radiated by the surfaces is

$$E_1 = A_1 \sigma T_1^4 \tag{2.6}$$

and

$$E_2 = A_2 \sigma T_2^4 \tag{2.7}$$

where $\sigma$ is the Stefan-Boltzman constant.

In terms of shape factor F, the radiation emitted by surface 1 and intercepted by surface 2 is

$$E_{1\to 2} = F_{1\to 2} A_1 \sigma T_1^4 \tag{2.8}$$

with an analogous expression

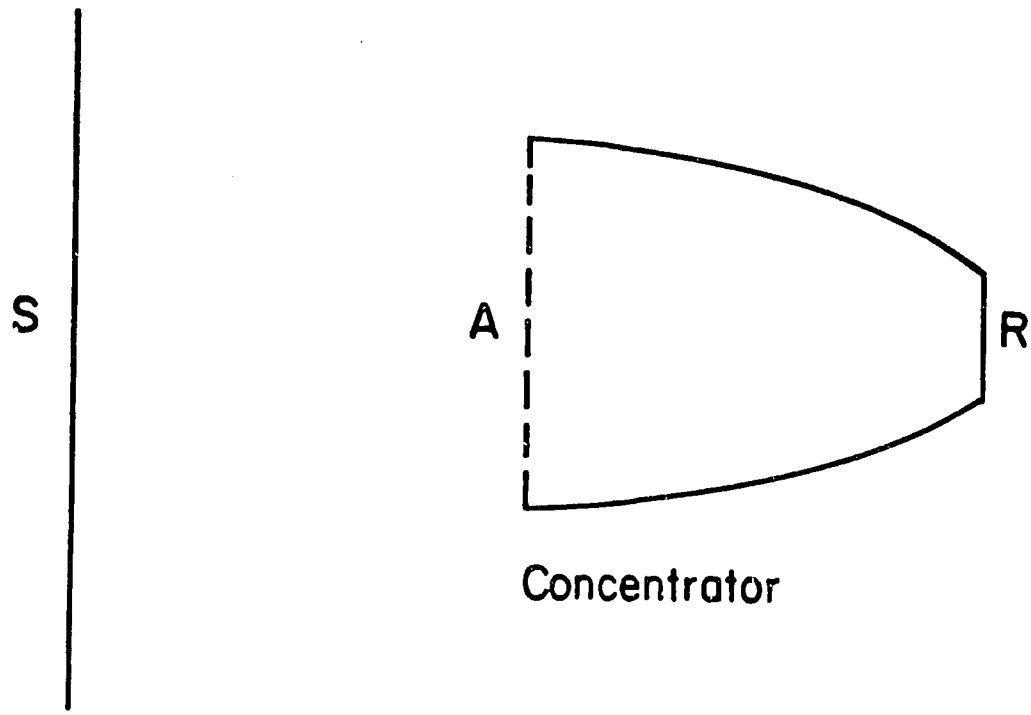


S : Source of Radiation
A : Aperture of Concentrator
R : Receiver of Concentrator

Figure 2-6 Schematics of Radiation Concentrator

$$E_{2\to1} = F_{2\to1}\, A_2\, \sigma\, T_2^4 \tag{2.9}$$

for radiation in the opposite direction. The net radiation transfer between surface 1 and 2 is

$$E_{net} = E_{1\to2} - E_{2\to1} \tag{2.10}$$

and is equal to zero if both surfaces are at the same temperature, which implies

$$A_1\, F_{1\to2} = A_2\, F_{2\to1} \tag{2.11}$$

Consider the configuration in Fig. 2-6 and apply the above result

$$A_s\, F_{s\to A} = A_A\, F_{A\to s} \tag{2.12}$$

and

$$A_s\, F_{s\to R} = A_R\, F_{R\to s} \tag{2.13}$$

Geometric concentration ratio CR is defined as the ratio of aperture area to absorber area, that is

$$CR = \frac{A_A}{A_R} \tag{2.14}$$

Substituting $A_A$ and $A_R$ for the shape factors in eqns. (2.12) and (2.13)

$$CR = \frac{F_{s\to A}\, F_{R\to s}}{F_{A\to s}\, F_{s\to R}} \tag{2.15}$$

If the incident radiation is within the acceptance angle of the collector, all the radiation received by the aperture will reach the receiver, therefore

$$F_{s\to A} = F_{s\to R} \tag{2.16}$$

resulting in

$$CR = \frac{F_{R\to s}}{F_{A\to s}} \tag{2.17}$$

Since the largest possible value of $F_{R\to s}$ is one, the thermodynamics

concentration ratio limit is

$$CR \leq CR_{max} = \frac{1}{F_{A \to s}} \tag{2.18}$$

For the case of solar concentrator, the sun is assumed to be at infinity and if $2\delta$ is the maximum angle within which radiation is to be collected, the shape factor $F_{A \to s}$ was found to be [5]

$$F_{A \to s} = \sin \delta \tag{2.19}$$

for the two dimensional case and

$$F_{A \to s} = \sin^2 \delta \tag{2.20}$$

for the three dimensional case. The corresponding maximum concentration limits are

$$CR_{max,\ 2D} = \frac{1}{\sin \delta} \tag{2.21}$$

and

$$CR_{max,\ 3D} = \frac{1}{\sin^2 \delta} \tag{2.22}$$

## 2.4 Compound Parabolic Concentrator (CPC)

One type of non-tracking concentrator is the compound parabolic concentrator or CPC. Descriptions of the CPC appeared independently in the United States, Germany, and the U.S.S.R. during the mid-1960's. The CPC consists of two symmetrical half parabolic cylinders which form the reflective sidewalls of a groove as shown in Fig. 2-7. The foci of the two distinct parabolic segments are located at the end of the receiver on the opposite side from the reflector. The axis of the parabolic segments are oriented away from the CPC optical axis by the amount equal to the acceptance angle $\delta$ of the collector. The slope of the reflector

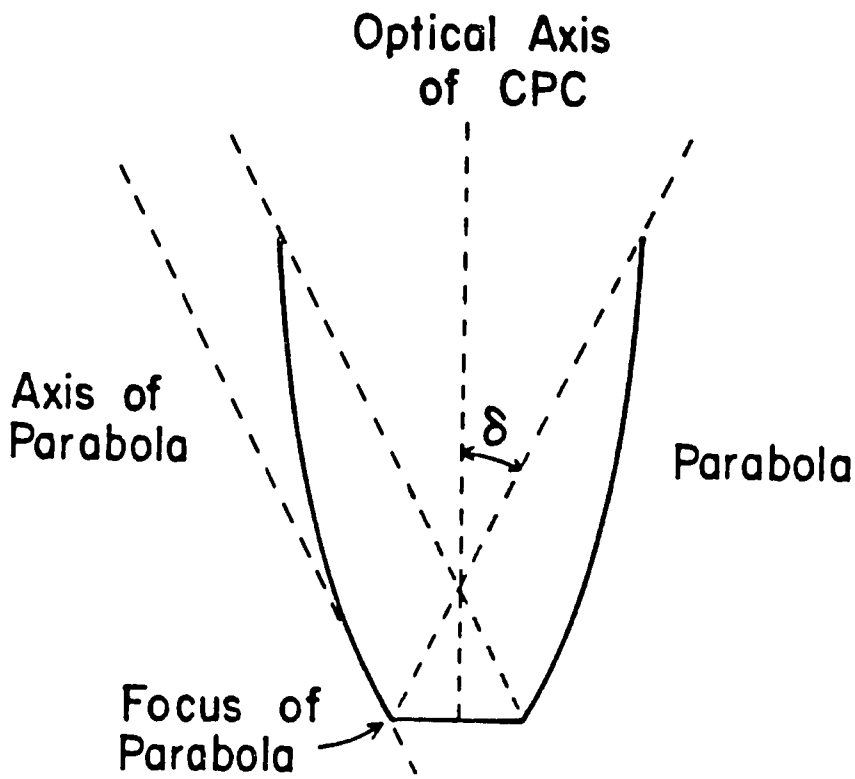


Figure 2-7 Compound Parabolic Concentrator CPC

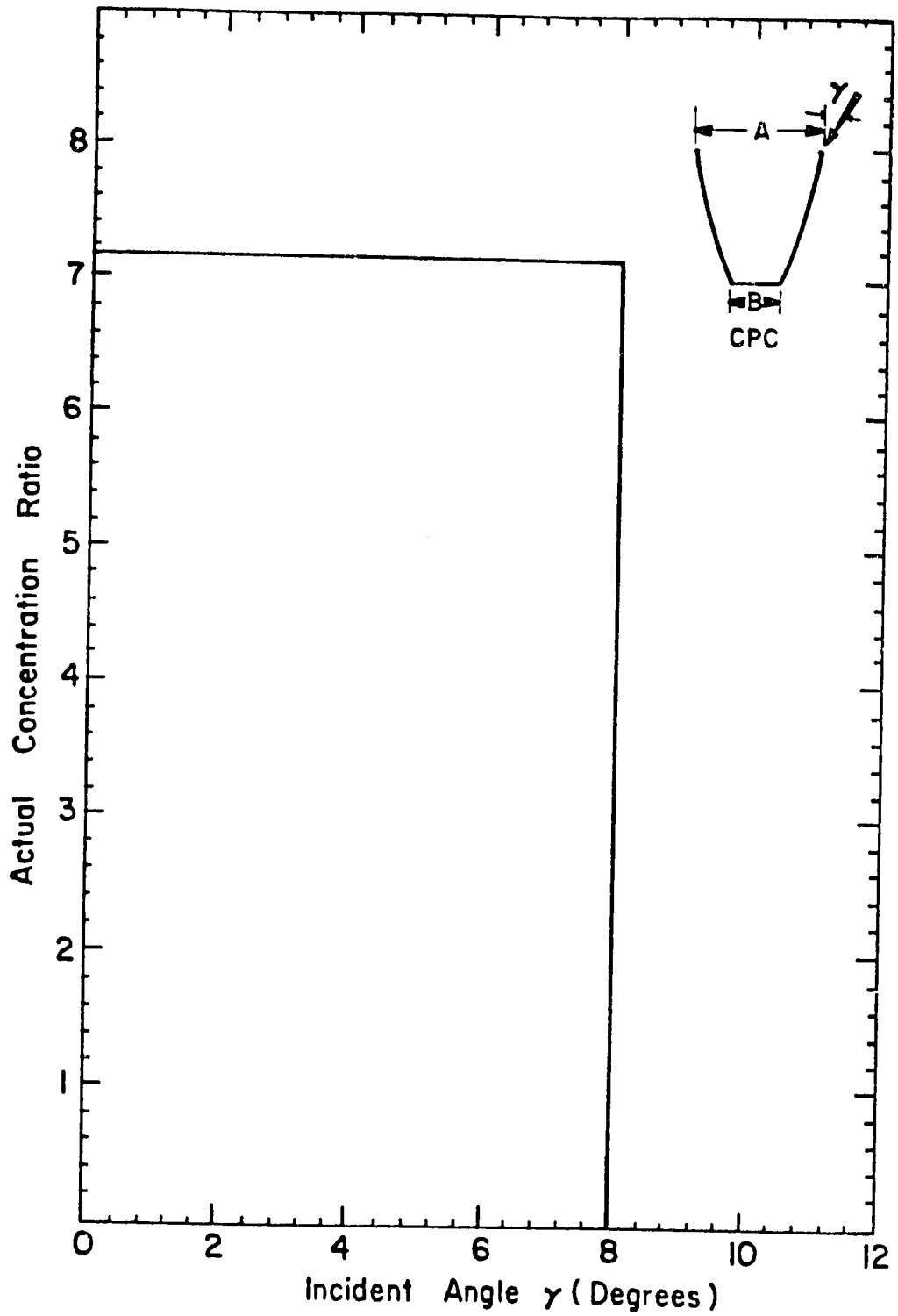


Figure 2-8 Illustration of the Sharp Cut Off Angle of CPC (Perfect Wall)

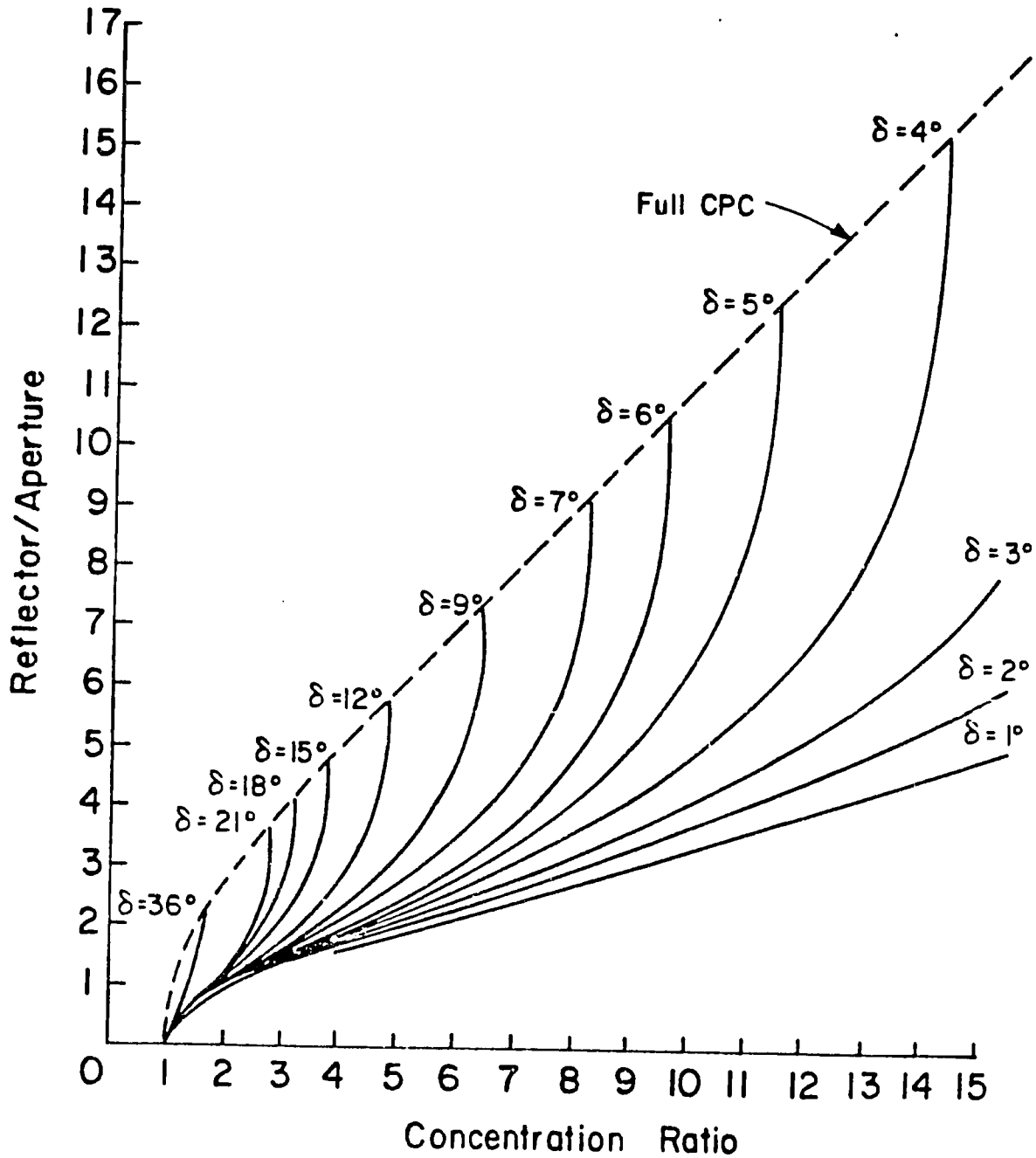


Figure 2-9 Reflector/Aperture Ratio as Function of Concentration Ratio for Full and Truncated CPC

surfaces at the aperture is parallel to the CPC optical axis.

Winston [6] has calculated the concentration ratio as a function of incidence angle for a two-dimensional CPC and it is shown in Fig. 2-8. Furthermore, Winston has demonstrated that the CPC is in fact an ideal concentrator which can achieve the maximum theortical concentration ratio for a given acceptance angle. One major drawback of the CPC is that it has quite precise optical requirements which make it comparatively expensive to manufacture. Less-developed countries such as those in Africa or Southern Asia may not have the necessary resources to mass produce such precise designs. The CPC also requires a relatively large area of reflector per unit of aperture opening. However, as shown in Fig. 2-9, a large portion of the reflector can be removed from the CPC without significantly affecting the performance of the collector. In Fig. 2-9, the reflector to aperture area ratio is plotted as a function of aperture to base area ratio (concentration ratio) with acceptance angle $\delta$ as a parameter. Only the limiting points, labeled full CPC, exhibit the absolute acceptance angle characteristic of Fig. 2-8. As one follows the design curve for a given acceptance angle, one sees a significant decrease in reflector for only a small decrease in concentration ratio. This trend is of course good. A practical design would therefore be near the knee of the curve. The truncated CPC is therefore a more realistic design.

## 2.5 Trapezoidal Groove Concentration

Another type of non-tracking concentrator is the trapezoidal groove collector. It has a trapezoidal geometry in cross section. Flat mir-

rors on either side of the groove redirect insolation to the base receiver. The trapezoidal groove collector can be of one-facet, two-facet, or multi-facet design depending on the optical criteria employed. Unlike the CPC, trapezoidal collectors cannot reach the thermodynamic concentration ratio limit.

Due to the simple configuration of the trapezoidal collectors, they have the benefit of being relatively easy to manufacture at relatively low cost. Such features make trapezoidal collectors especially attractive to countries where labor is cheap and technology less advanced. These countries may not be able to fabricate and maintain sophisticated collectors such as tracking concentrators or the CPC. Trapezoidal collectors thus enable less-developed countries to utilize solar energy by relatively simple means.

Trapezoidal groove collectors also fill in the performance gap between the flat plate collector and the more sophisticated CPC. If the temperature requirement for a specific application is greater than that usually associated with a flat plate collector, then the use of CPC may not be cost effective since CPC is rather expensive. Trapezoidal collectors can be designed to operate in this intermediate temperature range.

## Chapter Three

## Non-Tracking Concentrator Concepts

The use of side mirrors to boost the performance of flat plate solar collectors is an idea that has been around for a long time. In his third attempt at a large scale demonstration at Tacomy, Pennsylvania in 1911, Frank Shuman [7] utilized two plane mirrors attached to the upper and lower edges of a tiltable flat plate array. A concentration ratio of approximately two was achieved. Tilt adjustments were made every three weeks. The maximum instantaneous efficiency of the array was reported to be about 30%.

### 3.1 Design Criteria (one reflection or less)

Previous work [8-11] has been reported on the optical design of non-tracking, but tilt adjusted, trapezoidal solar concentrators. Mannan and Bannerot [11] proposed a "one reflection or less criterion" (i.e., radiation incident within the acceptance angle of the collector will strike the base in one reflection or less). Figure 3-1 illustrates the resulting geometric constraint for the one-facet and two-facet cases. Based on the geometry of Fig. 3-1, it can be shown that for the one-facet case, the geometric concentration ratio,

$$CR = \frac{A}{B} = \frac{\sin(3\alpha + \delta)}{\sin(\alpha + \delta)} \tag{3.1}$$

and the depth to base ratio

$$\frac{D}{B} = \frac{\cos(2\alpha + \delta)\cos\alpha}{\sin(\alpha + \delta)} \tag{3.2}$$

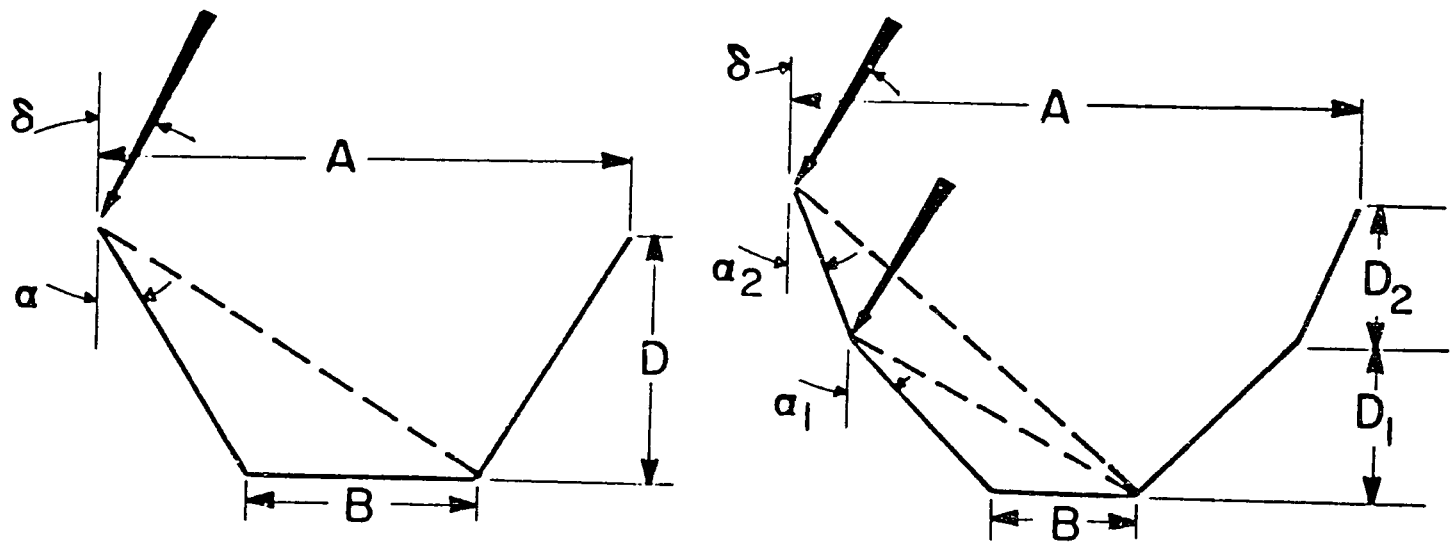


Figure 3-1 Geometric Constraint Imposed by the One Reflection or Less Criterion for Trapezoidal Groove Collector

For the two-facet case

$$CR = \frac{A}{B} = \frac{2 \cos \alpha_1 \sin(2\alpha_1 - \alpha_2 + \delta) \sin(2\alpha_2 + \delta)}{\sin(\alpha_1 + \delta) \sin(\alpha_2 + \delta)} - 1 \tag{3.3}$$

$$\frac{D}{B} = \frac{CR + 1}{2 \tan(2\alpha_2 + \delta)} \tag{3.4}$$

Figures 3-2 and 3-3 are plots generated from eqns. (3.1) and (3.3). Concentration ratio is plotted as a function of the design acceptance angle $\delta$ and wall angle(s) $\alpha$. The maximum concentration ratios shown under the one-reflection or less criterion in the one-facet case is 3 and for the two-facet case is 4.7. These maxima correspond to acceptance angles of $0^\circ$ and $1^\circ$, respectively, and are of course not practical designs. Also the results generated from eqn. (3.1) neglect wall absorption losses and assume perfect specular reflections. Both of these idealizations lead to overly optimistic performance predictions. Furthermore, the non-tracking devices concentrate but do not focus so that one of their advantages is that they do not require high quality optical materials. The perfect wall assumption is not justified.

A more realistic estimate of the grooves' optical performance has been obtained from a ray-trace computer simulation which has been developed as part of this work. It is discussed in the next section.

## 3.2 Computer Simulation

A computer simulation, based on a Monte Carlo [12] or ray-tracing technique, has been developed to estimate the performance of a given design. In the Monte Carlo simulation, the incident solar beam is subdivided into a large number (typically 1000) of energy packets (pho-

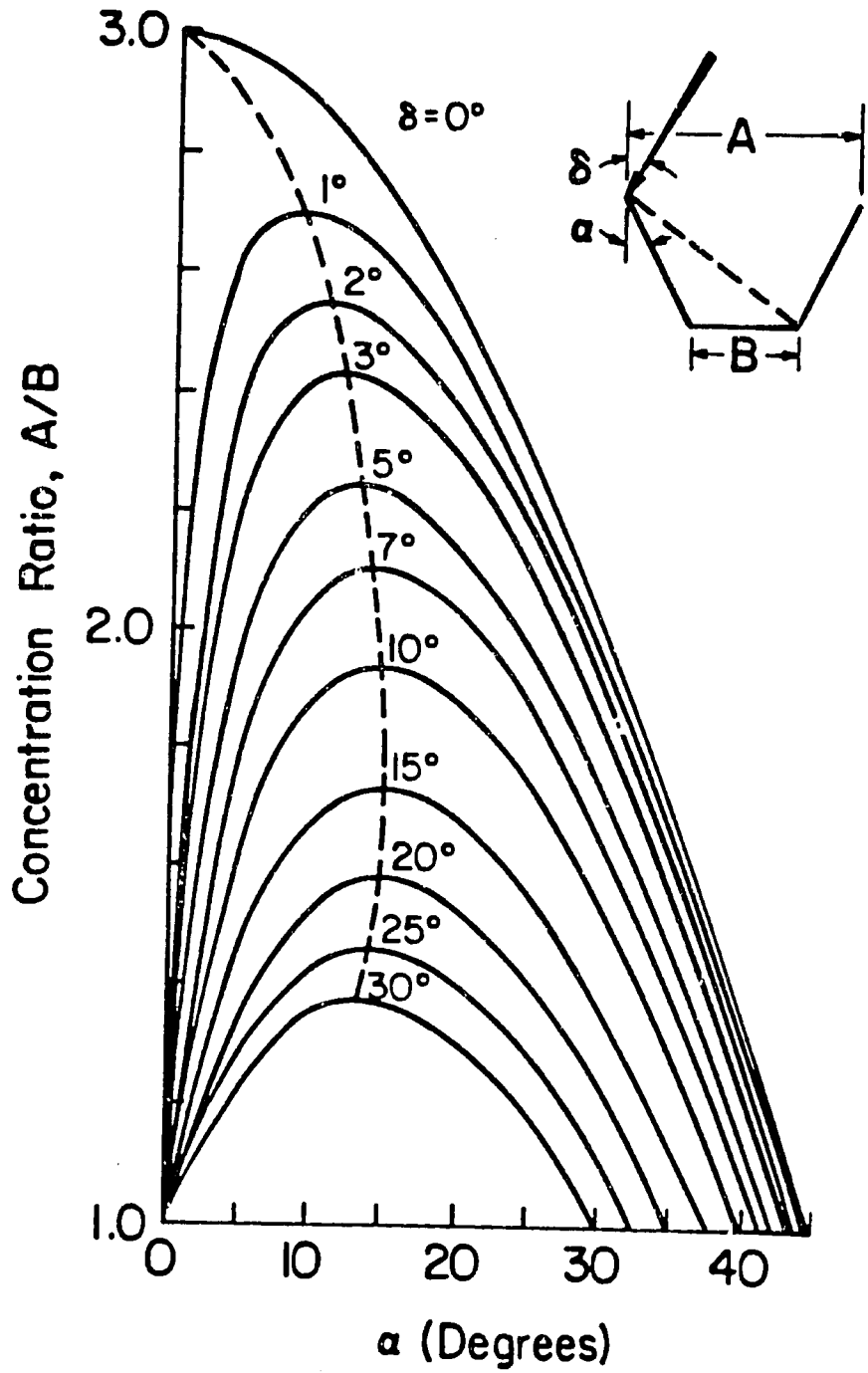


Figure 3-2 Performance of One-Facet Groove Based on One Reflection or less Criterion (Perfect Wall)

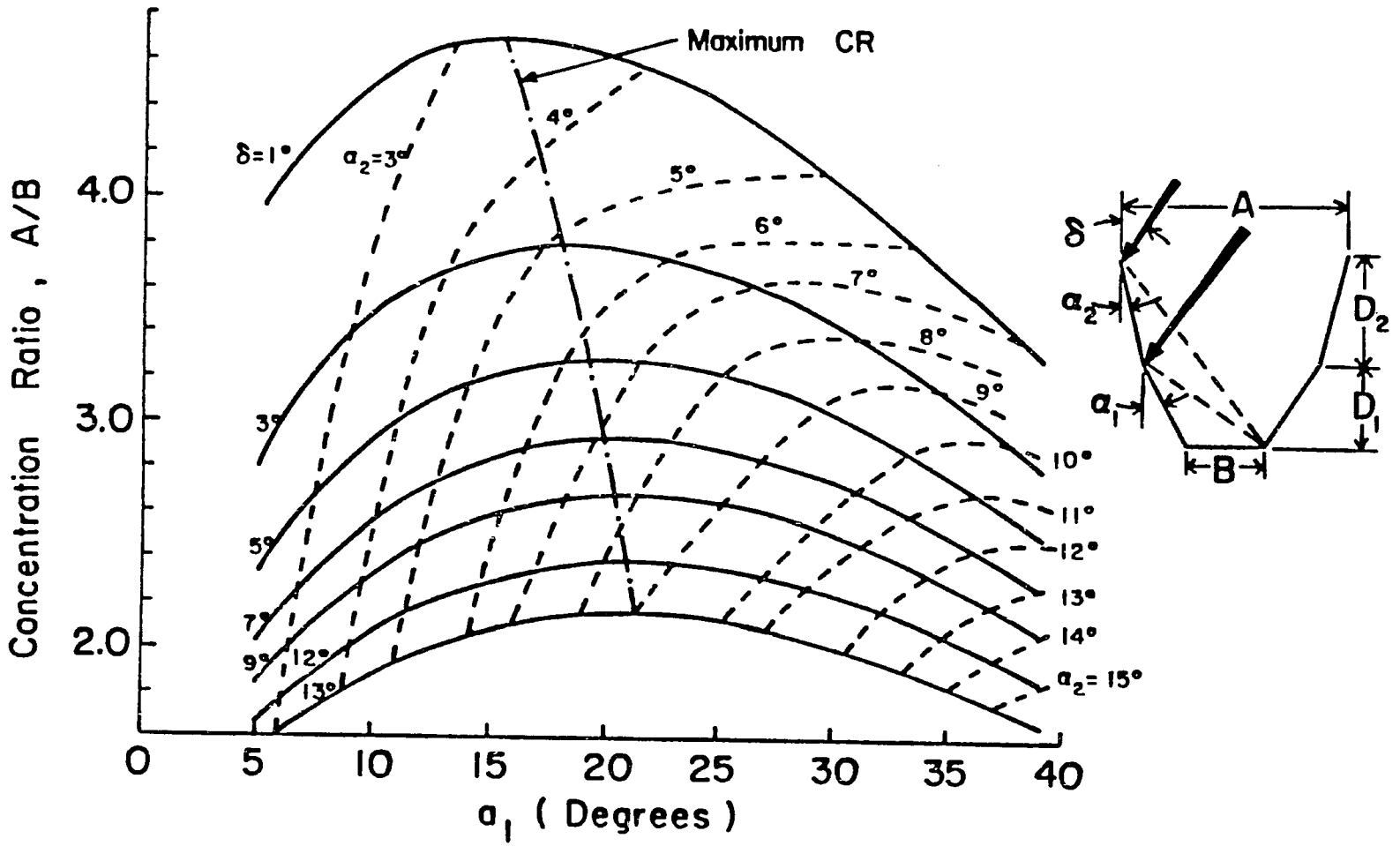


Figure 3-3 Performance of Two-Facet Groove Based on One Reflection or Less Criterion (Perfect Wall)

tons). The individual photons are allowed to interact with the groove. A record is kept on the fate of the individual photons. The aperture of the collector is subdivided into as many small sections as there are photons. Each section is struck by an incident photon. The incident angle of all the photons is set by the assumed incident angle of the solar beam. The program then calculates where the incident photon will strike the collector or the base. Once this is determined, a probabilistic analysis determines whether this particular photon is absorbed or reflected away by the reflector. If the photon is reflected, another analysis determines what type of reflection, specular or diffuse, takes place. All the probabilistic decisions are based on the surface properties of the reflectors that are part of the simulation input. After determining the type of reflection, the program calculates the angle of reflection and where the photon strikes next. The process is continued until the photon is either absorbed at the base or the wall, or reflected out of the groove. The whole procedure is repeated over and over until all the photons that strike the aperture have been accounted for. Details of the simulation can be found in Appendix A.

The result of all these computations for a given incident angle is a tally sheet that indicates where each of the photons was finally absorbed on the base or reflector or lost back through the aperture. This information is then used to determine the fraction of the incident photons (the fraction of the incident beam) that actually is absorbed at the base. This fraction is the "transmittance" of the groove. Therefore, for a given incident angle for the solar beam and for a given groove (geometry and radiative properties), the groove's radiative per-

formance can be determined.

### 3.3 Results for the One-Reflection or Less Criterion

The performance of a two-facet trapezoidal collector determined from the ray-tracing simulation is shown in Fig. 3-4. The collector geometry was determined from the one reflection or less criterion for a design acceptance angle, $\delta$, equal to $5^\circ$. The walls are perfectly reflecting. Thus the wall solar absorptivity is 0 (i.e., $\alpha_{sw} = 0$) and all reflections are specular (i.e., the specularity function f, defined as the fraction of total reflections that are specular, = 1). It can be seen that the groove is able to collect radiation incident at angles greater than the design acceptance angle. This is because some rays outside the design acceptance angle of the collector can still reach the base after multiple reflections. The incident angle at which the actual concentration ratio of the collector begins to decrease is called the actual acceptance angle of the collector, $\delta_a$. A performance evaluation based on the design acceptance angle is overly conservative. Conversely, a higher concentration ratio could have been achieved in practice for the same actual acceptance angle.

Previously, improved performance (higher concentration ratios) have been sought by increasing the number of wall facets, while imposing a one reflection or less criterion [13]. This approach now appears to be unfruitful. A better approach may be to use the results of Hollands [4]. By methods of images he demonstrated that the concentration ratio for a trapezoidal collector is proportional to the number of reflections that take place before the ray strikes the base.

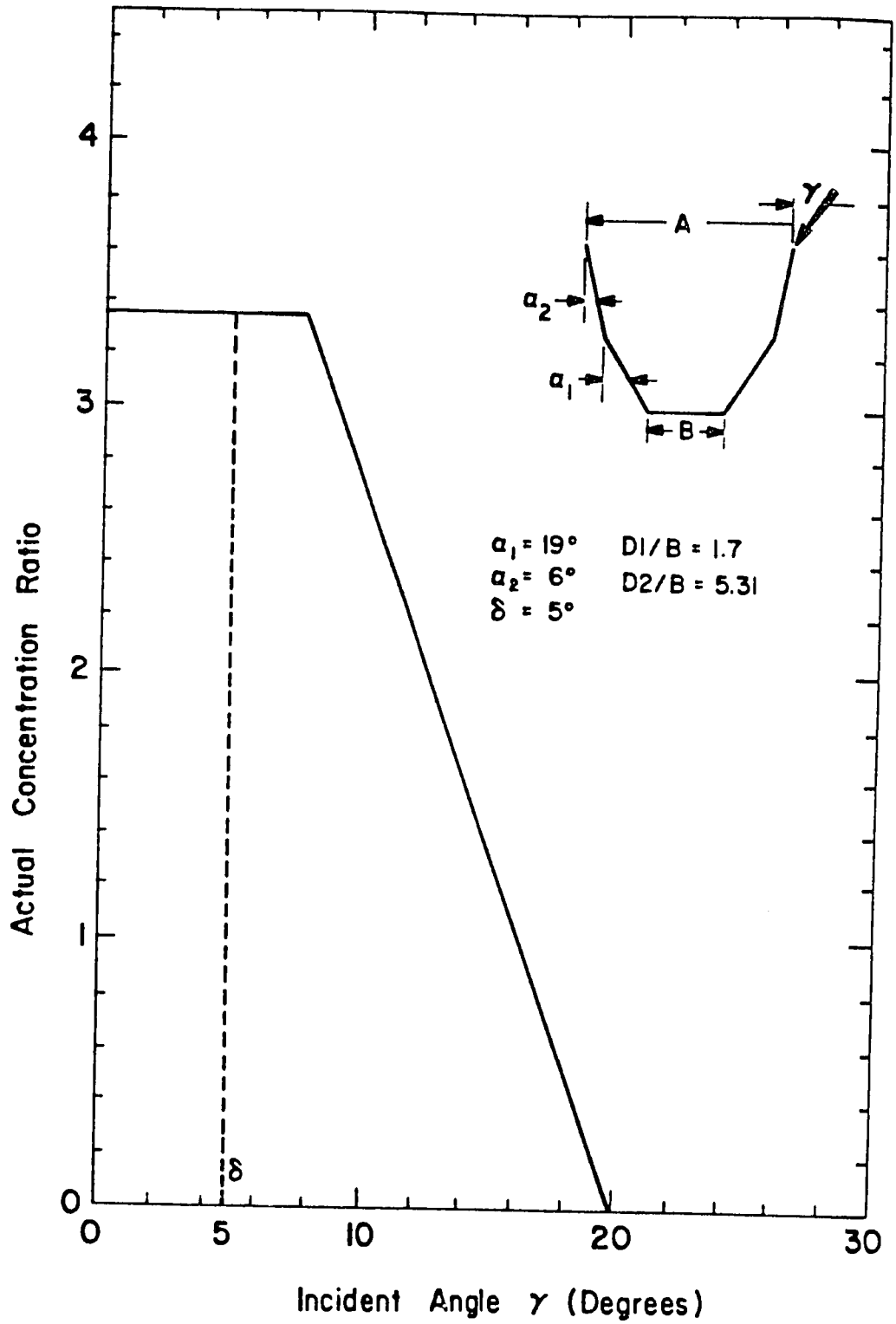


Figure 3-4 Effect of Incident Angle on the Performance of a Given One Reflection or Less Design (Perfect Wall)

By examinating the performance of many designs, it has been concluded that the number of wall facets plays a surprisingly minor role in determining the achievable concentration ratio. For example, for a given actual acceptance angle and with perfect walls, a one-facet design based on a criterion which allows several reflections can exhibit a higher geometric concentration ratio than a two-facet design based on the one reflection or less criterion. Thus a large number of reflections theoretically will result in higher geometric concentration ratios, but in practice, when the number of reflections becomes greater than about two, optical losses and wall absorption will outweigh the gain in geometric concentration ratio. The next logical step in the development of trapezoidal groove geometries is to incorporate a two reflections or less criterion into the design process.

### 3.4 The Two Reflection or Less Criterion

A two reflections or less criterion (i.e., radiation incident within the acceptance angle of the collector will strike the base in two reflections or less) has been used to develop a new set of trapezoidal designs. Figure 3-5 illustrates the resulting geometric constraint for the two-facet case. The ray striking the top of the upper reflector is constrained to reflect to the junction of the two facets on the opposite side and then to the opposite corner of the base as shown. The design criterion does not place any restriction on how the rays that directly strike the lower wall are reflected. The reason is that the geometry of the collector has already been defined by the constraints placed on the extreme ray that strikes the upper wall. An additional constraint would

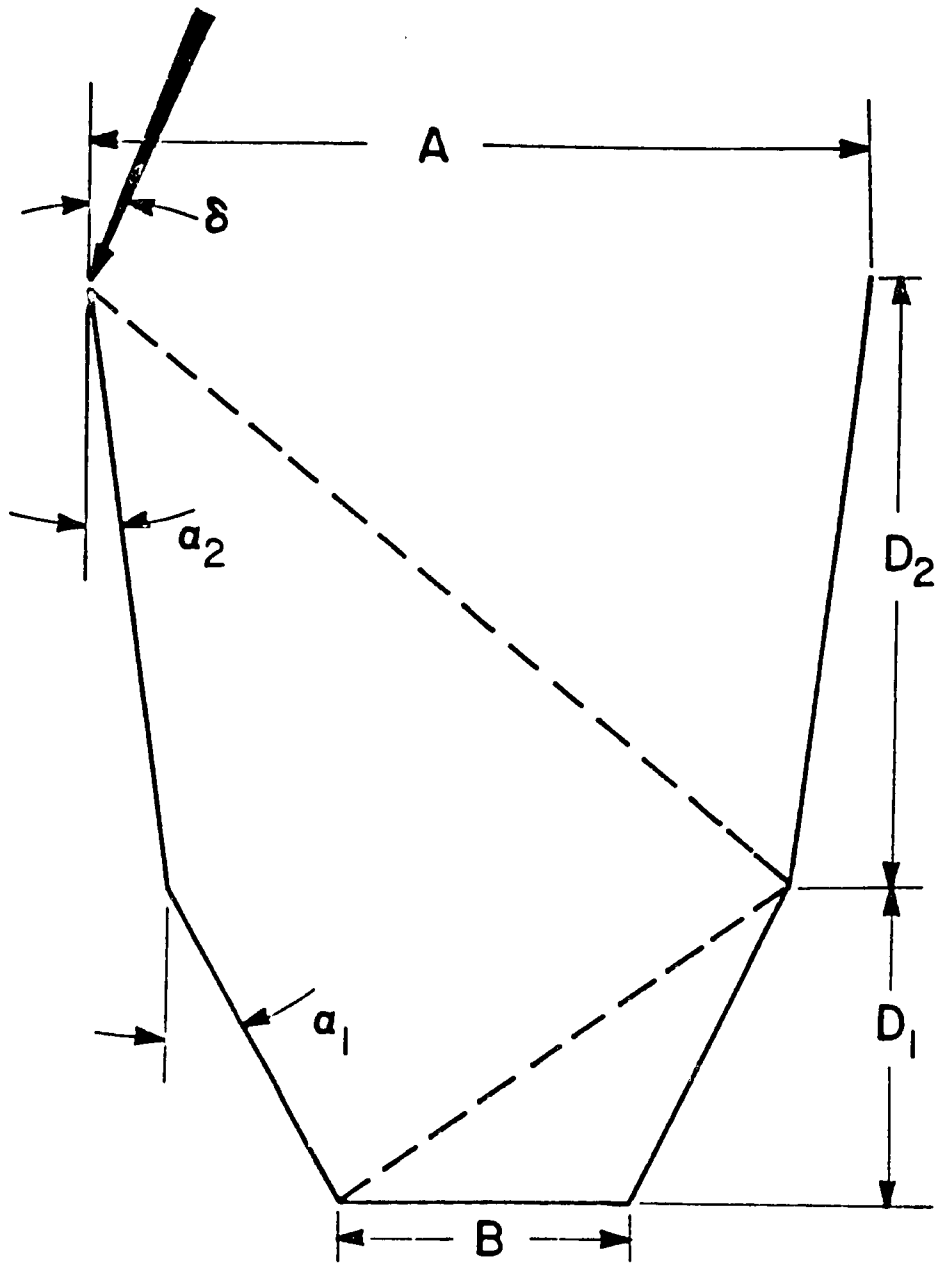


Figure 3-5 Geometric Constraints Imposed by the Two Reflection or Less Criterion for a Two-Facet Groove

over determined the system. It turns out that the rays striking the lower wall directly are reflected to the base anyway. From Fig. 3-5, it can be shown that the concentration ratio for a trapezoidal collector with a two-facet wall is

$$CR = \frac{\sin(3\alpha_1 + 2\alpha_2 + \delta)\ \sin(\delta + 3\alpha_2)}{\sin(\delta + 2\alpha_2 + \alpha_1)\ \sin(\delta + \alpha_2)} \tag{3.5}$$

and the depth to base ratio

$$\frac{D}{B} = \frac{D_1 + D_2}{B} \tag{3.6}$$

where

$$\frac{D_1}{B} = \frac{\cos(\delta + 2\alpha_2 + \alpha_1)\ \cos\alpha_1}{\sin(\delta + 2\alpha_2 + \alpha_1)} \tag{3.7}$$

$$\frac{D_2}{B} = \frac{\sin(3\alpha_1 + 2\alpha_2 + \delta)\ \cos(\delta + 2\alpha_2)\ \cos\alpha_2}{\sin(\delta + \alpha_2)\ \sin(\delta + 2\alpha_2 + \alpha_1)} \tag{3.8}$$

The conditions for maximum concentration can be obtained by differentiating the concentration ratio with respect to the wall angles $\alpha_1$ and $\alpha_2$ and requiring that both

$$\left(\frac{\delta\ CR}{\delta\ \alpha_1}\right)_{\alpha_2, \delta} = 0 \tag{3.9}$$

and

$$\left(\frac{\delta\ CR}{\delta\ \alpha_2}\right)_{\alpha_1, \delta} = 0 \tag{3.10}$$

be satisfied. The two transcendental equations below result, and, for a given $\delta$, they must be solved simultaneously for $\alpha_1$ and $\alpha_2$

$$\sin(2\delta + 4\alpha_1 + 4\alpha_2) = 2 \sin (2\alpha_1) \tag{3.11}$$

and

$$\begin{aligned} 2 \sin(\delta + \alpha_2) \sin(\delta + 3\delta_2) \sin(2\alpha_1) &= \sin(\delta + 2\alpha_2 + \alpha_1) \\ \sin(3\alpha_1 + 2\alpha_2 + \delta) \left(\sin(2\delta + 4\alpha_2) - 2 \sin(2\alpha_2)\right) \end{aligned} \tag{3.12}$$

The remainder of the geometry can be specified from values of $\alpha_1$, $\alpha_2$, and $\delta$ (eqns. 3.5 - 3.8). The one-facet case is simply a special case where $\alpha_1$ equals $\alpha_2$ in the above equations. It can be seen that eqns. (3.11) and (3.12) are quite complex. An explicit analytical solution for $\alpha_1$ and $\alpha_2$ was not possible. The desired solutions were found by inspecting Fig. 3-6 and 3-7 which were generated by eqn. (3.5). Concentration ratio is plotted as a function of wall angle(s) and acceptance angle for the one and two facet designs for the two reflections or less criterion. Comparing the above results with those obtained by the one reflection or less criterion, Fig. 3-2 and 3-3, a marked increase in performance is observed. The improvement in performance is more profound for the one-facet case. For example, the maximum geometric con-

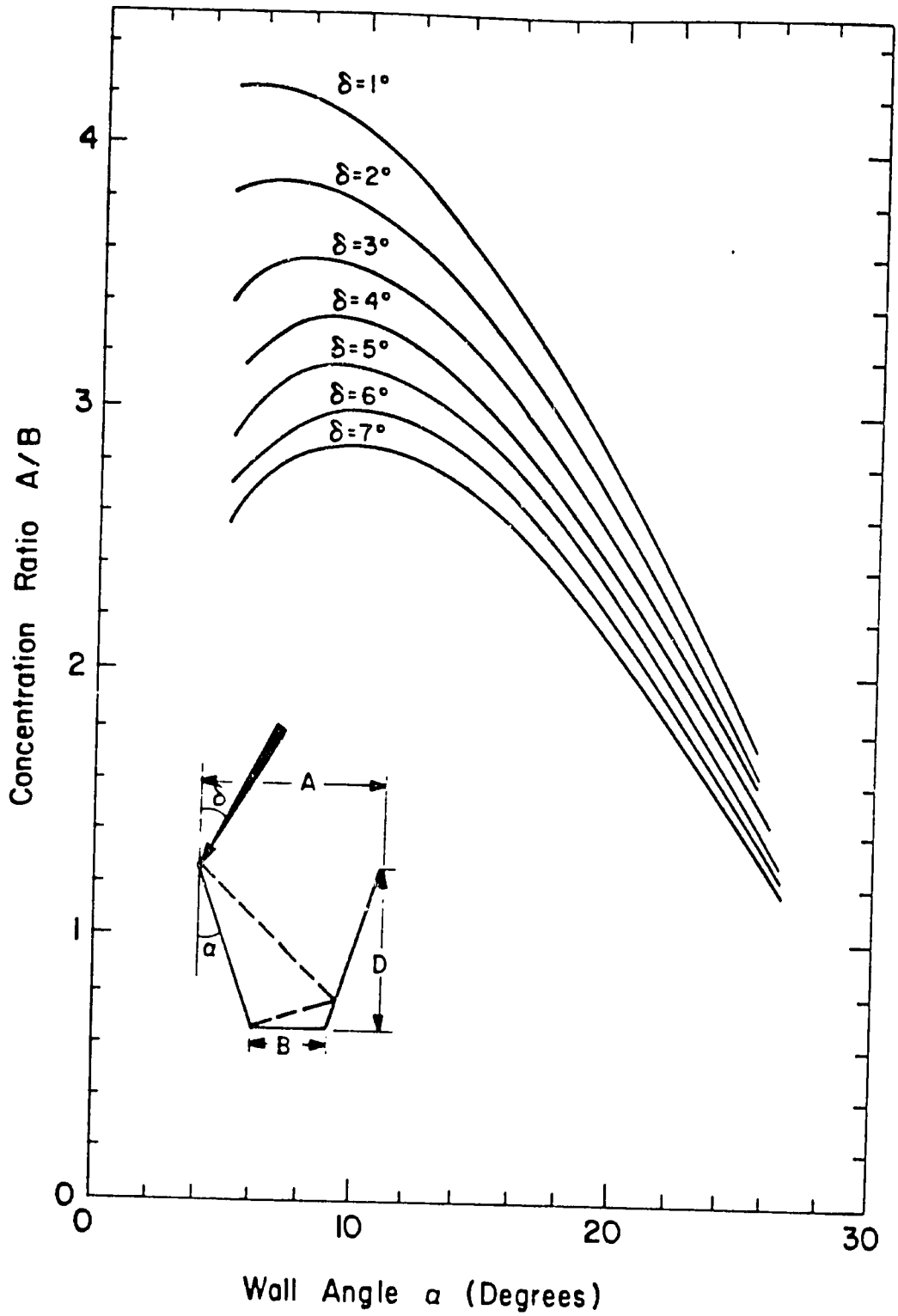


Figure 3-6 Performance of the One-Facet Groove Based on a Two Reflection or Less Criterion (Perfect Wall)

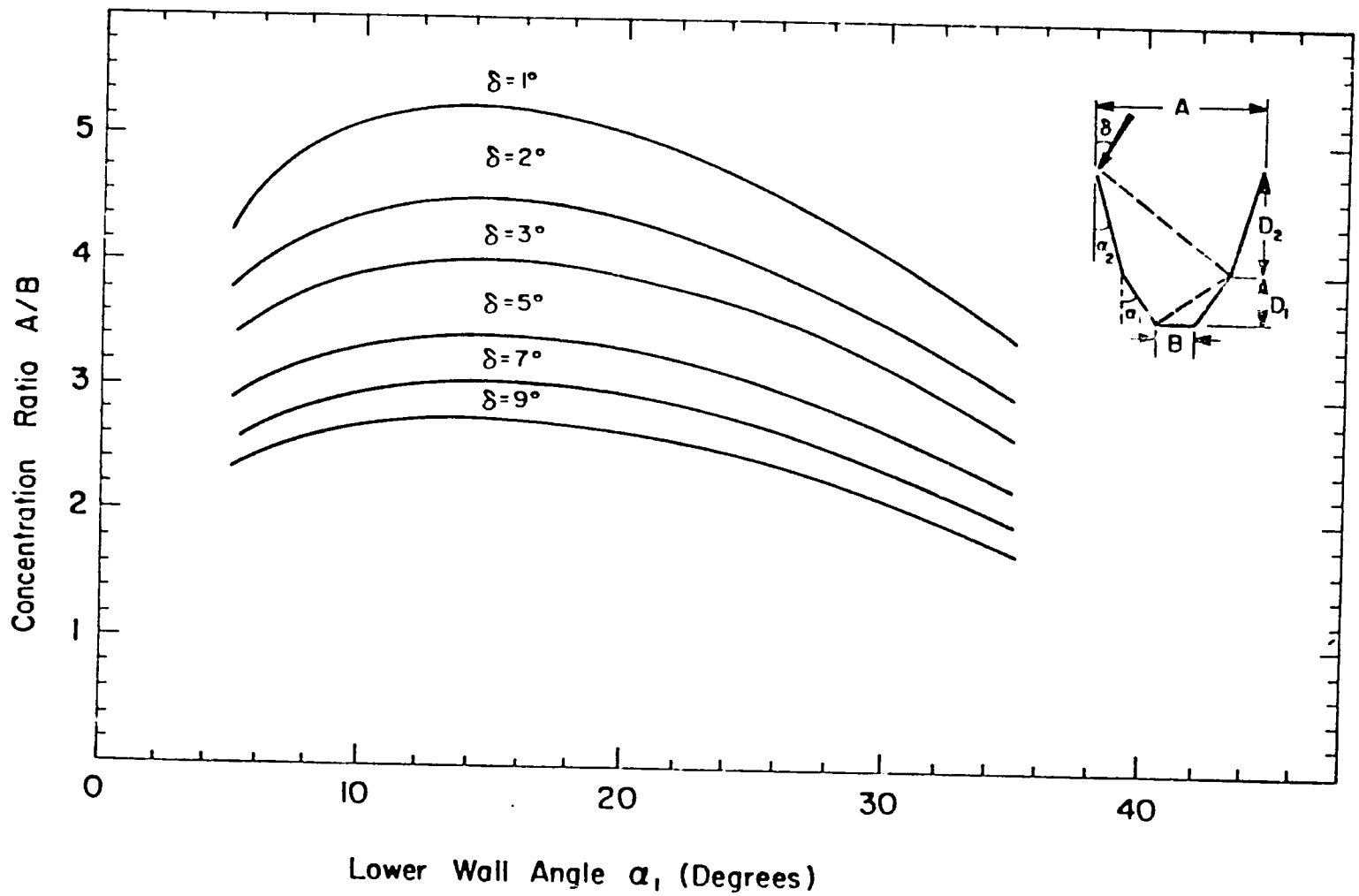


Figure 3-7 Performance of the Two-Facet Groove Based on a Two Reflection or Less Criterion (Perfect Wall)

centration ratio attainable by a collector with acceptance angle of 5 degrees is 2.33 and 3.15 for the one reflection and two reflection or less criterion, respectively. This represents a forty percent increase in concentration ratio.

### 3.5 Performance Characteristic

Selected geometries defined by the two reflection or less criterion were used to define designs for which the ray-trace simulation generated performance curves. Figure 3-8 is typical of the performance curves obtained for the one-facet designs with perfect reflectors (no absorption by the reflectors, all specular reflections). The actual concentration ratio is plotted as a function of incident angle and the wall angle. For small wall angles, the actual acceptance angle (the largest incident angle for which all incident radiation reaches the base) is significantly greater than the design acceptance angle and decreases as shown. Figures B-1 to B-4 in Appendix B are the performance curves obtained from the simulation of a wide range of collector geometries. In these simulations the walls of the collectors were assumed to be perfect. The actual concentration ratio remained constant (at the geometric concentration ratio for perfect walls) as the incident angle increased from zero to the design acceptance angle. At some point at or beyond the design acceptance angle performance began to degrade gradually. This behavior is contrasted with that of the compound parabolic concentrator CPC [6] shown in Fig. 2-8 where for the untruncated design, the design and acceptance angle coincide. The cutoff is sharp; no incident radiation outside the design acceptance angle reaches the

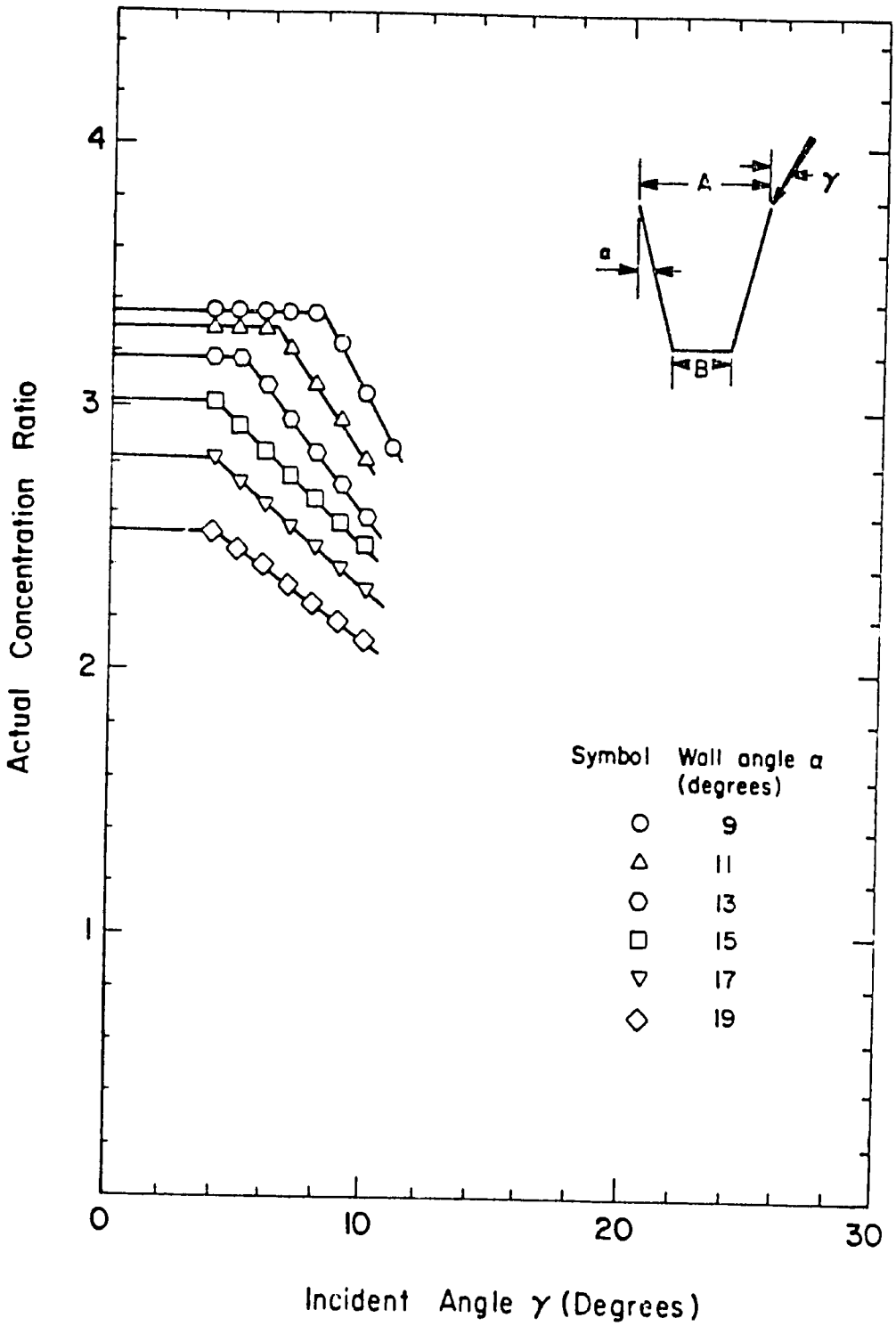


Figure 3-8 Effect of Incident Angle on the Performance of a Given Two Reflection or Less Design (Perfect Wall)

receiver. Truncation of the CPC results in a less sharply defined acceptance angle. The top and bottom corners of the curve in Fig. 2-8 become more and more rounded as one proceeds down the design curve (Fig. 2-9). In other words, the performance approaches that exhibited by the trapezoidal designs.

# Chapter Four

# Performance

## 4.1 90% Actual Acceptance Angle Criterion

In attempting to compare the radiative performance of the trapezoidal collector and the CPC it is clear that a comparison (with perfect walls) based on a definition of acceptance angle for which all incident energy must reach the receiver (the base) would not be fair to the trapezoidal design since it would disregard a large portion of the collectable energy. Conversely, a definition based on the largest incident angle for which any radiation reaches the receiver would favor the trapezoidal design.

To help establish a basis for a fair comparison, the following definition is made: the angle of incidence at which the actual concentration ratio of the collector is equal to 90% of the concentration ratio at zero incident angle is defined as the 90% actual acceptance angle $\delta_A*$. For smaller incident angles the actual concentration ratio would be greater and in fact equal to the geometric concentration ratio (for perfect walls) for most values $\gamma < \delta_A*$. For example, the design acceptance angle for the geometry utilized in Fig. 4-1 is $3^\circ$; the actual acceptance angle is $7^\circ$ and the 90% actual acceptance angle is $9^\circ$. This 90% actual acceptance angle will now be used as the basis for comparing the performance of the trapezoidal groove and the CPC.

## 4.2 Design Comparison with Perfect Walls

The relationship between actual concentration ratio and the incident angle has been examined for many geometries developed from the two

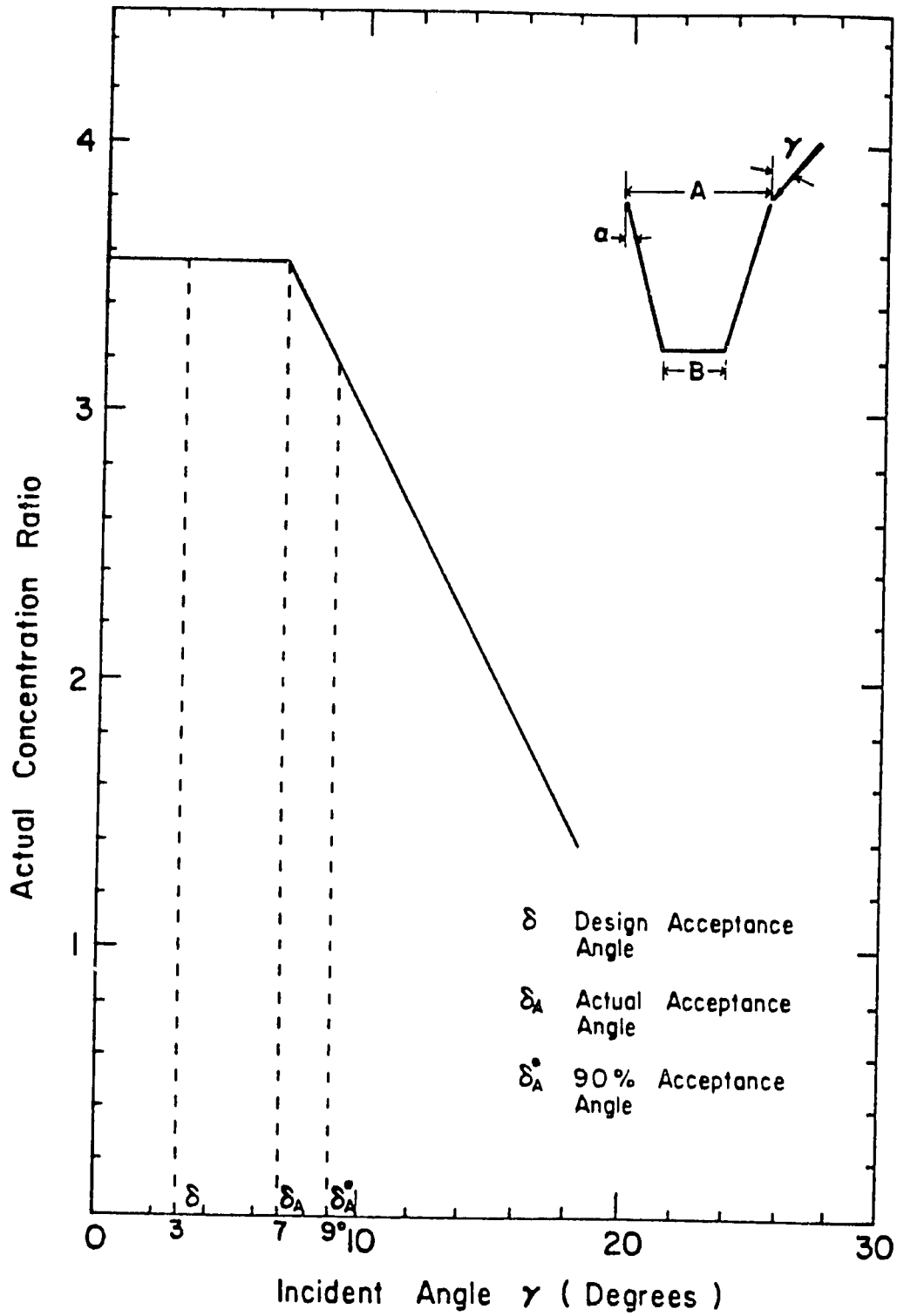


Figure 4-1 Illustration of the Design, Actual and 90% Acceptance Angle

reflection or less criterion. Usually 6 to 8 simulations at different incident angles were required for each geometry. From results like Fig. 4-1 the 90% actual acceptance angle was determined for each configuration. The designs with similar 90% actual acceptance angles were grouped and plotted.

The first significant conclusion is illustrated in Fig. 4-2. The total reflector to aperture ratio, R/A, is plotted against the geometric concentration ratio, A/B, for a 90% actual acceptance angle of 9° for both the one-facet and two-facet designs. Each point represents a different geometry. Generally, the best designs would have the highest concentration ratio for a given amount of reflector material or conversely the least amount of reflector material for a given concentration ratio. The modest scatter in the data is due to a lack of precision in grouping the results to a specific 90% actual acceptance angle. The points actually correspond to a specified angle (9° in Fig. 4-2) plus 0.5°, minus 0° (between 9° and 9.5° in Fig. 4-2). The line drawn through the limiting points on the right should be interpreted as the results for the stated value of the 90% actual acceptance angle. A line (not shown) through the limiting points on the left would correspond to design with a 90% actual acceptance angle 0.5° greater.

It is seen that the two-facet geometries enjoy only a slight performance advantage over the one-facet geometry for this acceptance angle. In fact comparisons at all acceptance angles studied from 3° to 12° demonstrated the same results. Based on this marginal performance advantage and on the increased complexity of the construction, the two-facet geometry seems an unlikely design choice. Therefore discussion

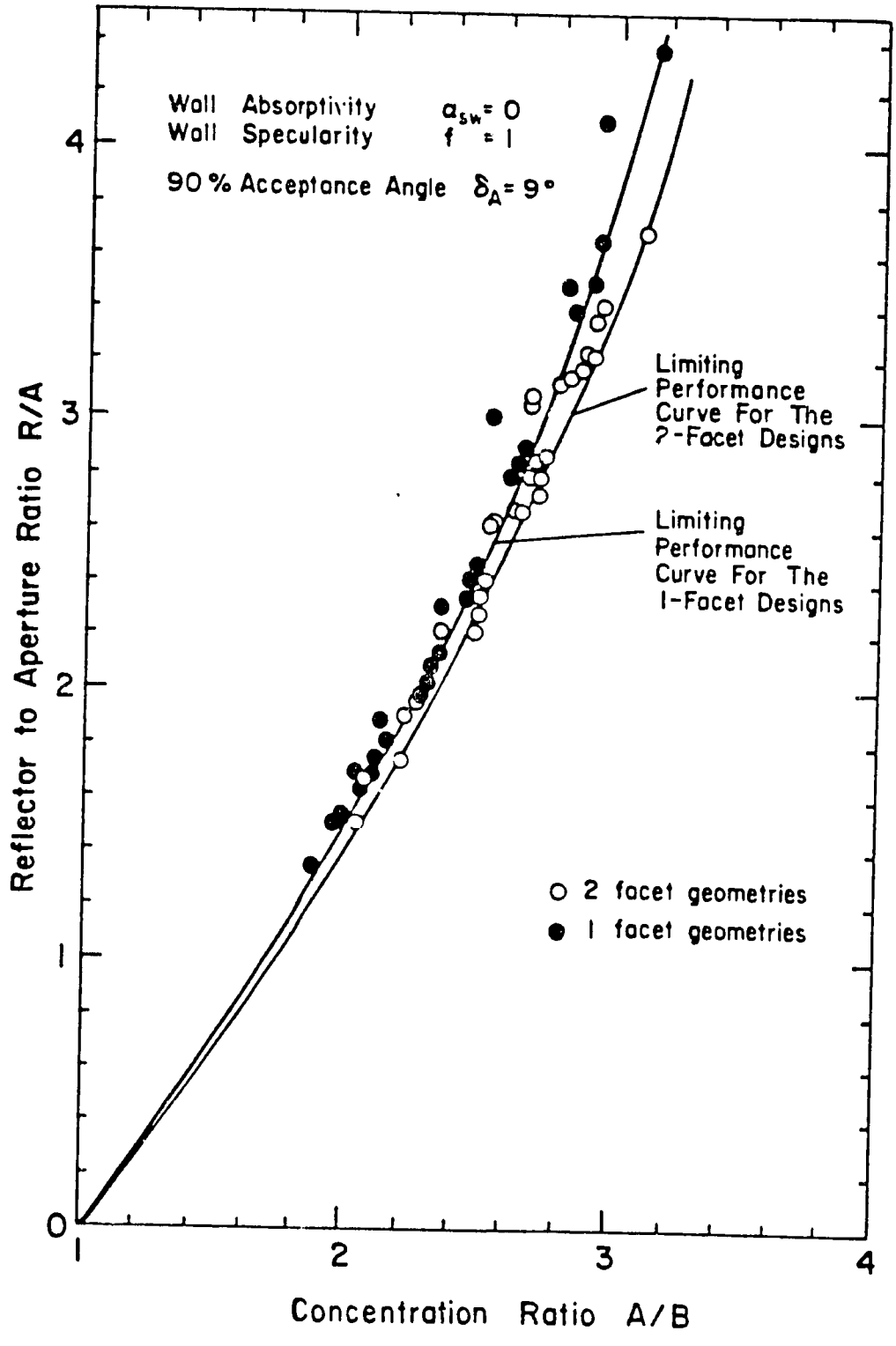


Figure 4-2 Comparison of the Performance of One- and Two-Facet Design Based on a Two Reflection or Less Criterion (Perfect Wall)

will be limited to the one-facet geometry for the remainder of this thesis.

Figures 4-3 through 4-5 are a summary of results for the one-facet designs for perfect walls. Each figure presents three curves: 1) designs based on the design acceptance angle (directly from Fig. 3-6), 2) designs based on the 90% actual acceptance angle (from curves like Fig. 4-1) and 3) the compound parabolic design (Fig. 2-9). The new interpretation of the collector "acceptance angle" results in a revised set of design options for the trapezoidal configuration which will result in improved performance, at least at the higher concentration ratios. However, the improvement leaves the trapezoidal designs still far short of the CPC performance.

The information in Figs. 4-3 to 4-5 together with the constraints of geometry allows one to establish the geometries of the optimal designs. For example, for a 90% actual acceptance angle of $7^\circ$ and a concentration ratio of 3, the minimum R/A is 3.12 (from Fig. 4-3). For the one-facet design, the wall angle

$$\alpha = \sin^{-1}\left(\frac{(A - B)/2}{R/2}\right)$$

$$= \sin^{-1}\left(\frac{A}{R}\left(\frac{CR - 1}{CR}\right)\right)$$

$$= \sin^{-1}\left(\frac{1}{3.12}\left(\frac{2}{3}\right)\right)$$

$$= \sin^{-1}(0.2137) = 12.34^\circ$$

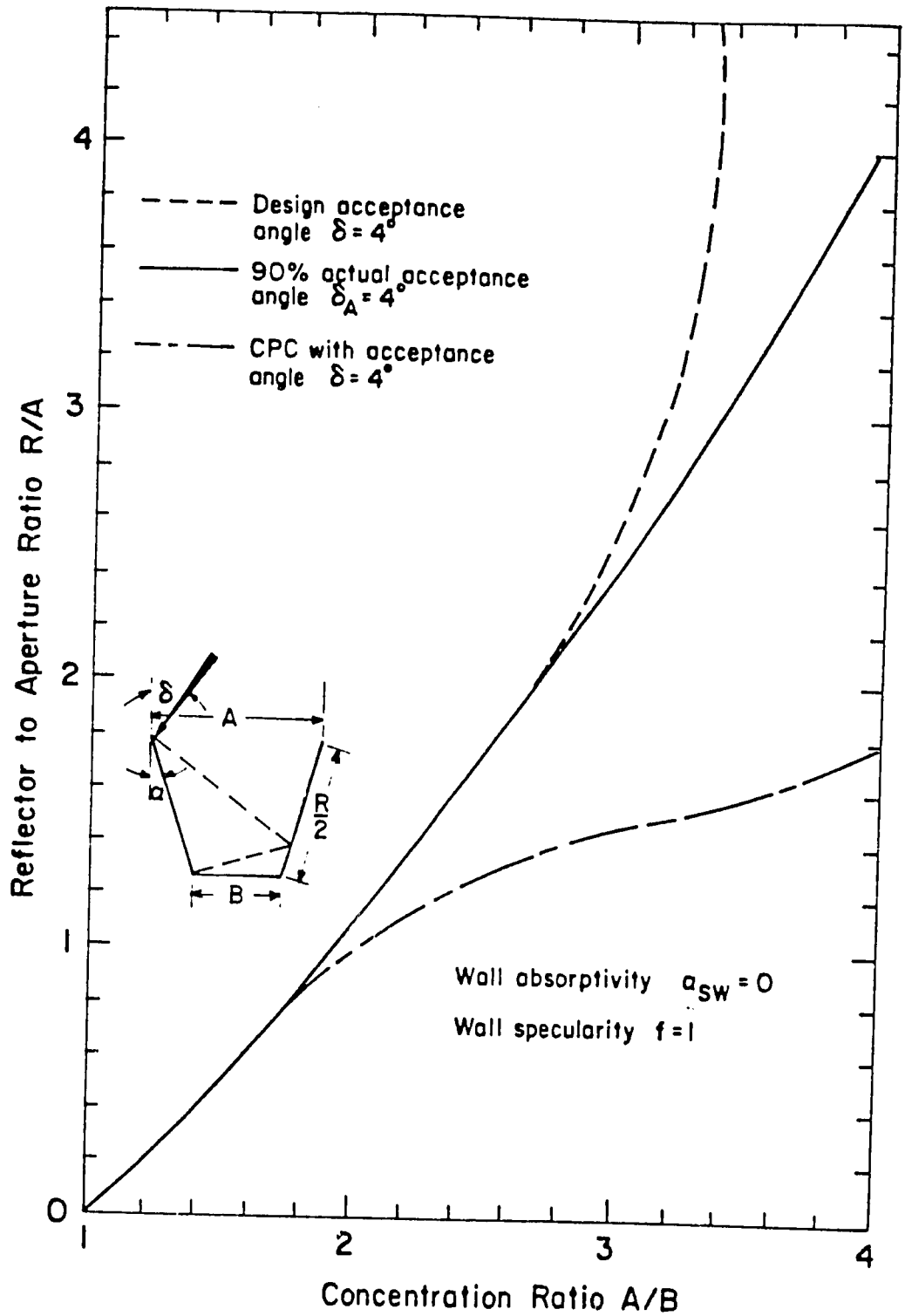


Figure 4-3 Performance Comparison Among Design Based on Design Acceptance Angle, 90% Actual Acceptance Angle and CPC with Acceptance Angle of 4°

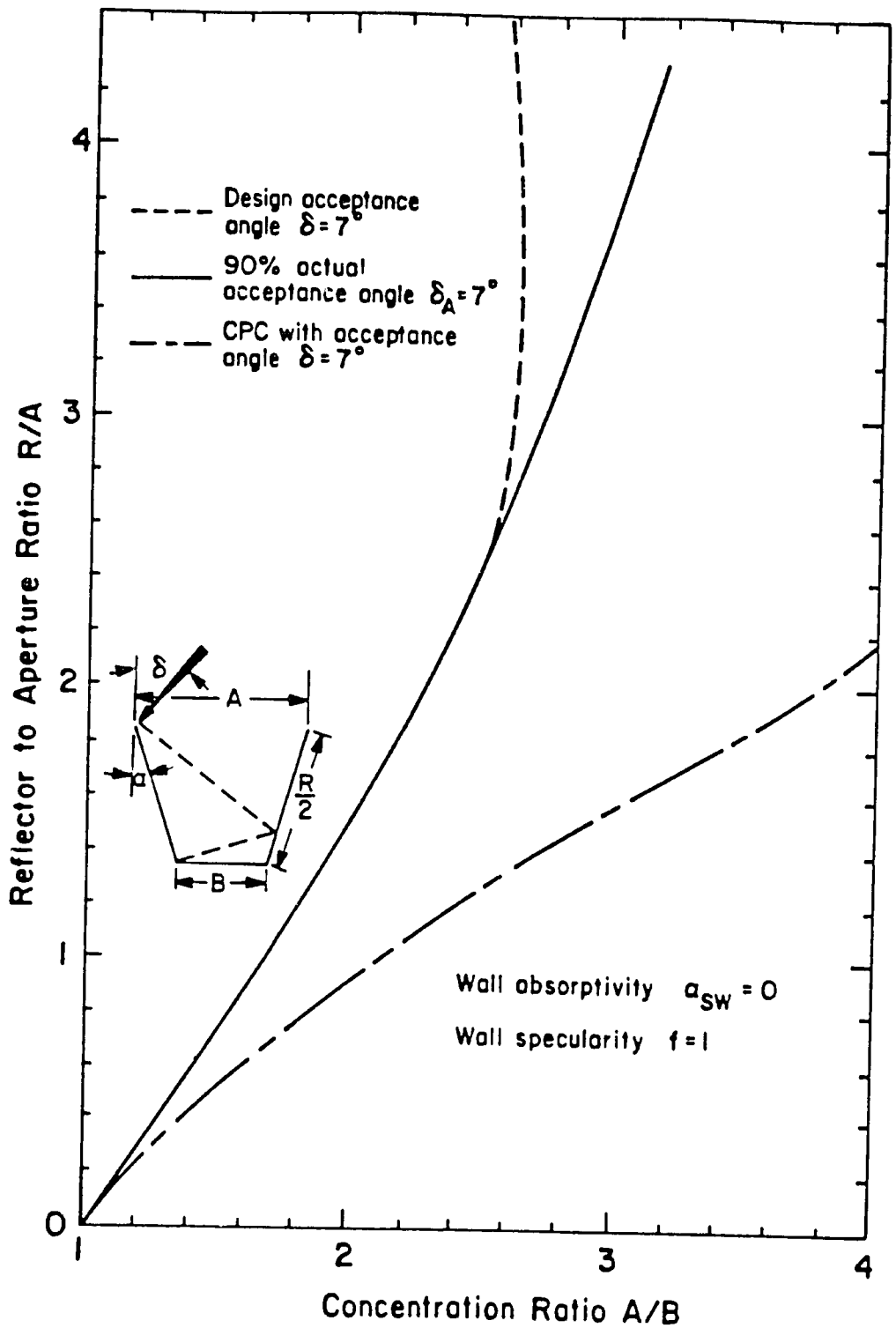


Figure 4-4 Performance Comparison Among Designs Based on Design Acceptance Angle, 90% Actual Acceptance Angle and CPC with Acceptance Angle of 7°

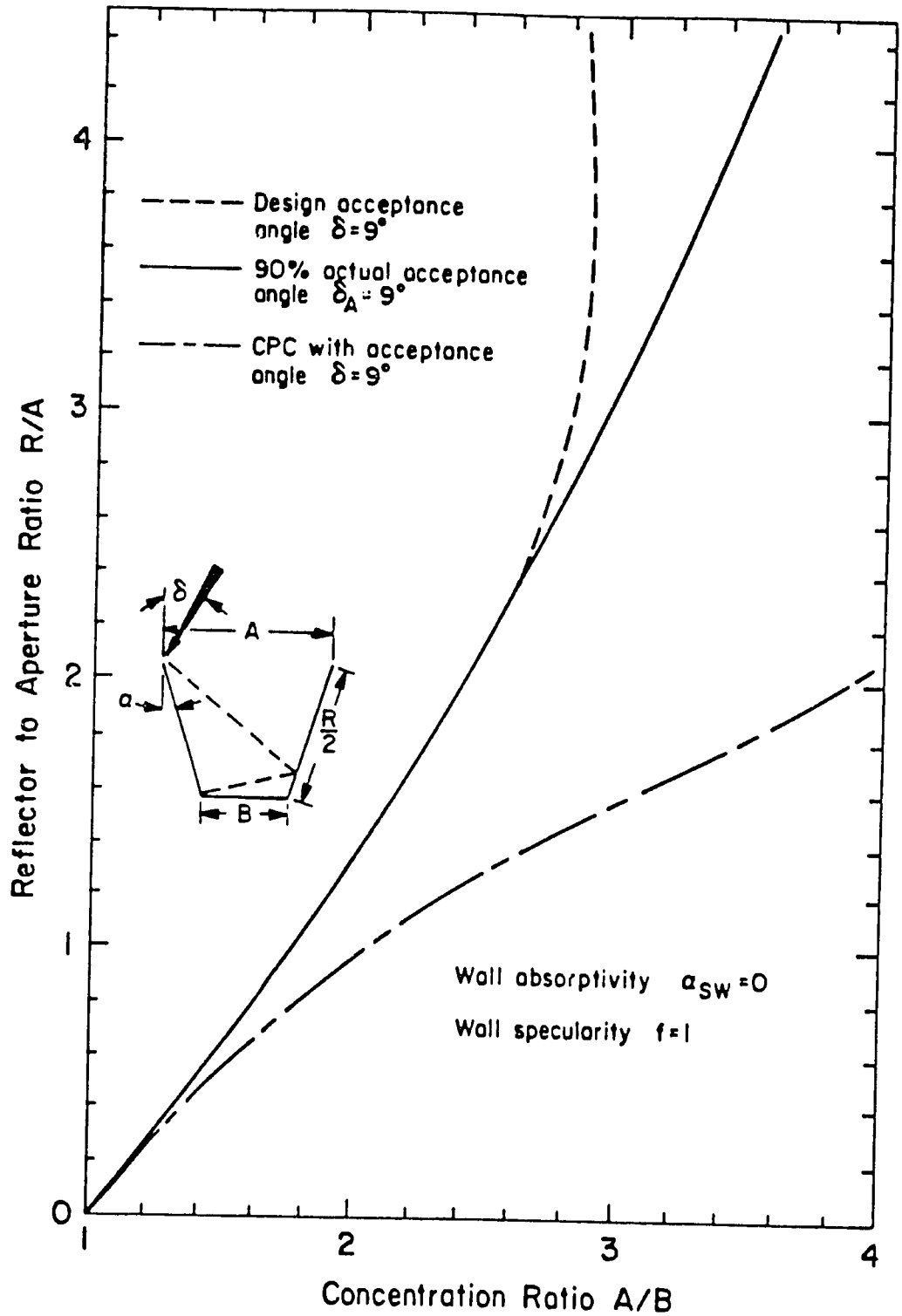


Figure 4-5 Performance Comparison Among Designs Based on Design Acceptance Angle, 90% Actual Acceptance Angle and CPC with Acceptance Angle of 9°

$$\frac{R}{B} = \left(\frac{R}{A}\right)\left(\frac{A}{B}\right)$$

$$= \left(\frac{R}{A}\right)^{CR}$$

$$= 9.36$$

$$\frac{D}{B} = \left(\frac{R}{2B}\right)^{\cos\alpha}$$

$$= 4.572$$

## 4.3 Design Comparison with Imperfect Walls

As mentioned before, the above results were obtained by assuming optically perfect walls. Figures 4-6 and 4-7 present results for 90% actual acceptance angles of $7^{c}$ and $9^{\circ}$ with more realistic walls.[1] The effects of real walls on the performance of the groove were approximated in the computer simulation by using a two parameter model of the actual wall performance. As previously mentioned the parameters were the wall absorptivity and the specularity factor. The specularity factor can range from 0 (diffuse reflections) to 1 (mirror like or specular reflections). The three curves in each figure represent performance for 1) ideal walls, $\alpha_{sw} = 0$ and $f = 1$, 2) walls with $\alpha_{sw} = 0.1$ and $f = 0.9$, and 3) walls with $\alpha_{sw} = 0.2$ and $f = 0.8$. The last case was considered to be the poorest wall quality acceptable for this application. These same results are tabulated in Table 4.1 and the percent decrease in actual concentration ratio is also noted. It can be seen that collectors with high concentration ratios suffer a greater loss in performance with wall imperfections. This is expected because the total number of reflections that are needed for all the rays that strike the aperture to reach the

---

[1] A $9^{\circ}$ acceptance angle will allow up to eight hours of operation on the solstices when the sun's north-south "swing" attains its maximum amplitude. This point is discussed further in the next chapter.

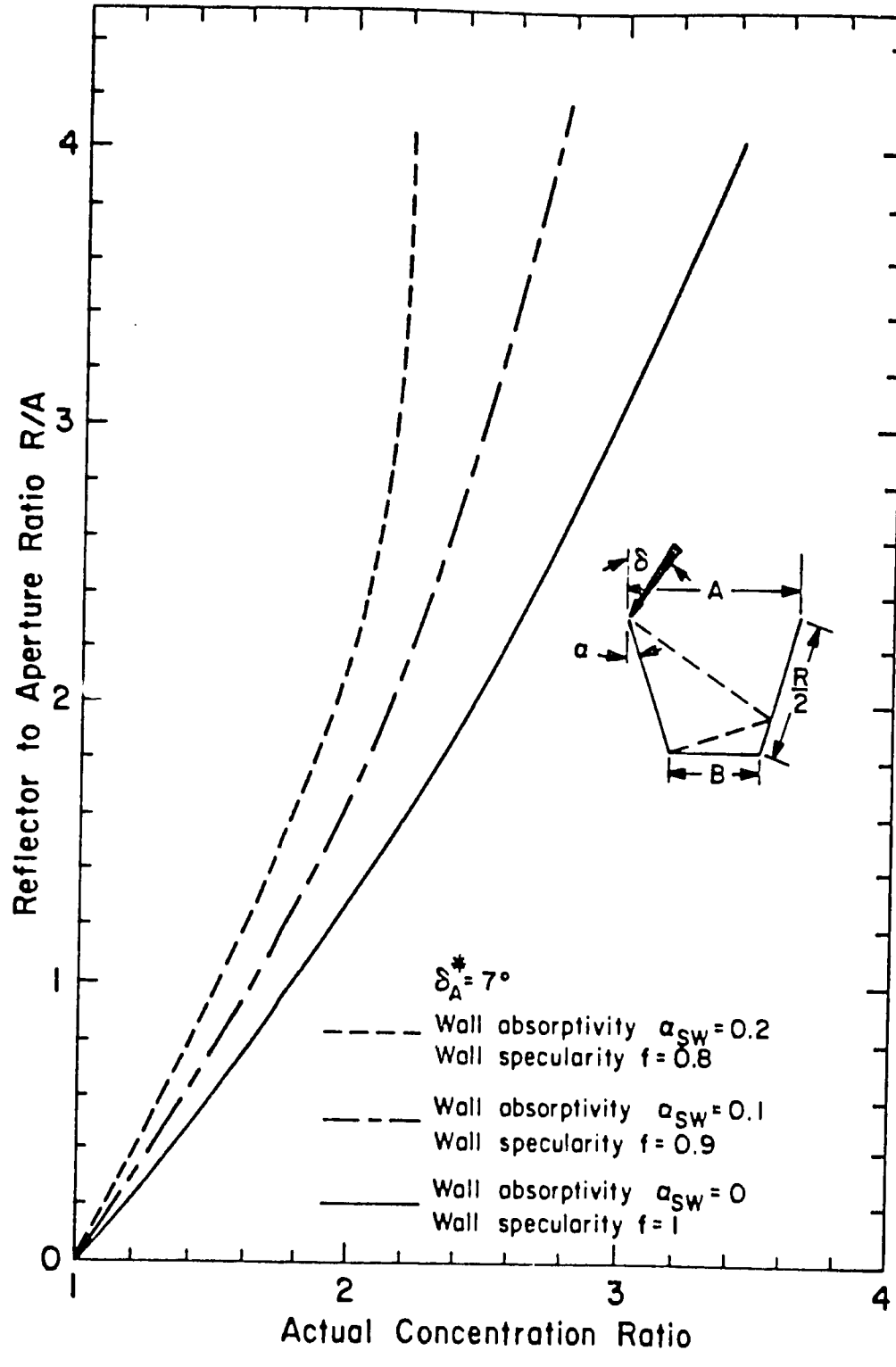


Figure 4-6 Effect of Real Walls on the Performance $\delta = 7°$

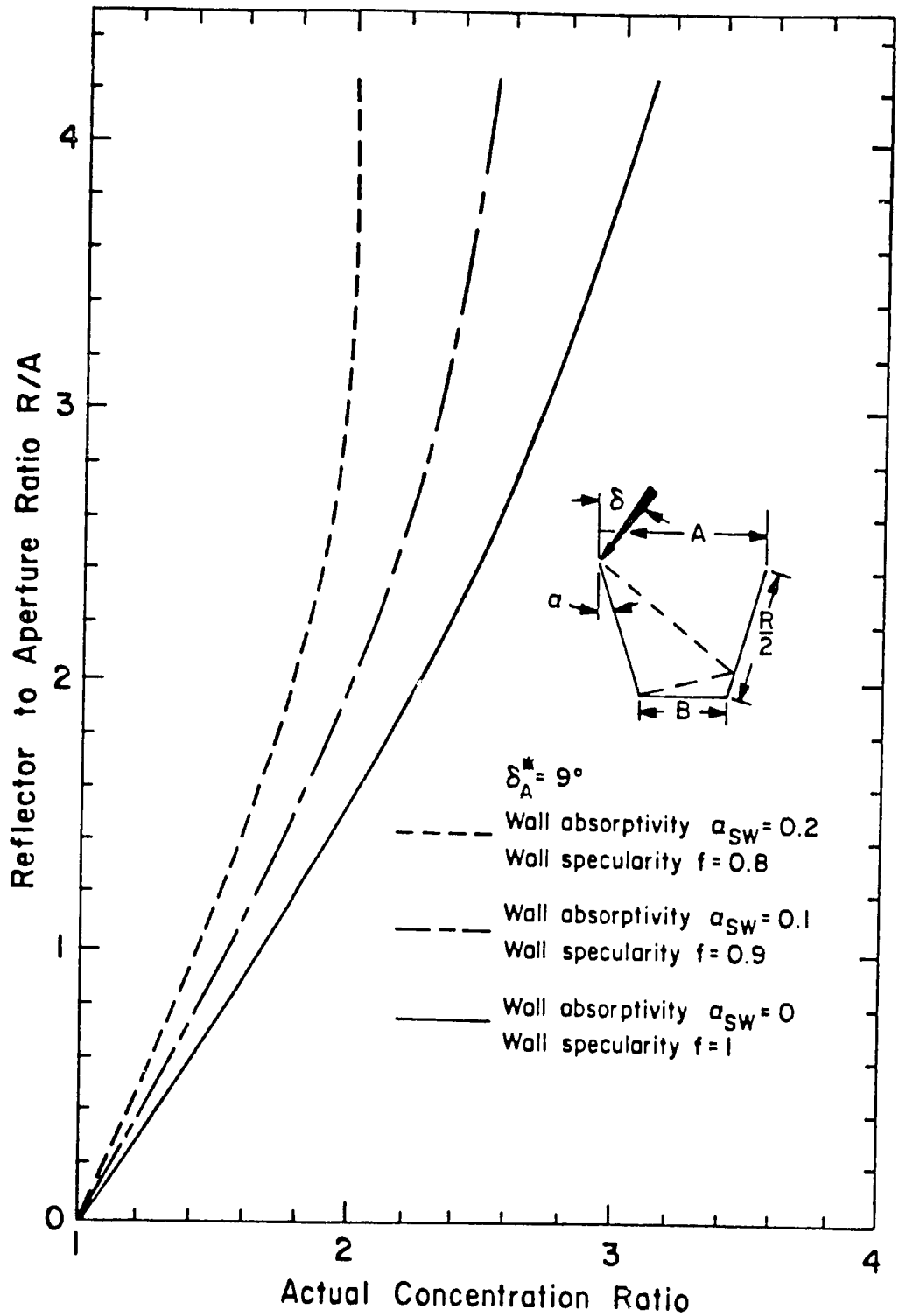


Figure 4-7 Effect of Real Walls on the Performance $\delta = 9°$

TABLE 4-1

EFFECTS OF REALISTIC REFLECTORS ON PERFORMANCE

$\delta_{A^*} = 7^\circ$

| $\alpha_{sw}$ | f | CR | % DEGRADATION |
|---|---|---|---|
| 0.0 | 1.0 | 3.24 | - |
| | 0.9 | 3.00 | 7.8 |
| | 0.8 | 2.70 | 16.7 |
| 0.1 | 1.0 | 2.96 | 8.6 |
| | 0.9 | 2.65 | 18.2 |
| | 0.8 | 2.46 | 24.1 |
| 0.2 | 1.0 | 2.62 | 19.1 |
| | 0.9 | 2.42 | 25.3 |
| | 0.8 | 2.28 | 29.6 |

| $\alpha_{sw}$ | f | CR | % DEGRADATION |
|---|---|---|---|
| 0 | 1.0 | 3.0 | - |
| | 0.9 | 2.74 | 8.7 |
| | 0.8 | 2.55 | 15.0 |
| 0.1 | 1.0 | 2.69 | 10.3 |
| | 0.9 | 2.5 | 16.7 |
| | 0.8 | 2.32 | 22.7 |
| 0.2 | 1.0 | 2.45 | 18.3 |
| | 0.9 | 2.27 | 24.3 |
| | 0.8 | 2.15 | 28.3 |

TABLE 4-1(a) CONTINUED

| $\alpha_{sw}$ | f | CR | % DEGRADATION |
|---|---|---|---|
| 0 | 1.0 | 2.50 | - |
| | 0.9 | 2.36 | 5.6 |
| | 0.8 | 2.18 | 12.8 |
| 0.1 | 1.0 | 2.32 | 7.2 |
| | 0.9 | 2.19 | 12.4 |
| | 0.8 | 2.05 | 18.0 |
| 0.2 | 1.0 | 2.12 | 15.2 |
| | 0.9 | 2.04 | 18.4 |
| | 0.8 | 1.96 | 21.6 |

| $\alpha_{sw}$ | f | CR | % DEGRADATION |
|---|---|---|---|
| 0 | 1.0 | 2 | - |
| | 0.9 | 1.89 | 6.7 |
| | 0.8 | 1.80 | 9.9 |
| 0.1 | 1.0 | 1.87 | 6.4 |
| | 0.9 | 1.78 | 11.0 |
| | 0.8 | 1.72 | 14.0 |
| 0.2 | 1.0 | 1.76 | 12.0 |
| | 0.9 | 1.73 | 14.0 |
| | 0.8 | 1.65 | 17.5 |

TABLE 4-1(b) $\varepsilon_A^* = 9^\circ$

| $\alpha_{sw}$ | f | CR | % DEGRADATION |
|---|---|---|---|
| 0.0 | 1.0 | 3.00 | - |
| | 0.9 | 2.74 | 8.6 |
| | 0.8 | 2.45 | 18.3 |
| 0.1 | 1.0 | 2.68 | 10.6 |
| | 0.9 | 2.48 | 17.3 |
| | 0.8 | 2.25 | 25.0 |
| 0.2 | 1.0 | 2.38 | 20.6 |
| | 0.9 | 2.21 | 26.3 |
| | 0.8 | 2.02 | 32.6 |

| $\alpha_{sw}$ | f | CR | % DEGRADATION |
|---|---|---|---|
| 0 | 1.0 | 2.75 | - |
| | 0.9 | 2.54 | 7.6 |
| | 0.8 | 2.35 | 14.5 |
| 0.1 | 1.0 | 2.52 | 8.4 |
| | 0.9 | 2.35 | 14.5 |
| | 0.8 | 2.16 | 21.4 |
| 0.2 | 1.0 | 2.29 | 17.7 |
| | 0.9 | 2.11 | 23.3 |
| | 0.8 | 1.99 | 25.6 |

TABLE 4-1(b) CONTINUED

| $\alpha_{sw}$ | f | CR | % DEGRADATION |
|---|---|---|---|
| 0.0 | 1.0 | 2.49 | - |
| | 0.9 | 2.30 | 7.4 |
| | 0.8 | 2.16 | 13.3 |
| 0.1 | 1.0 | 2.26 | 9.1 |
| | 0.9 | 2.16 | 13.3 |
| | 0.8 | 2.01 | 19.3 |
| 0.2 | 1.0 | 2.10 | 15.7 |
| | 0.9 | 2.00 | 19.7 |
| | 0.8 | 1.90 | 23.7 |

| $\alpha_{sw}$ | f | CR | % DEGRADATION |
|---|---|---|---|
| 0 | 1.0 | 2.0 | - |
| | 0.9 | 1.90 | 4.9 |
| | 0.8 | 1.84 | 8.2 |
| 0.1 | 1.0 | 1.90 | 5.0 |
| | 0.9 | 1.82 | 9.0 |
| | 0.8 | 1.77 | 11.5 |
| 0.2 | 1.0 | 1.81 | 9.5 |
| | 0.9 | 1.73 | 13.5 |
| | 0.8 | 1.66 | 17.0 |

base is larger for higher concentration ratios. As a result, the chance that radiation would be absorbed or diffuse reflected would be correspondingly higher. For the $7^\circ$ 90% actual acceptance angle, the degradation of performance ranges from about 30% for concentration ratio equal to 3.24 to 18% for concentration ratio equal to 2.

The effect on the optical performance due to changes in $\alpha_{sw}$ and f are numerically essentially the same. That is, increasing (or decreasing) $\alpha_{sw}$ with f fixed has essentially the same effect as decreasing (or increasing) f with $\alpha_{sw}$ fixed. The wall absorptivity has a slightly greater effect since it directly influences the loss of incident rays (by absorption) while f only indirectly influences the loss of incident rays by increasing the diffuse reflections which in turn may or may not cause a loss.

# Chapter Five

## Annual Performance of Trapezoidal Collectors

### 5.1 Annual Time Distribution of Tabor Angle

Solar geometry plays an important role in the design of efficient concentrating collectors. The amount of time which the sun spends at any particular location in the sky is of great interest to fixed or tilt adjusted concentrators. Since the sun spends different amounts of time in different locations in the sky, it is necessary for a fixed collector to be oriented in a direction that will enable it to operate efficiently for the longest period of time. The projection of the sun's direction vector onto the north-south vertical plane determines whether or not the sun beam will reach the base of an East-West aligned groove collector. The angle which the projected beam makes with the normal of the groove tilted at local latitude is the Tabor angle as discussed earlier in Chapter Two. The distribution of the total time on an annual basis during which the Tabor angle is within a specific angle has been determined by a numerical method. The result is shown in Fig. 5-1 and has been compared with good agreement to the result of D.C. Larson and C.R. Acqusta [14] who employed an analytical method. Figure 5-1 is a probability distribution curve of the number of hours per degree during which the Tabor angle is at a specified angle as a function of collector cut off time, $t_c$ (daily collection period is 2 $t_c$); if a collector is designed to collect 6 hours of insolation, then the corresponding cut off time will be 3 hours. For example, if a fixed concentrator is tilted at an angle equal to the local latitude and has actual acceptance

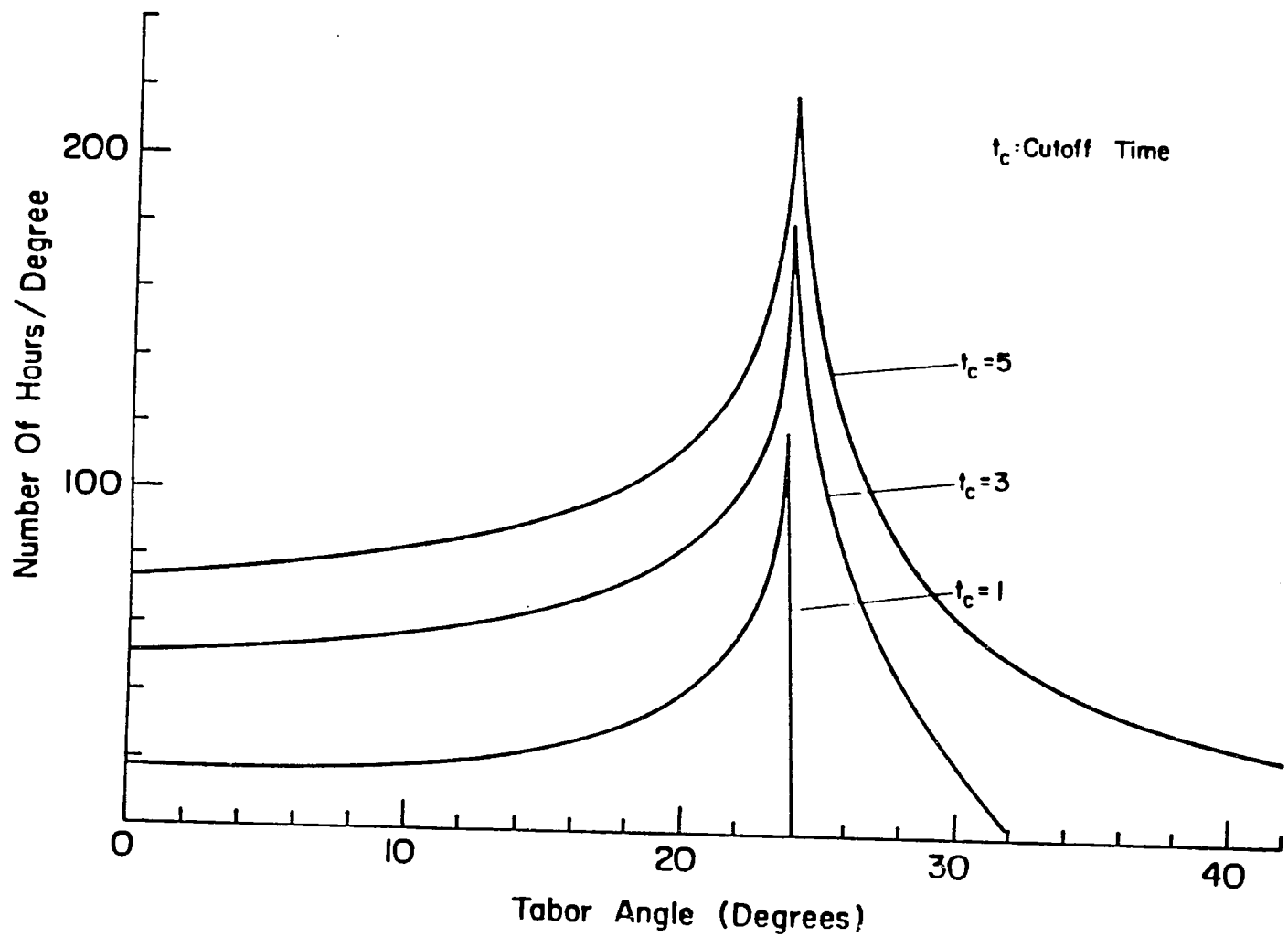


Figure 5-1 The Time Probability Function in Hours/Degree vs. Tabor Angle for Several Values of Cut off Time $t_c$

angle of $10^\circ$ ; then the total number of hours that the concentrator will have full concentration on an annual basis will be equal to the area under the specified cut off time curve up to $10^\circ$ . As is seen from Fig. 5-1, the time distribution function increases from $0^\circ$ to a peak at an angle of about $24^\circ$ and then decreases. Thus, a two dimensional fixed concentrator designed for year round operation should have an acceptance angle of at least $24^\circ$ . Interpolating from Fig. 2-9 for the ideal CPC, one can determine that the maximum concentration ratio obtainable would be less than 2. The fixed non-tracking concentrator is therefore severely limited if designed to be used throughout the year. Hence some type of tilting routine must be established to accommodate the north-south swing of the sun.

## 5.2 The Daily North-South Swing Curve

Trapezoidal groove concentrators are designed to be non-tracking. However, to be practical, occasional tilt adjustments are necessary as pointed out above. The daily north-south swing of the sun is described by the Tabor angle $\phi$ as mentioned earlier. Figure 5-2 is a plot of Tabor angle (measured from the direction of the local latitude) as a function of days from equinox and hours from solar noon. The $t=0$ curve indicates the noon time position of the sun. The $t=4$ curve indicates the amplitude of the solar swing four hours from solar noon. The difference in degrees between the noon time and the $t=4$ curve on a given day gives the north-south solar swing for eight hours (8 a.m. to 4 p.m. solar time) on that day. For instance, at the solstice where the daily swing is most severe, the eight hour swing (noon plus or minus 4

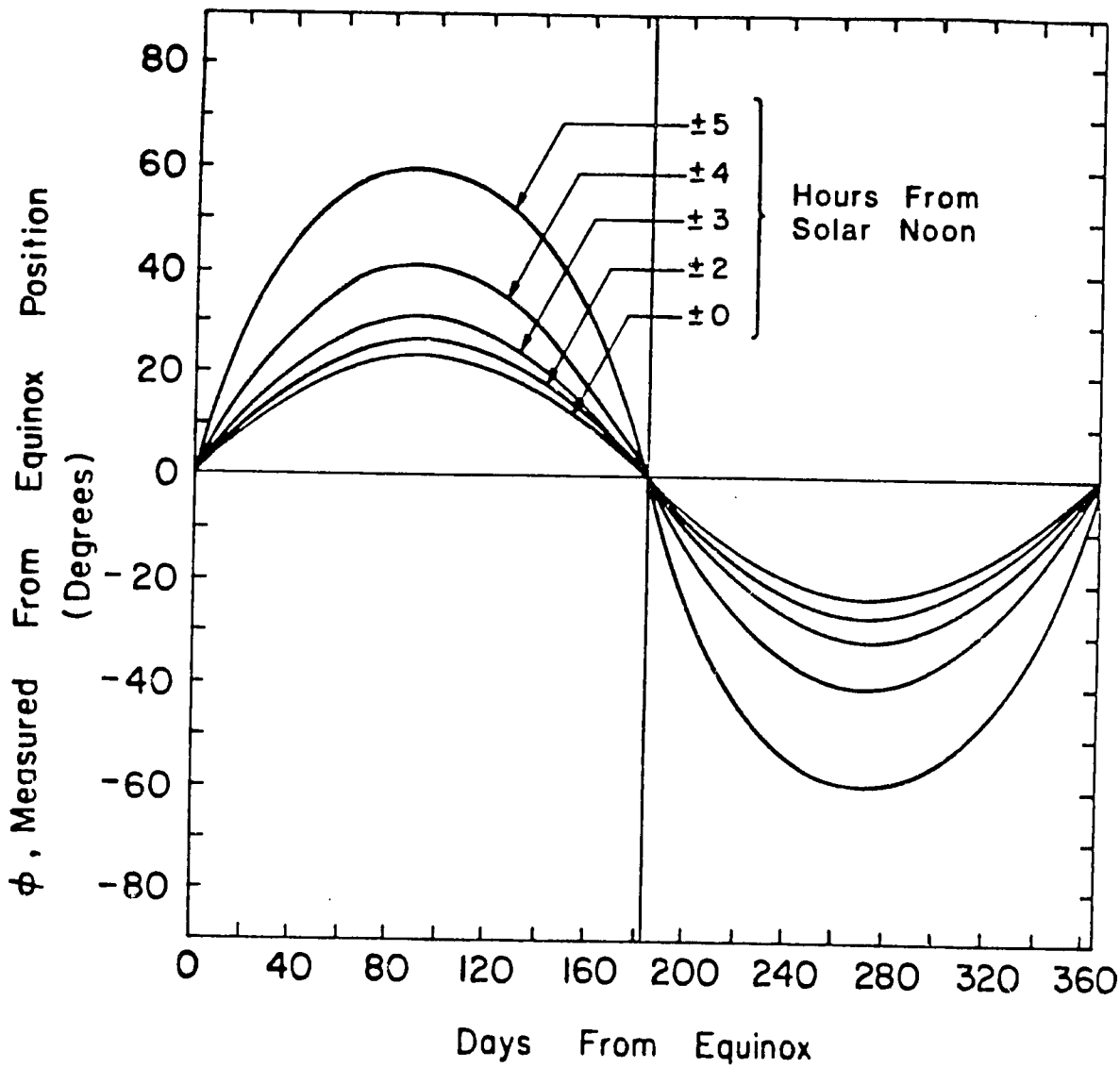


Figure 5-2 Variation of the Tabor Angle Throughout the Year

hours) is 17.5° (40.94° - 23.45°, from Fig. 5-2 or eqn. (2.4)). Thus a 9° acceptance angle is necessary to assure eight hours of full concentration on solstice if the trough is tilted to bisect the diurnal swing of the sun. The noon-time position of the sun swings approximately 47° from winter to summer solstice. The daily swing is accommodated for by the collector acceptance angle. The tilt adjustments must accommodate for the seasonal swing. Before discussing the criteria for tilt routines, it will be informative to discuss the factors which will affect the intensity of radiation.

## 5.3 Atmospheric Absorption of Solar Radiation

As radiation passses through the atmosphere, it is being absorbed and scattered by molecules and particles such as dust and water droplets that are present in the atmosphere. The simplest model used to estimate the relative magnitude of atmospheric absorption and scattering of solar radiation at any time for a clear sky is based on the air mass principle. Air mass is defined as the ratio of the actual slant path the radiation has to travel in the atmosphere to the vertical path length in the atmosphere to the same depth. Figure 5-3 is a graph showing the variation of air mass for different times of the day throughout the year. It is seen that the path length which radiation has to travel is greatest early in the morning and late in the afternoon. The intensity of the transmitted radiation decreases exponentially with air mass and is usually approximated as

$$I = I_o e^{-km}$$

where $I$ = transmitted intensity of the solar beam

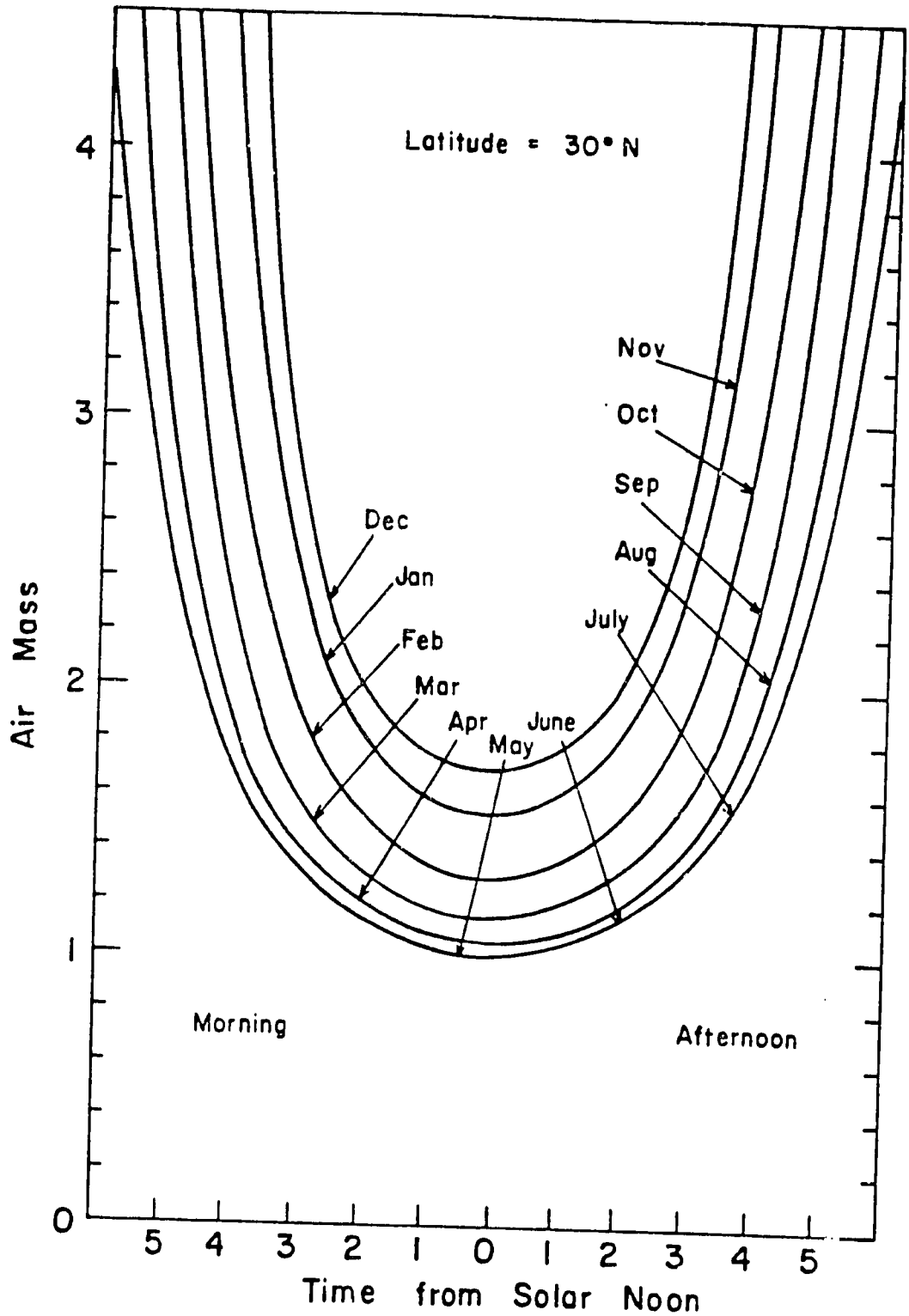


Figure 5-3 Air Mass vs. Time for the Year

$I_o$ = extraterrestial intensity of the solar beam

k = absorption coefficient of the atmosphere

m = no. of air mass

An important consequence of atmospheric attenuation of the solar beam is that the intensity of the beam can be significantly reduced early and late in the day. The fact that non-tracking concentrators are usually limited to operate only in the middle of the day due to their acceptance angle restriction may not be so restrictive then since the energy available outside these middle hours has been reduced, especially in the winter as seen in Fig. 5-3.

## 5.4 Criterion for Tilt Routine

As discussed previously in this chapter, the number of hours of full concentration actually sets the requirement for the collector acceptance angle. For example, at times near the solstices, in order to have eight hours of full concentration, the concentrator has to have an acceptance angle of at least $9^{\circ}$; a concentrator with a smaller acceptance angle will have less than eight hours of full concentration because the daily solar swing is so severe. The various curves in Fig. 5-4 represent the hourly swing of the sun (same as Fig. 5-2) from summer solstice (June 21) to winter solstice (Dec. 21). Each rectangle superimposed on the curves represents a different fixed collector tilt. The horizontal length of each box represents the period during which the tilt of the concentrator is fixed. The vertical width of each box corresponds to the angular range (twice the acceptance angle) that the concentrator is able to accommodate. In Fig. 5-4, the tilt routine shown

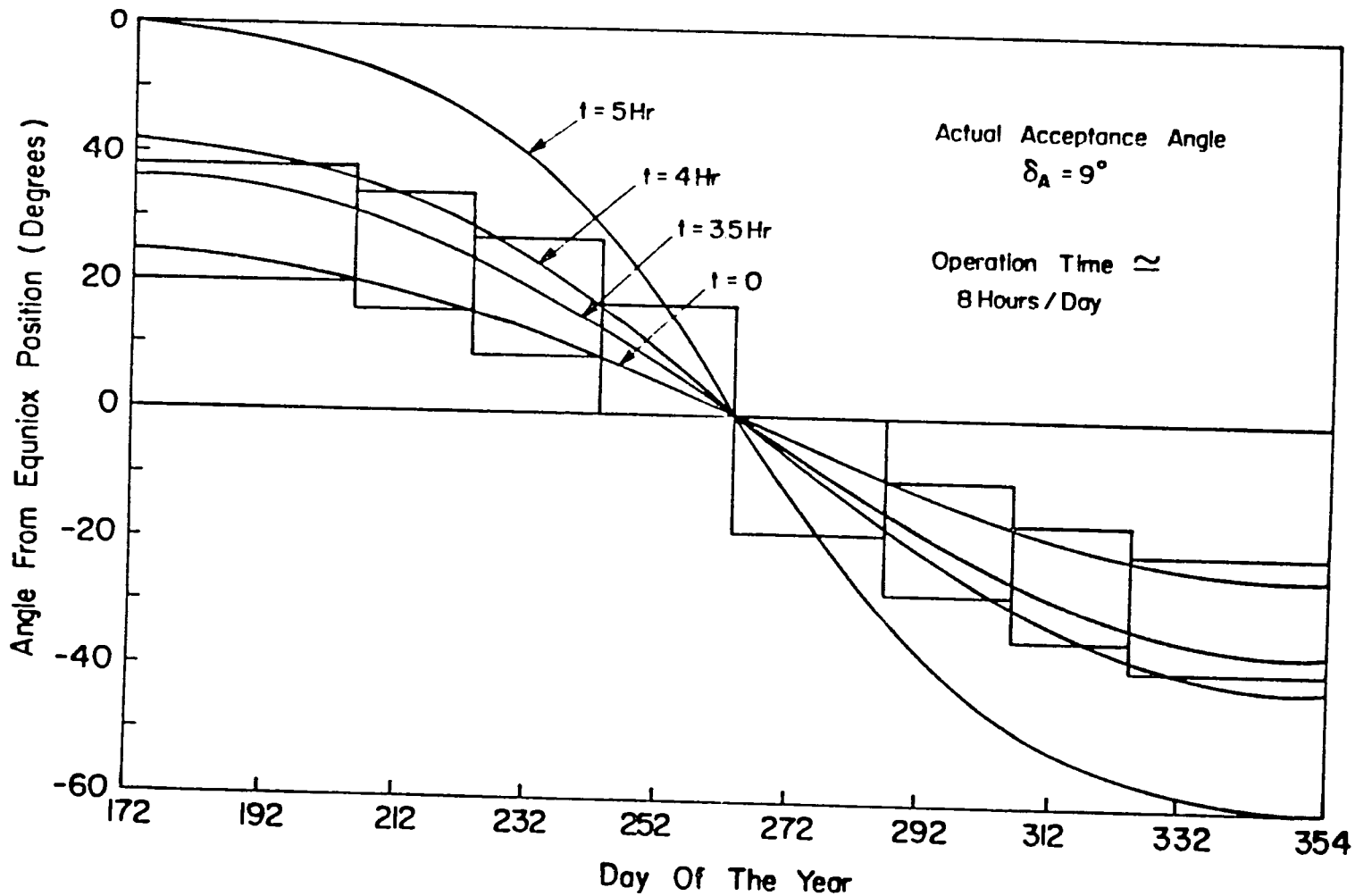


Figure 5-4 Tilt Routine for a Collector with Acceptance Angle of 9°

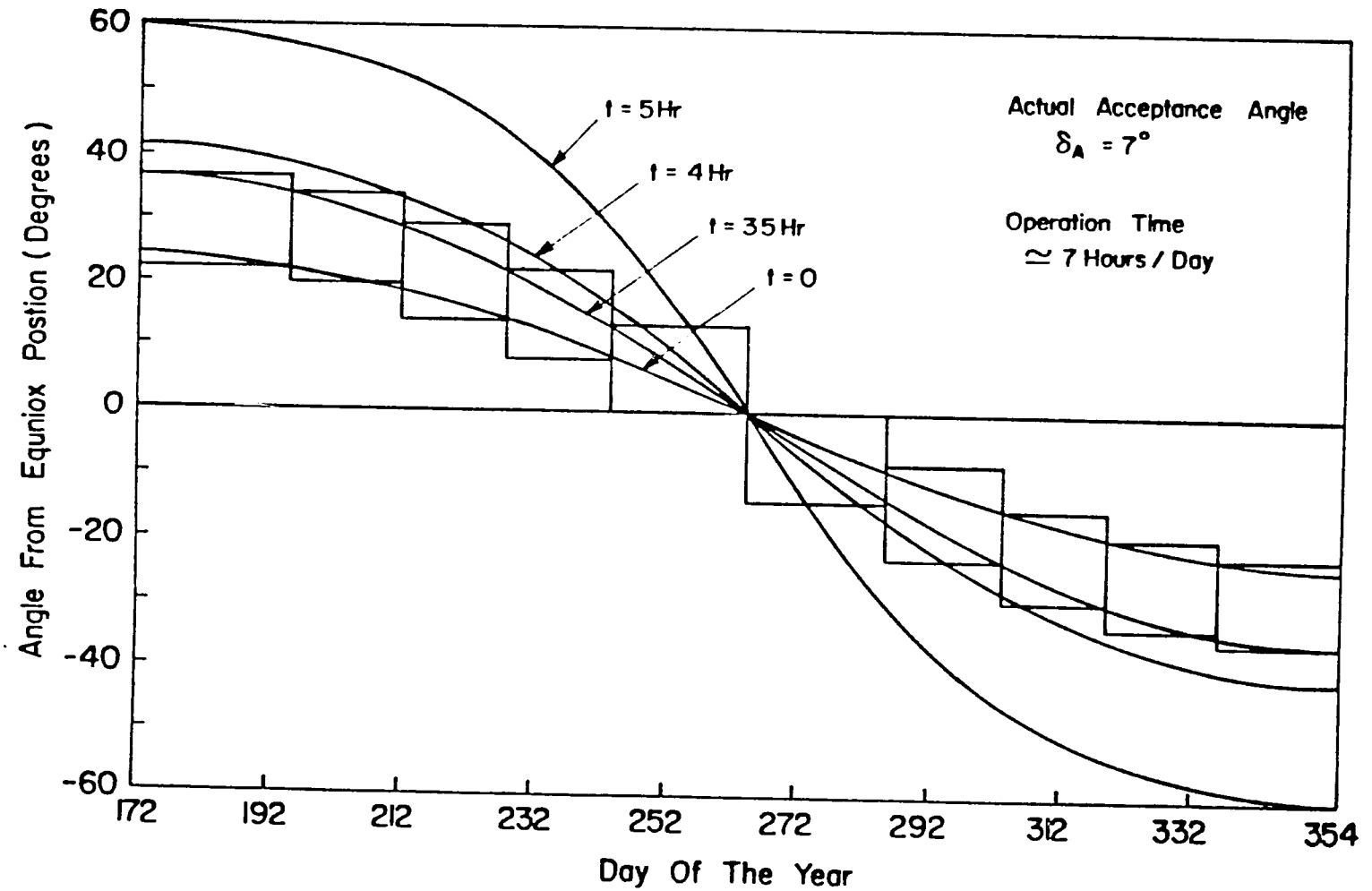


Figure 5-5 Tilt Routine for a Collector with Acceptance Angle of 7°

requires 14 adjustments per year and is designed to have at least eight hours of full concentration (except for days near solstice where the daily swing is so severe that the tilt adjustment has to be made every three or four days if eight hours of full concentration are needed). The acceptance angle of the concentrator used is $9^{\circ}$ and the angular range of the concentrator is $18^{\circ}$. As the daily swing changes periodically with time, tilt adjustments have to be made at various times to re-orient the concentrator so that its acceptance angle can cover the $\pm 4$ hr. of daily swing from solar noon. Tilt adjustments are made whenever the collector fails to receive full concentration at noon time. At noon, the intensity of the radiation is strongest, therefore, the time around solar noon is the most desirable collection period. Fig. 5-5 represents a tilt routine for a collector with an acceptance angle of $7^{\circ}$, and in this case the maximum number of hours with full concentration is about $\pm 3.5$ hours from solar noon during solstice. It requires 18 tilt adjustments per year.

By allowing the concentrator not to have full concentration for the full $\pm 4$ hours from the solar noon around the solstices reduces the required number of tilt adjustment greatly. However, the effect of this non-operating time on the annual performance of the system is minimum. During the early morning or late in the afternoon, the air mass is considerably larger than for the period near solar noon. The intensity of radiation at times greater than four hours from noon is greatly reduced from the noon time intensity especially in the winter period. Thus the loss of usable energy due to the lack of full concentration early and late in the day is very small. The hours of operation and the available

energy were determined for the tilt routines shown in Figs. 5-4 and 5-5. These values were compared to those obtained for a daily tilt routine (tilt adjusted every day) for the corresponding acceptance angle. Results from the comparison indicated that on an annual basis, the difference in collection time and total energy available between the tilt routines shown in Figs. 5-4 and 5-5 and the daily tilt routine model is within 1% in both cases.

Based solely on the hours of operation and for uniform annual performance, the optimal tilt routine as determined from figures like 5-4 and 5-5, can be fairly easily established. There is a little more uncertainty in establishing a tilt routine based on available insolation due to the air mass effect. There are two practical problems that can arise which make the design and schedule of tilting somewhat more complex. These have to do with seasonal energy requirements and pointing accuracy. Suppose the primary use of the collection system were to supply energy for a space cooling system. Then it may be desirable to pay close attention to the collector orientation in the summer, but not to be too concerned during the other seasons where space cooling is not required. This is particularly true on the winter side of equinox (October, November, February, March) where frequent adjustments would be required. Pointing accuaracy can also be important. In theory, there is not much margin for error for a system with a sharp cut off angle like the CPC. For a collector of the trapezoidal design, it is not so critical since the cut off angle is not sharp. However, in both cases it is important that the noon time solar angle be accommodated even if it means the loss of some energy early and late in the day. One way to

assure optimal operation in the middle of the day is to install, on the collector, a sun sight or shadow indicator designed for the acceptance angle of the particular collector so that someone could determine in the field, during operation, whether the collector is properly aligned at solar noon.

The information presented in this chapter and Chapter 4 will enable one to specify the optics of trapezoidal concentrating collectors. For example, if one decided a minimum number of hours of full concentration is needed daily for a specific purpose, then by inspecting the daily swing curves like the one shown in Fig. 5-3, the minimum required acceptance angle of the collector can be calculated. Once the acceptance angle of the concentrator is known, one can refer to curves like those in Figs. 4-6 or 4-7 which give the relationship between concentration ratio and quantity of material (and the geometry) that is needed to construct the concentrator. If circumstances arise where cheaper but lower quality reflective material is being considered, then one can examine the figures which include these non-ideal effects and locate the geometric concentration ratio that will give the desired concentration ratio when lower grade reflective material is used. From the geometric concentration ratio and the corresponding reflector to aperture ratio, the configuration of the groove collector can be reconstructed. Finally, by following the tilt routine criterion described above, one can determine when the tilt adjustments have to be made in order to maintain the predeterminated operation hours.

## Chapter Six

## Conclusions

It is clear that the optical performance of trapezoidal collectors designed on the basis of the one or two reflection criteria does not compare favorably with that of the compound parabolic concentration CPC which in fact is an ideal concentrator. On the other hand, because of its simplicity in configuration, the trapezoidal collectors may have other advantages such as low cost and less sophisticated fabrication, therefore the choice between the two is not so obvious. The two reflection or less criterion proved to be a better design criterion than the one reflection or less criterion. The improvement in the maximum concentration ratio is about 30% to 40% for the one facet case. For the results obtained here it appears that increasing the number of wall facets (above one) is not a viable approach in improving the optical performance of the trapezoidal groove at least for the geometric design criterion of two reflections or less. Clearly not all the geometric configurations have been examined and the possibilities exist that better multi-facet geometries could be found. As a general rule, for every 10% decrease in the wall properties (either $\alpha_{sw}$ or f), a corresponding 6% to 8% degradation in performance is expected. The higher the concentration ratio, the more severe will be the effect of wall imperfection.

From the tilt routine analysis, it was found that with the help of the daily swing curve like the one in Fig. 5-3, tilt routines can easily be formulated. And in fact any tilt routine which will guarantee to deliver the pre-determined number of hours of full concentration is as

good as any other tilt routine including the daily tilt routine model.

More work has to be done in the area of developing better design criteria for the trapezoidal collector if it is to compete with the CPC at reasonable concentration ratios. Once the initial cost of solar energy system can be reduced substantially, popularity of solar energy both in domestic and industrial use will not be too far away.

## References


1 H. Baird Tenny et altera, "Financial Barriers to the Use of Solar Industrial Process Heat Low Return on Solar Investment Precludes Most Industrial Applications," Proceedings of the Solar Energy Division Fourth Annual Conference, Albuquerque, New Mexico, April 26-29, 1982, pp. 189-94.

2 C. Thomas Brown, "A 400 KW High Temperature Solar Test Facility," Proceedings of the ERDA Conference on Concentrating Solar Collectors, Atlanta, Georgia, September 26-28, 1977, pp. 13-19.

3 H. Tabor, "Stationary Minor System for Solar Collectors," Solar Energy 2, 1958, pp. 27-33.

4 K. G. T. Hollands, "A Concentrator for Thin Film Solar Cells," Solar Energy 13, 1971, pp. 149-163.

5 W. C. Dickinson and P. N. Cheremisinoff, Solar Energy Technology Handbook, Marcel Dekker, Inc. 1980, pp. 258-64.

6 W. T. Welford and R. Winston, The Optic of Nonimaging Concentrators, Academic Press, 1978, pp. 47-103.

7 A. S. E. Ackerman, "The Utilization of Solar Energy," Annual Report of the Board of Regents of the Smithsonian Institute, 1915, pp.

141-166.

8 R. B. Bannerot and J. R. Howell, "The Effect of Non-Direct Insolation of the Radiation Performance of the Trapezoidal Grooves Used as Solar Energy Collectors," Solar Energy 19, 1977, pp. 549-553.

9 R. B. Bannerot and J. R. Howell, "Predicted Daily and Yearly Average Radiative Performance of Optimal Trapezoidal Groove Solar Energy Collectors," Solar Energy 22, 1979, pp. 229-234.

10 R. B. Bannerot and J. R. Howell, "Moderately Concentrating Flat-Plate Solar Energy Collectors," ASME Paper 75-HT-54. Presented at the National Heat Transfer Conference, San Francisco, California, 1975.

11 R. B. Bannerot and J. R. Howell, "Trapezoidal Grooves as Moderately Concentrating Solar Energy Collectors," Radiative Heat Transfer and Thermal Control, Progress in Astronautics and Aeronautics, vol. 49, AIAA, 1976, pp. 277-289.

12 R. Siegel and J. R. Howell, Thermal Radiation Heat Transfer, McGraw-Hill Book Company, 1972, pp. 608-626.

13 K. D. Mannan, "Performance of Optimal Geometry Three Step Compound Wedge Stationary Concentrator," Paper presented at the 8th Annual Conference of All India Solar Energy Working Group, Ludhiana,

1977.

14 D. C. Larson and C. R. Acquista, "Solar Elevation Angle Probability Distribution," Solar Energy 24, 1980, pp. 417-420.

## Appendix A

## Mathematical Basis of the Ray-Trace Computer Simulation for the Groove's Optical Performance

### Incident Beam

An orthogonal x-y-z co-ordinate system is centered at the midpoint of the groove base as shown in Fig. (A-1). The x-axis is directed along the length of the groove. The y-axis traverses the base plane and the z-axis is vertical (perpendicular to the base plane). The groove is symmetric about the x-z plane. The base extends from $y = -B/2$ to $B/2$ and is infintely long. The lower sidewall has a vertical height of $D_1$ and is inclined at an angle of $\alpha_1$ from vertical. The upper sidewall has a vertical height of $D_2$ and is inclined at $\alpha_2$ from vertical. (See Fig. (3-5)).

The solar beam is determined by two incident solar angles ($\gamma_s$, $\theta_s$). The beam strikes the opening at a point ($x_1$, $y_1$, $z_1$). The direction cosines of the beam with respect to the x, y, z axes, respectively, are:

$$\cos \alpha_i = - \sin \gamma_s \cos \theta_s \qquad \text{. . . . . (A.1.a)}$$

$$\cos \beta_i = - \sin \gamma_s \sin \theta_s \qquad \text{. . . . . (A.1.b)}$$

$$\cos \gamma_i = - \cos \gamma_s \qquad \text{. . . . . (A.1.c)}$$

The minus signs indicate that the beam is directed toward the incident point. The equation of the line passing through (x, y, z) in the direction of the solar beam can be written as

$$\frac{x - x_1}{\cos \alpha_i} = \frac{y - y_1}{\cos \beta_i} = \frac{z - z_1}{\cos \gamma_i} \qquad \text{. . . . . (A.2)}$$

For infinitely long groove $x_1$ can be selected arbitrarily. At the

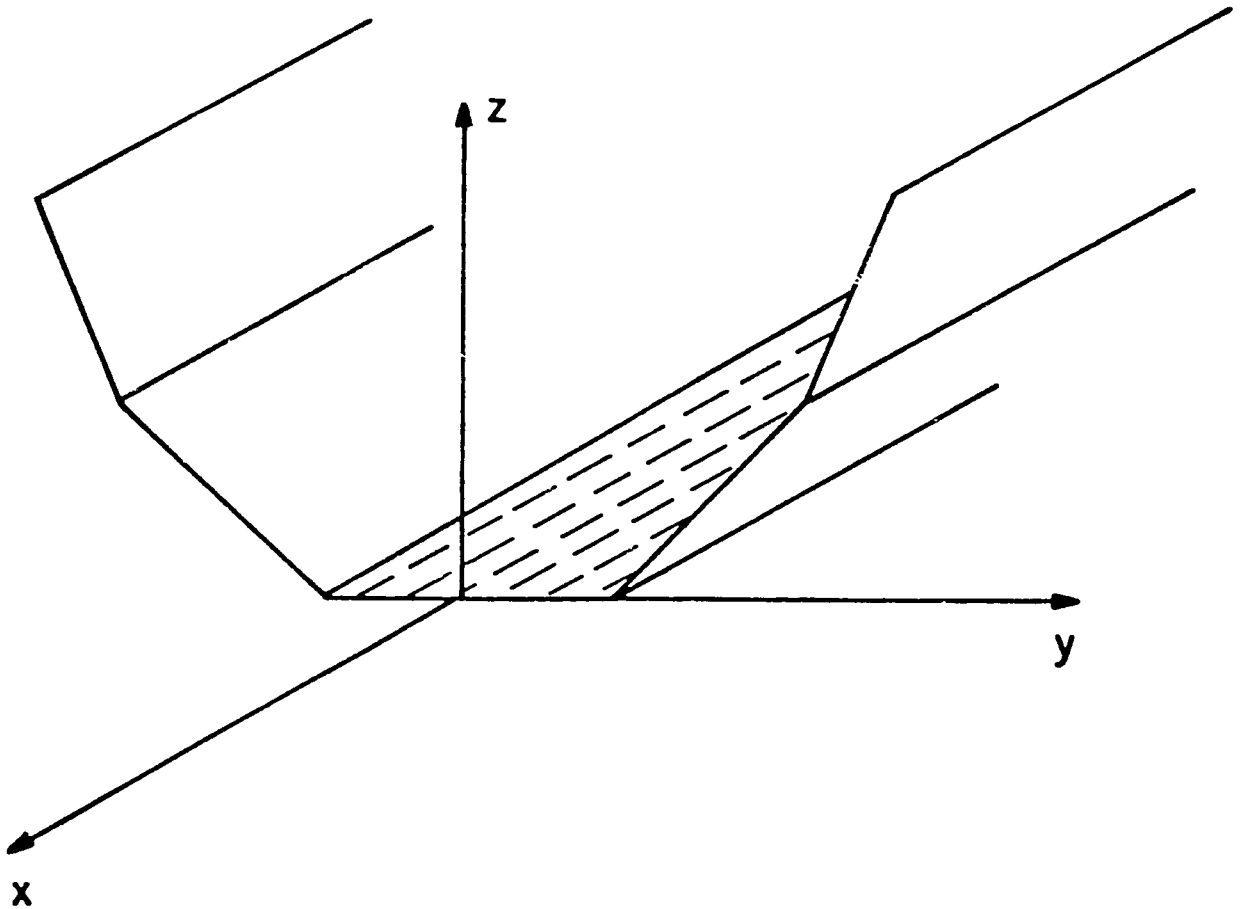


Figure A-1 Location of the Orthogonal Co-ordinate System in the Based Plane

opening,

$x_1 = 0,\ z_1 = (D_1 + D_2)$

Hence, the equation of the beam will be:

$$\frac{x}{\sin \gamma_s \ \cos \theta_s} = \frac{y - y_1}{\sin \gamma_s \ \sin \theta_s} = \frac{z - D_1 - D_2}{\cos \gamma_s} \qquad \ldots\ldots (A.3)$$

Now, the point, at which the beam strikes the base or a sidewall, can be determined as follows:

For the base plane, $z = 0$. Substituting $z = 0$ in eqn. (A.3),

$$\frac{y_b - y_1}{\sin \gamma_s \ \sin \theta_s} = \frac{-D_1 - D_2}{\cos \gamma_s}$$

or $\quad y_b = -(D_1 + D_2) \tan \gamma_s \ \sin \theta_s + y_1$

Depending upon the value of $y_b$,

| | |
|---|---|
| $y_b < B/2$, | the incident beam strikes either of the left side-walls. |
| $-B/2 \leq y_b \leq B/2$, | the incident beam strikes the base. |
| $y_b > B/2$, | the incident beam strikes either of the right side-walls. |

For $|y_b| > B/2$, it must be determined whether the upper or lower side wall is hit.

The plane parallel to the base plane at a height of $D_1$ can be identified by $z = D_1$. The incident beam would strike this plane at

$y_b' = -D_2 \tan \gamma_s \ \sin \theta_s + y_1$

Depending upon the value of $y_b'$

$y_b' \leq -B/2 - D_1 \tan \alpha_i$, the incident beam strikes the upper left wall.

$y_b' \geq B/2 + D_1 \tan \alpha_i$, the incident beam strikes the upper right wall.

Once, the wall or base, where the incident beam strikes, is known, the coordinates of the point of intersection can be determined.

Since the coordinates of various points on the wall and base are known, the equations of the planes forming the walls and base can be determined using the following general formula:

$$\frac{y - y_{I}}{y_{II} - y_{I}} = \frac{z - z_{I}}{z_{II} - z_{I}} \qquad \ldots\ldots (A.4)$$

Where $(y_{I}, z_{I})$ and $(y_{II}, z_{II})$ are two different points lying in the plane. From equations (A.2), an incident beam can be represented by

$$\frac{y - y_1}{\cos \beta_i} = \frac{z - z_1}{\cos \gamma_i} \qquad \ldots\ldots (A.2)$$

The point $(y_i, z_i)$, at which the incident beam strikes the plane denoted by eqn. (A.4), can be obtained by solving eqns. (A.2) & (A.4).

$$z_i = \frac{\left(z_{I}\left(\frac{y_{II} - y_{I}}{z_{II} - z_{I}}\right) - z_1\left(\frac{\cos \beta_i}{\cos \gamma_i}\right) - (y_{I} - y_1)\right)}{\left(\left(\frac{y_{II} - y_{I}}{z_{II} - z_{I}}\right) - \frac{\cos \beta_i}{\cos \gamma_i}\right)}$$

$$y_i = \left(\frac{z_i - z_l}{z_{ll} - z_l}\right) * (y_{ll} - y_l) + y_l$$

Specular Reflection from walls:

If the beam is not absorbed, it is reflected from the surface on which it is incident. As discussed in Chapter Four the sidewalls have been characterized as specular-diffuse. In the event of reflection from a sidewall, the beam may either be diffusely reflected or specularly reflected. Here analysis for only one wall will be given. The others are similar.

Specular Reflection from lower left wall:

A beam is incident at a point $(x_L, y_L, z_L)$ on the lower left wall. The direction cosines of this beam with respect to the base coordinate system (x, y, z) are $\cos \alpha_1$, $\cos \beta_1$, and $\cos \gamma_1$.

Consider a transformed orthogonal coordinate system (x', y', x') centered at the point $(x_L, y_L, z_L)$ and rotated clockwise about the x-axis by an angle $(90-\alpha_1)$ degrees. Now the z'-axis is perpendicular to the wall and y'-axis lies in the plane of the wall.

The rotation about the x-axis is a linear transformation with the x-axis as a pivot and can be expressed as the following matrix equation:

$$(\cos \alpha_i', \cos \beta_i', \cos \gamma_i') = \qquad \ldots\ldots (A.5)$$

$$(\cos \alpha_i, \cos \beta_i, \cos \gamma_i) \begin{bmatrix} 1 & 0 & 0 \\ 0 & \cos(90-\alpha_1) & \sin(90-\alpha_1) \\ 0 & -\sin(90-\alpha_1) & \cos(90-\alpha_1) \end{bmatrix}$$

Therefore, the direction cosines of the incident beam in the transformed

coordinate system are

$$\cos \alpha_i' = \cos \alpha_i \tag{A.5.a}$$

$$\cos \beta_i' = \sin \alpha_1 \cos \beta_i - \cos \alpha_1 \cos \gamma_i \tag{A.5.b}$$

$$\cos \gamma_i' = \cos \alpha_1 \cos \beta_i + \sin \alpha_1 \cos \gamma_i \tag{A.5.c}$$

In the transformed coordinate system, the reflected beam will have the same direction cosines with respect to the x' and y'-axes as the incident beam and the negative of the incident direction cosine with respect to the z'-axis. (See Fig. (A-2)). Therefore

$$\cos \alpha_r' = \cos \alpha_i' = \cos \alpha_i \tag{A.6.a}$$

$$\cos \beta_r' = \cos \beta_i' = \sin \alpha_1 \cos \beta_i - \cos \alpha_1 \cos \gamma_i \tag{A.6.b}$$

$$\cos \gamma_r' = \cos \gamma_i' = -\cos \alpha_1 \cos \beta_i - \sin \alpha_1 \cos \gamma_i \tag{A.6.c}$$

In order to transform these equations back into the base coordinate system, eqn. (A.5) will have to be inverted by an inverse linear transformation:

$$\cos \alpha_r = \cos \alpha_r' \tag{A.7.a}$$

$$\cos \beta_r = \sin \alpha_1 \cos \beta_r' + \cos \alpha_1 \cos \gamma_r' \tag{A.7.b}$$

$$\cos \gamma_r = \sin \alpha_1 \cos \gamma_r' - \cos \alpha_1 \cos \beta_r' \tag{A.7.c}$$

Equations (A.5) and (A.6) are substituted in eqns. (A.7) to obtain cosines of the reflected beam in the base co-ordinate system.

$$\cos \alpha_r = \cos \alpha_i \tag{A.8.a}$$

$$\cos \beta_r = -\cos 2\alpha_1 \cos \beta_i - \sin 2\alpha_1 \cos \gamma_i \tag{A.8.b}$$

$$\cos \gamma_r = -\sin 2\alpha_1 \cos \beta_i + \cos 2\alpha_1 \cos \gamma_i \tag{A.8.c}$$

Therefore, the equation of a line coincident with reflected beam is

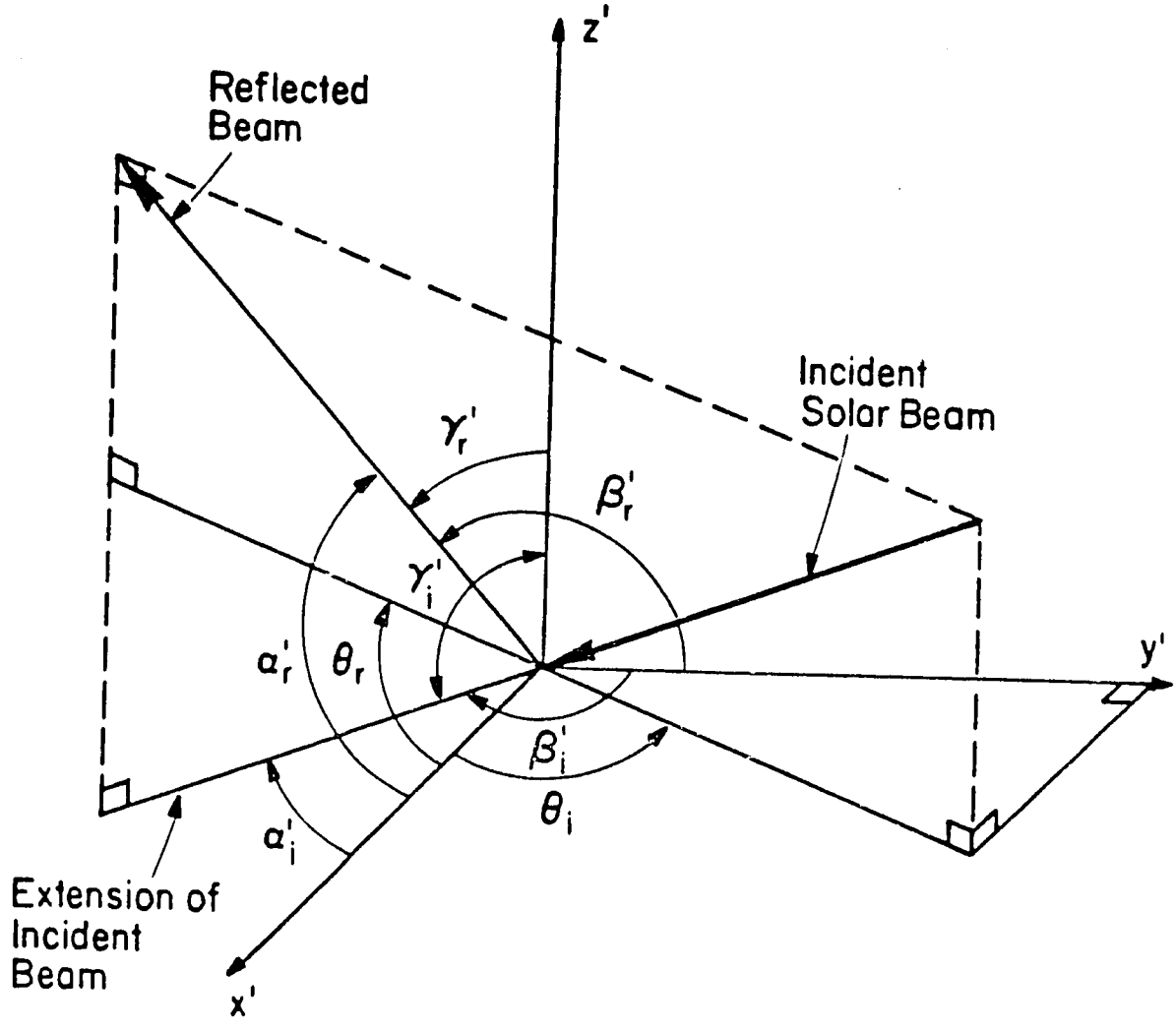


Figure A-2 Incident and Reflected Beam in Transformed Co-ordinate System

$$\frac{x - x_L}{\cos \alpha_r} = \frac{y - y_L}{\cos \beta_r} = \frac{z - z_L}{\cos \gamma_r}$$

Depending upon the values of $\alpha_r$, $\beta_r$, $\gamma_r$, $x_L$, $y_L$, and $z_L$, there are the following possible fates for the reflected beam (see Fig. (A-3)).

(a) It can escape the groove.

(b) It can strike the upper right wall.

(c) It can strike the lower right wall.

(d) It can strike the base.

(e) It can strike the upper left wall.

Now the reflected beam is extended to strike the extended planes of the base and other walls to determine the point of incidence or escape (to the surroundings from the top). This has been shown by dotted lines in Fig. (A-3). This process of reflection continues until the beam is absorbed in the groove or escapes back to the surroundings.

Diffuse Reflection from the walls and the base:

Diffuse reflection from a surface is taken to be uniformly distributed over all angles. That is why, here, the incident angles are not required; only the point of incidence. Howell [12] has suggested a Monte Carlo technique to determine the probable direction of a random diffuse reflection. He has determined the probability distribution functions for the longitudinal, $\theta_r$, and the colatitudinal, $\gamma_r$, angles for diffuse reflection. That is, functions which determine the probability that a given reflection might be in a direction which has given $\theta_r$ and $\gamma_r$, are known.

If $R_1$ & $R_2$ are two random numbers between zero and one, the direc-

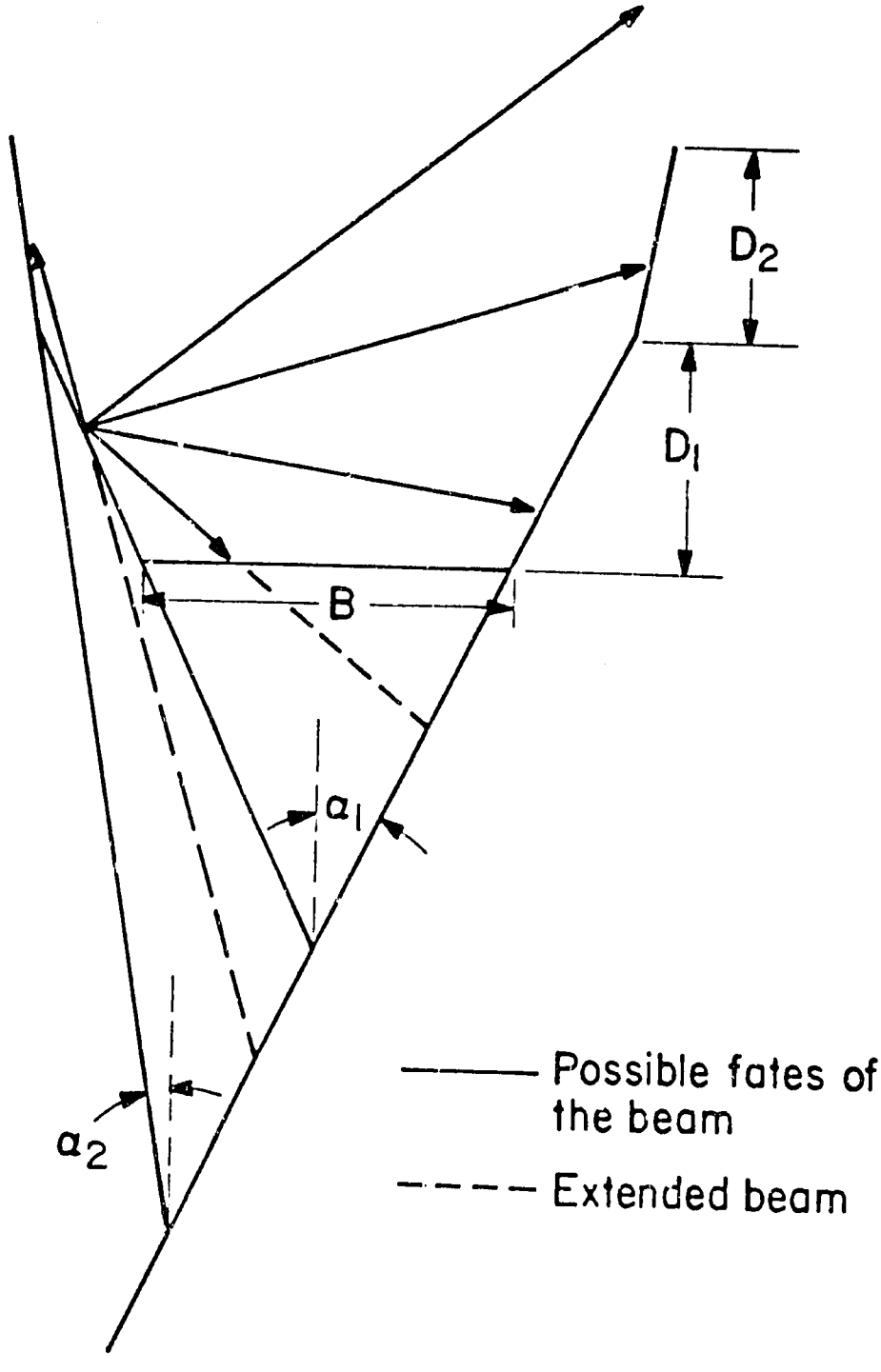


Figure A-3 Possible Fates of a Beam Reflected from Lower Left Wall (Specular or Diffuse Reflection)

tion of a random diffuse reflection may be expressed as:

$$\theta_r = 2 \pi R_1 \tag{A.9.a}$$

$$\gamma_r = \cos^{-1} \sqrt{R_2} \tag{A.9.b}$$

That is, all longitudinal directions are equally probable and the probability of a reflection into a particular colatitudinal direction varies as the inverse cosine of the square root of a random number. The random numbers are generated using a built in subroutine on the Honeywell 66/60 system.

Here, an analysis for the lower left wall will be given. Analysis for other walls is similar.

Diffuse Reflection from lower left wall:

A beam is diffusely reflected from a point $(x_L, y_L, z_L)$ located on the lower left wall. The probable longitudinal and colatitudinal angles for the direction of reflection are:

$$\theta_r' = 2 \pi R_1 \tag{A.9.a}$$

$$\gamma_r = \cos^{-1} \sqrt{R_2} \tag{A.9.b}$$

where the prime indicates that the angles are measured in the transformed coordinate system. (Introduced earlier in this Appendix.)

The direction cosines for the reflected beam are:

$$\cos \alpha_r' = \sin \gamma_r' \cos \theta_r' \tag{A.10.a}$$

$$\cos \beta_r' = \sin \gamma_r' \sin \theta_r' \tag{A.10.b}$$

$$\cos \gamma_r' = \cos \gamma_r' \tag{A.10.c}$$

These direction cosines in the base coordinate system are:

$$\cos \alpha_r = \cos \alpha_r' \tag{A.11.a}$$

$$\cos \beta_r = \sin \alpha_1 \cos \beta_r' + \cos \alpha_1 \cos \gamma_r' \tag{A.11.b}$$

$$\cos \gamma_r = - \cos \alpha_1 \cos \beta_r' + \sin \alpha_1 \cos \gamma_r' \tag{A.11.c}$$

Combining eqns. (A.9), (A.10), and (A.11).

$$\cos \alpha_r = \sqrt{1-R_2} \cos (2\pi R_1) \tag{A.12.a}$$

$$\cos \beta_r = \sqrt{1-R_2} \sin (2\pi R_1) \sin \alpha_1 + \sqrt{R_2} \cos \alpha_1 \tag{A.12.b}$$

$$\cos \gamma_r = - \sqrt{1-R_2} \sin (2\pi R_1) \cos \alpha_1 + \sqrt{R_2} \sin \alpha_1 \tag{A.12.b}$$

The procedure form this point is exactly the same as that explained for the specular reflected beam.

<u>Diffuse Reflection from the base</u>:

In the whole analysis, the base is assumed to be diffuse. The probable longitudinal and colatitudinal angles for the direction of the reflected beam are:

$$\theta_r = 2\pi R_1$$

$$\gamma_r = \cos^{-1} \sqrt{1-R_2}$$

(The angles are in the base coordinate system).

The direction of cosines of the direction of the reflected beam are:

$\cos \alpha_r = \sin \gamma_r \cos \theta_r$

$\cos \beta_r = \sin \gamma_r \sin \theta_r$

$\cos \gamma_r = \cos \gamma_r$

or

$$\cos \alpha_r = \sqrt{1-R_2} \cos (2\pi R_1) \tag{A.13.a}$$

$$\cos \beta_r = \sqrt{1-R_2} \sin (2\pi R_1) \tag{A.13.b}$$

$$\cos \gamma_r = \sqrt{R_2} \tag{A.13.c}$$

Therefore, the equation of the line coincident with reflected beam at point $(x_B, y_B, z_B)$ is

$$\frac{x - x_B}{\cos \alpha_r} = \frac{y - y_B}{\cos \beta_r} = \frac{z - z_B}{\cos \gamma_r} \tag{A.14}$$

Since the base is located at $z = 0$ and since the x-coordinate can be arbitrarily selected (set $x = 0$), the equation (A.14) becomes

$$\frac{x}{\cos \alpha_r} = \frac{y - y_B}{\cos \beta_r} = \frac{z}{\cos \gamma_r} \tag{A.15}$$

The destination of the diffusely reflected beam is now determined.

If,

$0 \leq \theta_r < \pi$, the beam is reflected to the right.

$\pi \leq \theta_r < 2\pi$, the beam is reflected to the left.

Case I: Beam reflected to the right

The equation of the plane of upper right wall is

$$z = (y - B/2 - D_1 \tan \alpha_1) \cot \alpha_2 + D_1 \tag{A.16}$$

The equation of the reflected beam may be written as

$$z = \frac{\cos \gamma_r}{\cos \beta_r} (y - y_B) \tag{A.15}$$

Using eqns. (A.15) and (A.16), the point of intersection of upper right wall with the reflected beam may be determined as

$$y_{int} = \frac{(B/2 + D_1 \tan \alpha_1) \cot \alpha_2 - D_1 - y_B(\frac{\cos \gamma_r}{\cos \beta_r})}{(\cot \alpha_2 - \frac{\cos \gamma_r}{\cos \beta_r})} \tag{A.17.a}$$

$$z_{int} = (y_{int} - B/2 - D_1 \tan \alpha_1) \cot \alpha_2 + D_1 \tag{A.17.b}$$

If

| | |
|---|---|
| $z_{int} \leq D_1$ | Beam strikes the lower right wall |
| $D_1 < z_{int} \leq (D_1 + D_2)$ | Beam strikes the upper right wall |
| $(D_1 + D_2) < z_{int}$ | Beam escapes to the surroundings |

Case II: Beam reflected to the left

The equation of the plane of upper left wall is

$$z = - (y + B/2 + D_1 \tan \alpha_1) \cot \alpha_2 + D_1 \tag{A.18}$$

The equation of the reflected beam is (from eqn. (A.15))

$$z = \frac{\cos \gamma_r}{\cos \beta_r} (y - y_B) \tag{A.15}$$

Using eqns. (A.15) and (A.18), the point of intersection of upper left wall with the beam reflected from the base may be determined as:

$$y_{int} = \frac{-(B/2 + D_1 \tan \alpha_1) \cot \alpha_2 + D_1 + y_B(\frac{\cos \gamma_r}{\cos \beta_r})}{(\cot \alpha_2 + \frac{\cos \gamma_r}{\cos \beta_r})} \tag{A.19.a}$$

$$z_{int} = - (y_{int} + B/2 + D_1 \tan \alpha_1) \cot \alpha_2 + D_1 \tag{A.19.b}$$

If

| | |
|---|---|
| $z_{int} \leq D_1$ | Beam strikes the lower left wall |
| $D_1 < z_{int} \leq (D_1 + D_2)$ | Beam strikes the upper left wall |
| $(D_1 + D_2) < z_{int}$ | Beam escapes to the surroundings |

# Appendix B

## Additional Results

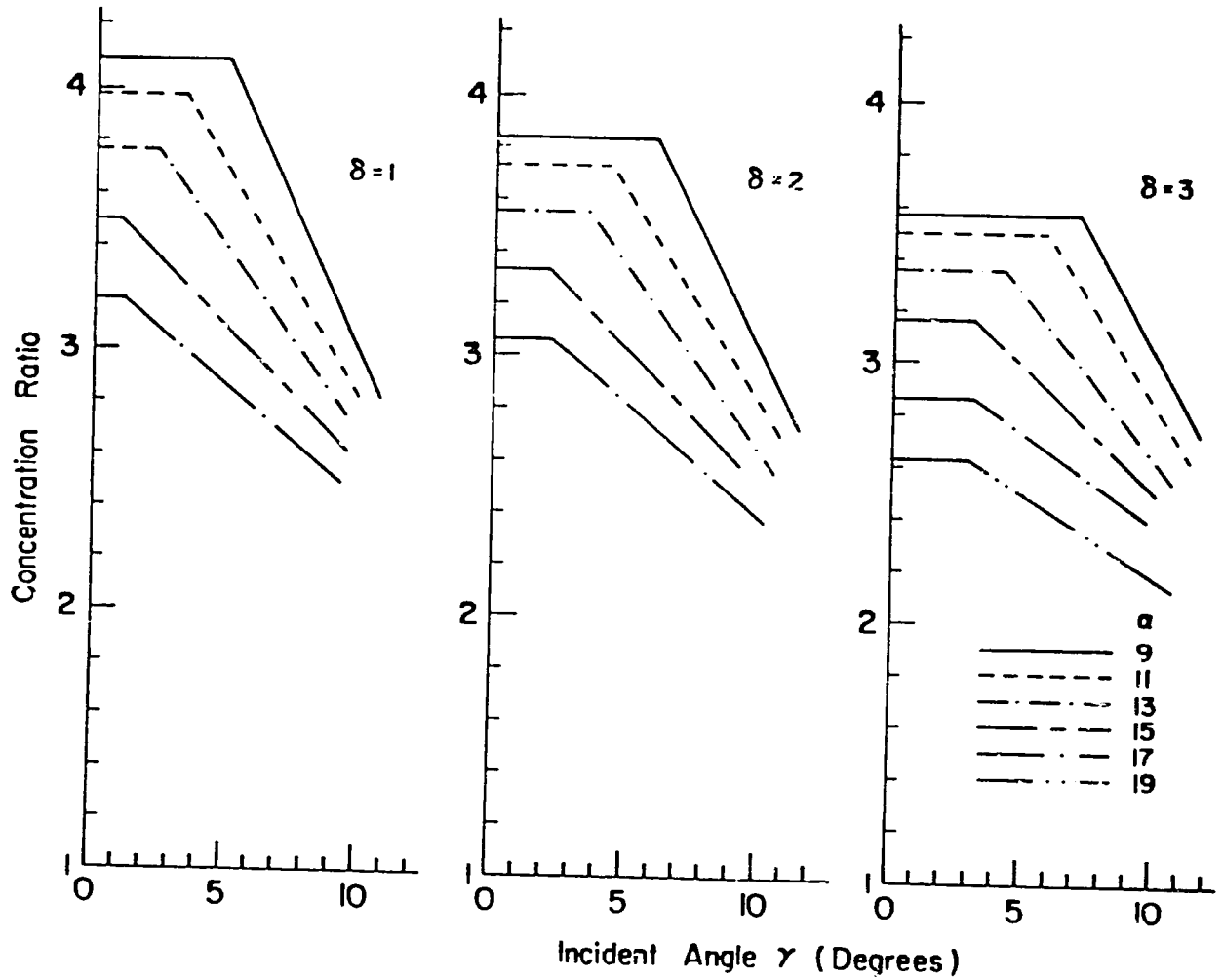


Figure B-1 Performance of One-Facet Groove Based on Two Reflection or Less Criterion (Perfect Wall)

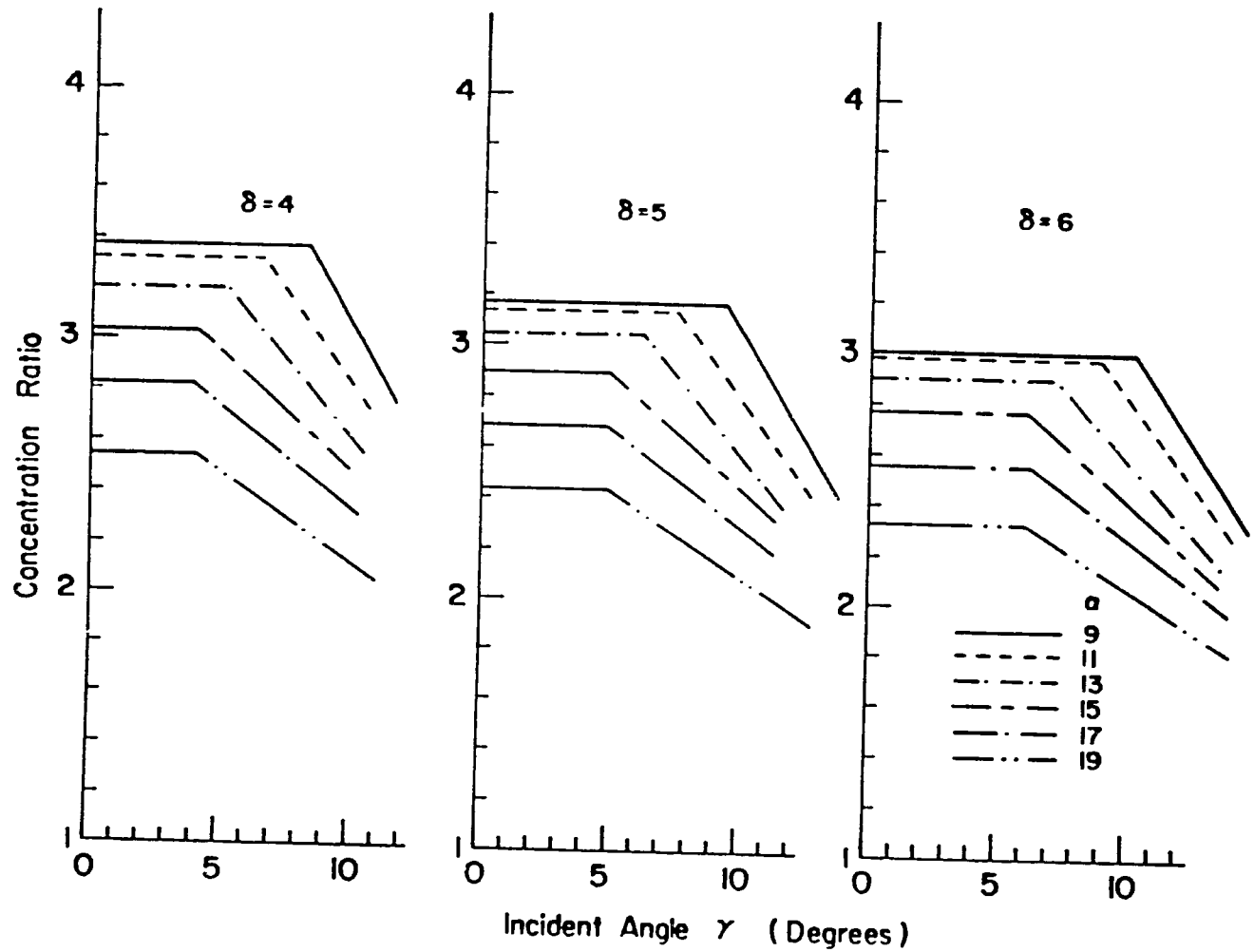


Figure B-2 Performance of One-Facet Groove Based on Two Reflection or Less Criterion (Perfect Wall)

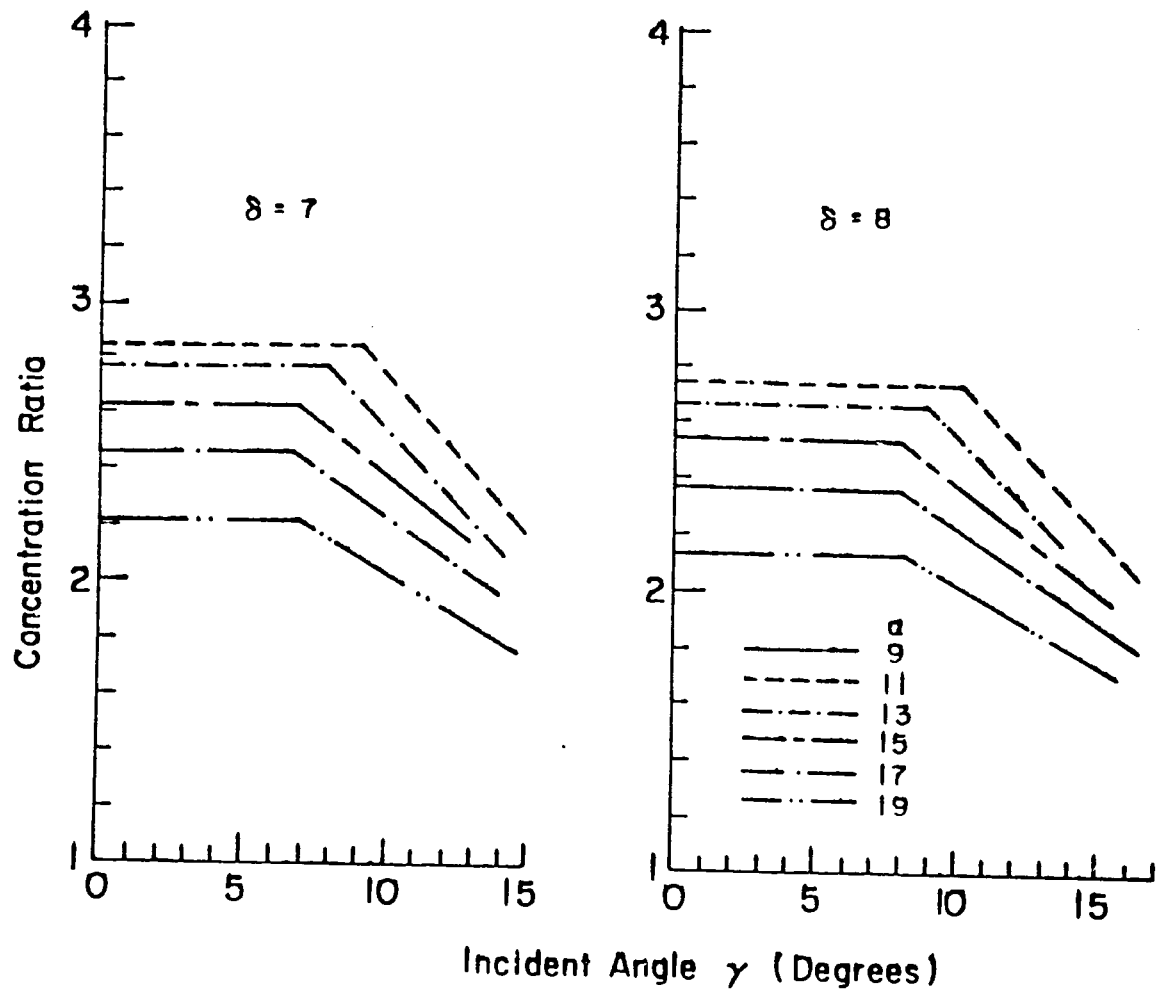


Figure B-3 Performance of One-Facet Groove Based on Two Deflection or Less Criterion (Perfect Wall)

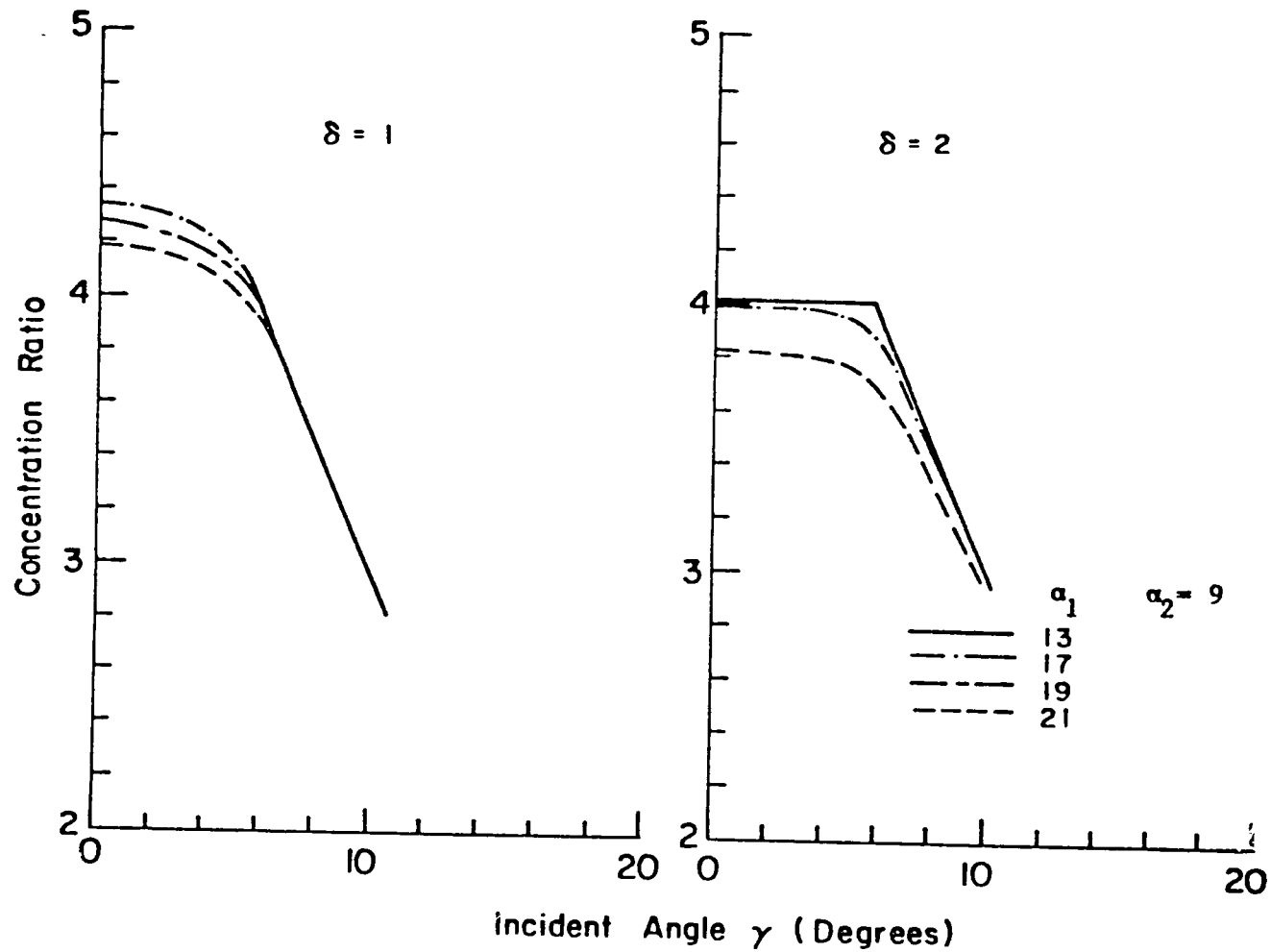


Figure B-4 Performance of Two-Facet Groove Based on Two Reflection or Less Criterion (Perfect Wall)

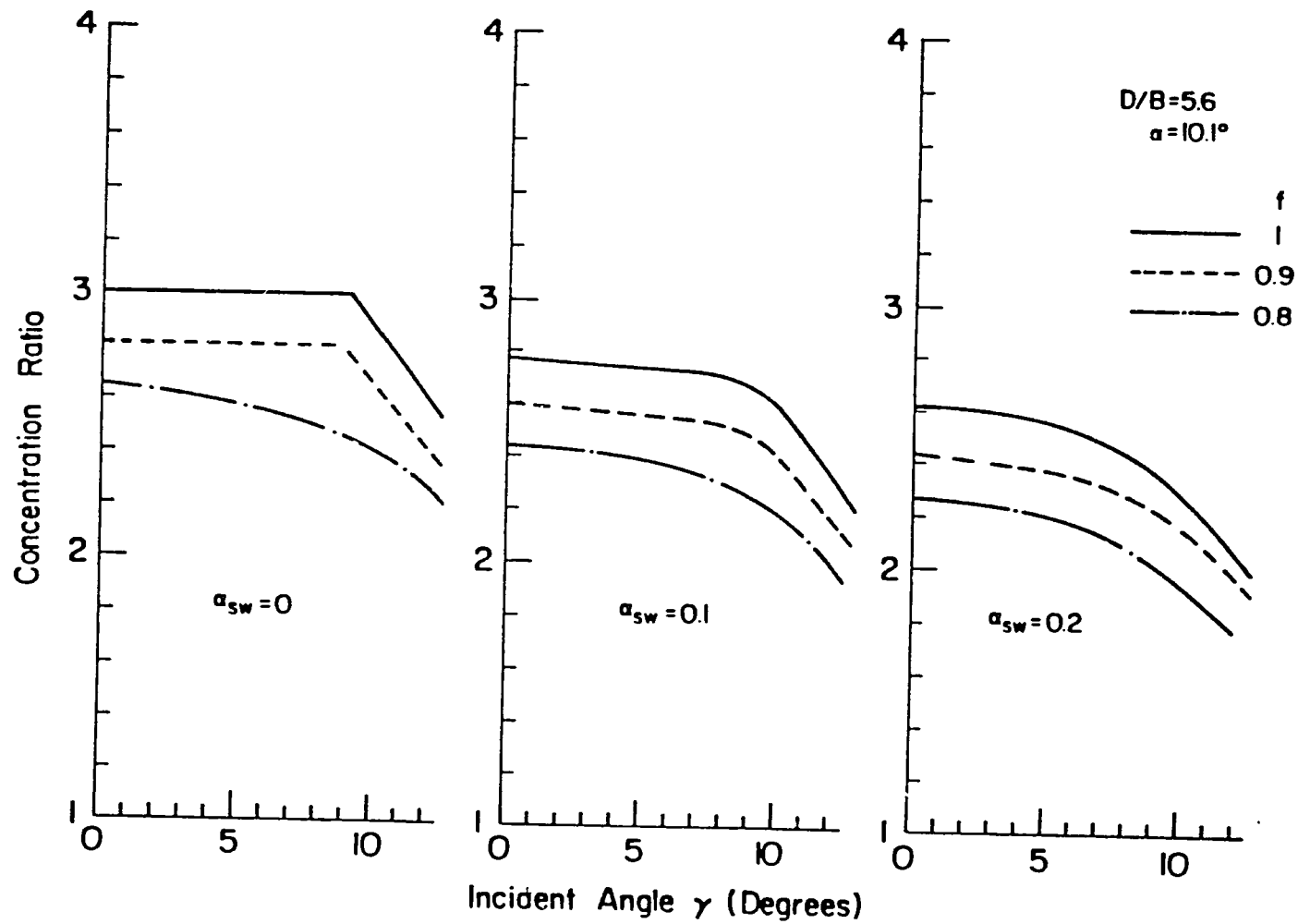


Figure B-5 Performance of One-Facet Groove Based on Two Reflection or Less Criterion (Real Wall)